RIVISTA DEL NUOVO CIMENTO Vol. 38, N. 5 2015
DOI 10.1393/ncr/i2015-10112-2

Fermi LAT: More than six years of insights and new puzzles

R. Rando and S. Buson

Dipartimento di Fisica e Astronomia, Università di Padova e INFN, Sezione di Padova Padova, Italy

received 18 December 2014

Summary. — We review the scientific output of more than six years of operation of the *Fermi*-LAT γ-ray space telescope, focusing in particular on the works by the *Fermi*-LAT Collaboration.

PACS 95.55.Ka – X- and γ-ray telescopes and instrumentation.

1. – Introduction

In August 2008, the Large Area Telescope (LAT) on board the *Fermi* Gamma-ray Space Telescope started nominal operations. Porting reliable high-energy physics technology into space, and building on the heritage of the CGRO-EGRET predecessor, expectations were high for a bountiful season in GeV astrophysics. Now, after more than six years of nearly continuous science operation, it is hard to overemphasize the *Fermi*-LAT contribution to the comprehension of the high-energy universe. In terms of sheer volume of scientific production *Fermi* is extremely succesful: a query on the *Fermi* Science Support Center database([1]) returns more than 1600 refereed papers having used *Fermi* data or results, with a cumulative citation number above 40000. Ranked by citation count in astrophysics, *Fermi* papers (sometimes several) are in the top 10 in 2009, 2010, and 2012. From the figures above it is evident how selecting highlights from the wealth of available material will be remarkably hard([2]). For this review we decided to emphasize the variety of phenomena the LAT has observed, ranging from thunderstorms to the investigation of the properties of the first stars to have appeared in the universe. Before moving to the scientific results, let us acknowledge the hard work of the worldwide *Fermi* community. All of the achievements have been made possible by a dedicated international team numbering over one hundred scientists, and with the support of several among the major research agencies and institutions in France, Germany, Italy, Japan, Sweden and USA: we thank everyone who joined in such an ambitious project and participated in making it real.

([1]) `http://fermi.gsfc.nasa.gov/cgi-bin/bibliography_fermi`
([2]) A complete updated list of *Fermi*-LAT Collaboration publications is available at `https://www-glast.stanford.edu/cgi-bin/pubpub`

2. – Puzzles and open questions in high-energy astrophysics

In this section we review a few of the open questions in high-energy astrophysics that fall within the range of the LAT investigation capabilities. Perhaps the most intriguing puzzle regards the origin of cosmic rays (CRs); in addition other astrophysical questions involving both Galactic and extragalactic accelerators will be mentioned. Finally, relevant issues in cosmology and frontier physics will be addressed.

2˙1. *Cosmic rays*. – We have know since 1912 that "radiation of very great penetrating power enters our atmosphere from above", to quote CR pioneer Victor Hess. Today we are aware that accelerated particles, mostly nuclei, populate the neighborhood of the Earth spanning over more than 10 decades in energy, but we remain far from a clear understanding of the particle origin and acceleration mechanism. To further complicate the picture, charged particles' trajectories are hopelessly twisted by the disordered cosmic magnetic fields, so that straightforward identification of the acceleration sites is impossible. A practical solution is to observe secondary γ rays: being neutral particles they are unaffected by magnetic fields and, as opposed to neutrinos, are relatively easy to detect.

The CR spectrum is featureless above the solar modulation threshold of a few GeV, and at least up to the so-called "knee" at $\sim 10^{15}$ eV (fig. 1). This remarkable lack of features naturally favors a single, universal acceleration mechanism and possibly a single class of CR sources. Supernova remnants (SNRs) are commonly suggested as sources of CRs, at least up to the knee, thanks to the success of the comprehensive theory of non-diffusive shock acceleration (NDSA), where particles are accelerated by repeatedly crossing a shock wave, gaining a small amount of energy with each passage. Accelerated electrons are easily identified in multiwavelength observation, while for a conclusive proof of hadronic acceleration we had to wait for the current generation of γ-ray observatories. CRs above the "ankle" ($\sim 10^{17}$ eV) are thought to be extragalactic in origin, possibly accelerated by active galaxies or in large-scale cosmic structures. In addition to this, isotopic abundances in CR composition show deviations from Solar System composition, indicating that up to 20% of CRs are accelerated in regions of massive-star formation [2]. Star-forming regions are complex environments, agitated by SN explosions and stellar winds: after acceleration, the turbulent medium may significantly influence the early propagation of CRs.

Regardless of the acceleration site, once CRs are released into the Galaxy they interact with the Galactic medium, producing secondary particles. The commonly accepted scenario describes the CR propagation as dominated by diffusion on disordered magnetic fields, with a possible contribution by convection. The ratio of stable-to-unstable isotopes confirms the picture of a Galactic halo surrounding the Milky Way where CRs are confined for time scales of $\sim 10^7$ years, occasionally interacting with the relatively dense disk. Observation of γ-ray emission from remote Galactic regions allows us to probe the local content of CRs and the concentration of target materials.

In addition to indirect measurements, the local abundance of CRs can be directly observed from Earth orbit. Given the high-energy loss rate of e^+ and e^-, the observation of the electron spectrum is a great probe of the local Universe (a few kpc). Primary electrons are accelerated as mentioned above in SNRs, massive-star associations, pulsars, etc. Secondary electrons, mainly from primary CR interactions with the Galactic medium, are produced as e^+ and e^- in equal number: the great asymmetry in the observed e^+ and e^- flux (roughly 1:20 at 10 GeV) indicates that e^- are mostly primary, while e^+

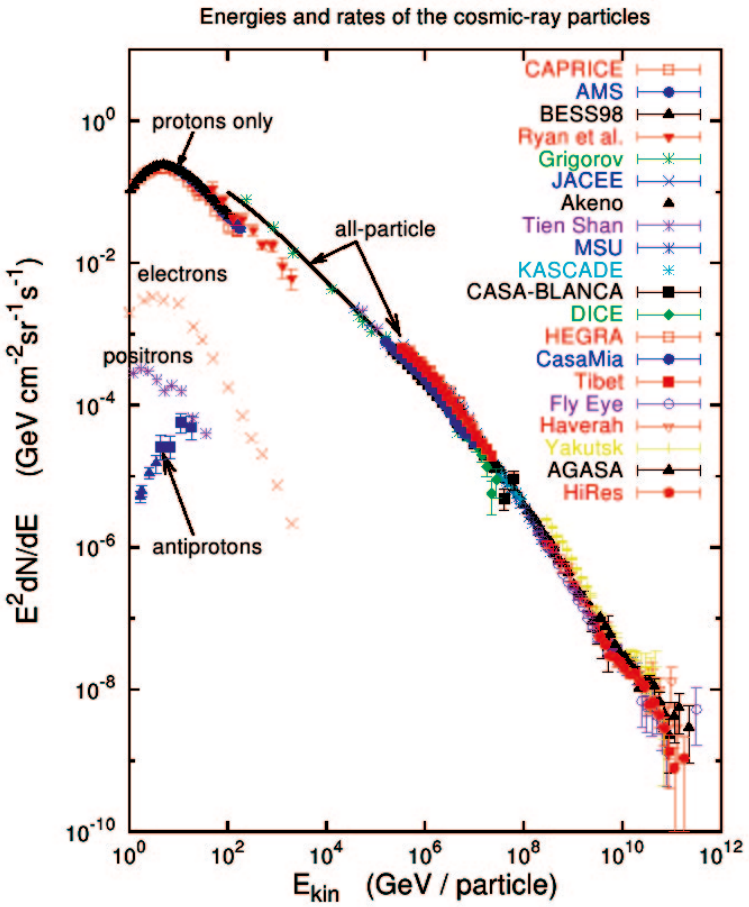

Fig. 1. – Compilation of measurements of the energy spectrum of charged CRs, from [1].

are mostly secondary particles; standard CR propagation models predict that the e^+ fraction should fall with increasing energy. In 2008 ATIC reported a bump in the electron spectrum around $\sim 500\,\mathrm{GeV}$ [3]; in 2009 H.E.S.S. reported an electron flux above expectation, but with no indication of such a spectral feature [4]. In 2009 PAMELA reported an anomalous abundance of e^+ above a few GeV: instead of falling as expected the e^+ fraction was shown to be increasing rapidly with energy [5]. All together, these new measurements of the local electron abundances show a scenario far from the expected, hinting to the presence of a local source of energetic CR in the nearby Galactic neighborhood.

In addition to direct observation, secondary γ-ray emission from the Earth atmosphere and from the other Solar System bodies can be used to derive the local primary proton spectrum. The Sun itself is a source of secondary γ rays due to hadronic CR interactions within its atmosphere, in addition to inverse Compton (IC) scattering on the low energy photons it radiates.

In summary, several processes allow us to derive the local CR spectrum, with different assumptions and different systematics. The question remains what exactly is accelerating

the CR to the observed energies. From isotopic abundances, roughly 80% of Galactic CRs have the same composition of Solar System material, with the remaining 20% being synthesized by Wolf-Rayet stars [6]. For the majority CR component SNRs have long been considered one of the most promising accelerators.

The CR spectrum is in agreement with a non-diffusive shock acceleration scenario (or *first-order Fermi mechanism*): because of scattering and turbulent motions, particles repeatedly cross a shock front, each time gaining a small amount of energy, leading to a power-law differential spectrum. The shocked medium left behind by an SN explosion is a perfect example of where such a process could take place; indeed the expectation placed on this mechanism led to it being labeled *SNR paradigm*. SNRs are historically classified by the remnant morphology as *shell-type*, in the presence of a shell of shocked plasma generated by the interstellar medium swept up by the shock wave, *plerions*, where a filled-center nebula is powered by a central pulsar, and *composite* SNRs, where filled nebula and a surrounding shell are both present. The time evolution of an SNR can be sketched as follows. During a first ejecta-dominated phase the material expelled by the SN freely expands, picking up interstellar material in the shock wave. During a second adiabatic phase the swept-up mass becomes greater than the expelled mass: a forward shock propagates in the interstellar medium and a reverse shock is generated, moving back towards the center of the SNR; radiative losses are negligible, hence the name. In a third, pressure-driven phase, radiative cooling causes the shock velocity to drop; the material inside the shock joins that outside, creating a dense shell. Finally, the shock merges into the interstellar medium. Once particles are accelerated in the SNR shock, they can produce γ-ray emission by the usual non-thermal processes: bremsstrahlung, inverse Compton and synchrotron for leptons, pion production and decay for hadrons, leading to observable emission with distinctive morphology.

2˙2. *Galactic sources*. – Among Galactic sources, pulsar science has witnessed the most dramatic advance. Pulsars are cosmic lighthouses: the rapidly rotating neutron star emits a beam of photons from its magnetosphere. The energy output is remarkable: up to 10^4 times the solar luminosity are emitted from radio to γ-ray energies; such energy expenditure causes the gradual increase of the rotation period. While the energy emitted at radio wavelengths is negligible, γ-ray efficiencies are as high as 10% of the spin-down power. γ rays are a probe of the acceleration processes in the pulsar magnetosphere and track the structure of the neutron star magnetic fields. Currently $\sim$ 2300 pulsars are known from radio observations. Pulsars can be divided into two families: *normal* (or *young*) pulsars have rotational periods in the range 0.1–10 s, while *millisecond pulsars* (MSPs) have rotational periods less than 0.1 s, down to a few ms. Such rapid rotation is usually interpreted as indication of a "spun-up" pulsar: an old pulsar in a binary system accelerates to high rotational frequencies by leaching angular momentum from the system. Indeed, the signal from most MSPs is observed to suffer from effects from orbital dynamics with a companion. γ-ray emission models introduce a *gap* region in the pulsar magnetosphere where the magneto-hydrodynamic force-free condition is violated, and particles can be accelerated up to TeV energies. Three gap regions were identified as possible acceleration sites: the *polar cap* region [7], the *slot gap*, along the last closed magnetic field line [8], the *outer gap*, between the null charge surface and the light cylinder [9], and a modified version of the latter, the *one pole caustic* [10]. Each model predicts specific pulsar emission patterns, *i.e.* a different γ-ray spectrum as a function of the pulsar rotational phase, according to the pulsar magnetic field, spin period, angle between rotational and magnetic axes, and gap width and position. Previously to *Fermi*-LAT,

only seven pulsars were detected at γ-ray energies, so a proper population study was impossible. *Fermi*-LAT observations transformed pulsar science from the study of a few bright sources into a science based on population characteristics. A corollary of the MSP age and their appearance in stellar binary systems is their relative abundance in globular clusters. Among the most ancient constituents of our Galaxy, rich in binary systems, these concentrations of 10^4–10^6 stars host large populations of MSPs [11], making them interesting targets at γ-ray energies.

2˙3. *Extragalactic sources.* – The study of *Active Galactic Nuclei* (AGNs) underwent a revolution with *Fermi*. Already at the very beginning of its operation *Fermi*-LAT proved to be a successful "AGN hunter", given the increased sensitivity and the whole sky observation strategy. The first three months of data pointed out 106 high-confidence associations with known AGNs [12] (by comparison the EGRET third catalog lists 66 objects [13]); many of them were later confirmed to be also among the brightest objects in the *Fermi* sky.

AGNs are extremely powerful objects: their γ-ray emission is thought to be powered by accretion of mass onto a supermassive black hole ($M \simeq 10^6$–$10^9 M_\odot$) located at the center of the host galaxy. Gravitational potential energy is converted into radiation observable through the whole electromagnetic spectrum. Their luminosity is second only to supernovae explosions, but while the latter are active just for a limited period, AGNs have a vast energy reservoirs and release energy almost continuously. After more than six years of operations *Fermi*-LAT has established AGNs as constituting the overwhelming majority of sources populating the γ-ray sky. The third LAT AGN catalog accounts for about 1600 objects detected at high significance in the high-energy band [14]. Within the γ-ray AGN population, most of the sources are of the *blazar* class: according to the so-called *AGN standard model*, in blazars a relativistic jet of plasma is closely aligned with the line of sight. They manifest the most dramatic emission and variability in the high-energy band. The LAT wide field of view enables observing the entire sky in only three hours, making it a suitable tool to follow the rapid variation of blazars and transient sources as well.

Regarding the AGN γ-ray emission, several questions were left open by EGRET observations and still have not found definite answers. First, the emission mechanism is poorly understood, namely how are jets collimated and confined, and what is their exact composition. Besides, other features still lack a reasonable interpretation: the ultra-short variability (of the order of few minutes) observed at γ-ray energies is much shorter than the black holes dynamical time scale; how very-high-energy (VHE; $> 100\,\mathrm{GeV}$) radiation can originate in FSRQs; several conflicting results have been obtained about the long controversial quest of the location of the γ-ray emission regions (see sect. **6˙2.2**); finally, there might be evidence for a hard spectral component in some objects.

Beside their intrinsic interest, AGNs can fruitfully be used for complementary studies in several parallel major fields: *e.g.*, extragalactic background light and high-energy horizon studies (more details below).

To conclude, the presence of intergalactic magnetic fields (IGMF) could blur the image of remote AGNs [15]. The origin of such fields in the early Universe is unknown, and according to the different models the expected magnitude is uncertain by more than 10 orders of magnitude: an indirect measurement by the observation of photon halos around AGNs is in principle within the LAT capabilities.

Gamma-Ray Bursts (GRBs) are bright flares of γ rays occurring at cosmological distances, over time scales ranging from less than one second to a few minutes. GRB science greatly benefits from *Fermi* as well: in particular, the complementarity of the two instruments aboard the *Fermi* spacecraft (*i.e.* LAT and Gamma-ray Burst Monitor) provides a wide, uninterrupted energy range over which to characterize these sources. Two classes of GRBs were identified before its launch: *long-duration* GRBs ($\tau > 2\,\mathrm{s}$), associated with low metallicity host galaxies and star-forming regions of galaxies, and *short-duration* GRBs, found in regions of much lower star formation rate in the host [16]. Gravitational collapse of supermassive stars and black hole formation are thought to be related to the activation of long-duration bursts [17] while short-duration bursts may arise from the coalescence of compact objects (such as neutron stars [18]).

The high-energy emission of GRBs was almost unexplored before *Fermi*. EGRET had the great merit of paving the way for *Fermi* studies: it earned the credit of detecting the first bursts at energies $> 100\,\mathrm{MeV}$, opening a new window of observation for these objects. The EGRET GRB sample, though limited to few bursts, already pointed out several common properties and peculiarities. The observed long-duration GRBs displayed two components: a $> 100\,\mathrm{MeV}$ emission, contemporaneous with the prompt emission detected in the 10–1000 keV band, and a delayed component, extending up to GeV energies, lasting more than an hour in the case of GRB 940217 [19]. Noteworthy, in the case of GRB 941017 [20], an additional power-law component unexpectedly emerged above the commonly used Band function spectrum [21].

These outcomes naturally directed interest toward the energy band that would have been soon covered by the LAT. EGRET capabilities did not allow to pinpoint temporal features patterns in the prompt component of the bursts (the spark chamber deadtime was of the order of $\sim 100\,\mathrm{ms/event}$). The new observation strategy and improved performance of *Fermi*, such as a lower deadtime per event of the order of $\sim 26\,\mu\mathrm{s}$, allowed to confirm GRB properties and discovery many more details, *e.g.* the delayed onset of emission above 100 MeV or the presence of an extra spectral component at high energy in some GRBs.

Extragalactic background light—high-energy horizon. Objects at cosmological distances, namely AGNs and GRBs, are powerful tools to explore the properties of the Universe on large scales and thus in past eras. In particular, γ-γ absorption of high-energy γ rays due to interaction with the diffuse, low-energy photon fields [22], allows us to indirectly probe the radiation content of the Universe. The effect is of extreme intrinsic interest, and indeed a clear detection of this absorption mechanism in the case of AGNs was one of the key science objectives of *Fermi*-LAT. In this process a γ ray photon interacts with a low-energy photon from the Extragalactic Background Light([3]) (EBL), causing a suppression of the high-energy spectrum of remote sources. The opacity of the Universe as a function of the photon energy can be modeled, based on assumptions on the primordial star populations and on the evolution thereof over cosmological time scales [23], and predicted suppression of high-energy blazar spectra can be compared with observations. In standard Big Bang cosmology, after the recombination at $z \sim 1000$ and the "Dark Ages", where no light source existed except the rapidly cooling Cosmic Microwave Background (CMB), a second ionization of hydrogen occurred, before $z \sim 6$ and possibly as early as

([3]) The interaction takes place when the γ ray photon energy, E_γ, and the EBL photon energy, E_{EBL}, satisfy: $E_\gamma \cdot E_{\mathrm{EBL}} \geq 2(m_e c^2)^2$, where $m_e c^2$ is the rest mass energy of the electron.

$z \sim 10$ [24]. The mode of re-ionization and the energy sources are still unknown, but UV radiation from the first stars in the earliest galaxies is a likely suspect. Direct observation of the primordial UV field is difficult, but indirect observations are possible, *e.g.* via the impact on GRB spectra.

2˙4. *Dark matter and new physics*. – Eighty years have passed since Zwicky first spoke of "dark matter" (DM), based on the vast discrepancy between the observed mass in the Coma galaxy cluster and the amount implied by the virial theorem. Experimental evidence has since accumulated: see, *e.g.*, [25] for a review. Perhaps the most striking evidence is given by the anisotropies of the CMB. Primordial density fluctuations left an imprint on the last scattering surface (at a redshift $z \sim 1000$) which COBE, WMAP and recently Planck [26] have measured; the agreement between the observed power spectrum and the expectation from models with a DM component totaling about 6 times the baryonic mass is really something unique in experimental physics. One could argue that from Zwicky's day we have learned a lot about what DM cannot be, but we still have no clear hint of what it is. Conventional matter, exotic matter and modified gravitational theories have been proposed, but the constraints that must be met are severe. One of the most successful candidates in the last 30 years is the family of elementary particles collectively known as *Weakly Interacting Massive Particles* (WIMPs). WIMPs are neutral, massive, and interact only through gravitational and weak forces. The general scenario is as follows: a primordial population of WIMPs, created at the Big Bang, decouple long before leptons and at the freeze-out leave a relic density which is approximately constant (per comoving volume) since it changes only due to the (relatively rare) annihilations. Strikingly, the typical relic density needed to explain the observed DM mass density translates into a velocity-weighted cross section ($\langle \sigma v \rangle$) of $\sim 1\,\mathrm{pb}$ ("thermal" cross section), that is a typical value for weak interactions. This connection between cosmology and fundamental physics has often been described as "the WIMP miracle".

DM detectors and accelerator searches have yet to provide evidence of DM candidates; indirect searches aim to detect the products of DM annihilation (or decay). As mentioned the average density and the expected cross sections ensure that on cosmological scales the amount of DM is comovingly constant. This is not true for regions where the DM density is greatly enhanced, such as in the DM clumps associated with cosmic structures, such as galaxies and galaxy clusters. A trivial calculation tells that the collision rate scales with the density squared, which for self-annihilating DM is also the annihilation rate. All predictions of DM product fluxes are thus composed schematically by two terms: a "particle physics" term, collecting all information on annihilation channels, cross sections, etc., and an "astrophysics" term, with DM density along the line of sight.

Detection of charged DM decay and annihilation products is possible, but given the abundance of primary CRs it is profitable to look for less frequently produced particles, such as e^+, that are mostly of secondary origin. DM indirect searches through γ-ray detection has the obvious advantages that γ rays do not lose energy in propagation and they are not deflected by magnetic fields. In particular the latter implies that the γ signal is clearly centered on the region where DM annihilation happens: logical targets are galaxy clusters, Galactic cores, the Galactic center (GC) and other Galactic clumps. Indeed numerical simulation of the DM clumping favors cuspy concentrations, while observed galactic rotation curves indicate constant density cores ("cusp-core problem") so models do not constrain very well the DM concentration in regions with the highest expected signal. Another numerical issue is the lower cutoff in the scale of substructures

that can be investigated in DM models (usually $\sim 10^5 M_\odot$); such unresolved structures can have a large impact, in particular in galaxy clusters. γ rays from DM annihilation can be divided into two main signatures: monochromatic signals due to annihilation into γX, and continuum signal due to annihilation into other particles and subsequent hadronic or leptonic γ production. The former kind leads to a "smoking gun" detection, since no other astrophysical phenomenon is known that could produce such a peculiar signature; unfortunately such channels are suppressed by a factor $1/\alpha^2 \sim 137^2$ since the DM particle must be neutral. The DM particle mass is easily derived in both cases: this is obvious for the monochromatic signal, but even the continuum spectrum has an exponential cutoff at the DM mass, while the exact spectral shape depends on the annihilation channel and hence on the DM mass scale.

3. – The Fermi Large Area Telescope

3˙1. *Fermi Gamma-Ray Space Telescope: some history.* – In 1995, NASA formed the *Gamma-Ray Astronomy Program Working Group*, to formulate recommendations for future space missions in NASA's γ-ray astrophysics program. In 1997 the Working Group presented a report, giving detailed recommendations for future NASA projects [27]. The highest priority one was called GLAST, a next-generation 10 MeV–100 GeV γ-ray mission to improve sensitivity 1 or 2 orders of magnitude with respect to the CGRO EGRET predecessor. In 1999 November a Flight Investigation proposal was submitted to the NASA Office for Space Science, addressing the instrument design, its capabilities and the scientific aims: the overall structure of the GLAST observatory was defined. The primary instrument, the Large Area Telescope (LAT), a high-energy pair conversion telescope, was designed based on the experience with EGRET, and on proven technologies with either flight heritage or widespread, documented performance in high-energy physics experiments. The GLAST Burst Monitor (GBM) was selected as complementary instrument to extend the sensitivity to γ and X rays down to ~ 5 keV.

After construction by a joint venture of NASA, the United States Department of Energy, and government agencies in France, Germany, Italy, Japan, and Sweden, and after integration and qualification, GLAST was launched on 2008 June 11 aboard a Delta-II rocket; on 2008 August 4, the LAT began nominal science operations. Renamed *Fermi Gamma-Ray Space Telescope* in honor of high-energy physics pioneer Enrico Fermi, it has given astronomers an increasingly detailed portrait of the universe's most extraordinary phenomena, from giant black holes in the hearts of distant galaxies to thunderstorms on Earth.

3˙2. *The Large Area Telescope.* – The *Fermi*-LAT is an imaging high-energy γ-ray telescope covering the energy range from ~ 20 MeV to more than 300 GeV. A detailed description of the LAT design and operation can be found in [28, 29]; here we summarize briefly the aspects relevant to this review.

The LAT consists of three detector subsystems. A tracker/converter (TKR), comprising 18 layers of paired x-y Silicon Strip Detector (SSD) planes with interleaved W foils to promote pair conversion, measures the directions of incident particles [30]. A calorimeter (CAL), composed of 8.6 radiation lengths of CsI(Tl) scintillating crystals stacked in 8 layers, provides energy measurements as well as some imaging capability [31]. An Anticoincidence Detector (ACD), featuring an array of plastic scintillator tiles and wavelength-shifting fibers, surrounds the TKR and rejects CR backgrounds [32]. In addition to these three subsystems a triggering and data acquisition system selects

and records the most likely γ-ray candidate events for downlink. A modular design is employed: 16 identical towers with TKR and CAL modules are assembled in a 4×4 matrix, enclosed by the ACD, a thermal blanket, and micrometeorite shield.

The TKR is the section of the LAT where ideally γ rays convert to e^+-e^- pairs and the charged particles are tracked. Starting from the top of each tower (farthest from the CAL), the first 12 paired layers are arranged to immediately follow converter foils composed of 3% of a radiation length of W (*thin* or *front* section). The next 4 layers are similar except that the W converters are 6 times thicker; designed to increase the conversion probability at the cost of a somewhat reduced angular resolution, these layers are referred to as the *thick* or *back* section. The last two layers have no converter, because the TKR trigger is insensitive to γ rays that convert in the last two layers.

The CAL is a 3D imaging calorimeter. This is achieved by arranging the CsI crystals in layers and rotating elements by 90° about the vertical axis in each layer. Energy deposition in each log is read out with a two-range readout system covering low energies ($< 1\,\mathrm{GeV}$ per crystal) and high energies ($< 70\,\mathrm{GeV}$ per crystal) respectively. For each log with some deposited energy, two position coordinates are derived simply from the geometrical location of the log within the CAL array, while the longitudinal position is derived from the ratio of signals at opposite ends of the log: the crystal surfaces were treated to provide monotonically decreasing scintillation light collection with increasing distance from an end. Thus, the CAL provides a 3D image of the energy deposition for each event. Since the CAL is only 8.6 radiation lengths thick at normal incidence, for energies greater than a few GeV shower leakage becomes relevant, limiting the energy resolution. The intrinsic 3D imaging capability of the CAL is key to mitigating the degradation of the energy resolution at high energy through an event-by-event 3D fit to the shower profile; it also plays a critical role in the rejection of hadronic showers.

The ACD is critically important for the identification of charged CRs. From the experience of the LAT predecessor EGRET came the realization that a high degree of segmentation was required in order to minimize self-veto due to hard X-ray back-scattering from showers in the CAL. The ACD consists of 25 scintillating plastic tiles covering the top of the instrument and 16 tiles covering each of the four sides. The design requirements for the ACD specified the capability to reject entering charged particles with an efficiency $> 99.97\%$. The required segmentation inevitably led to less than complete hermeticity: tiles overlap in one dimension, leaving gaps between tile rows in the other; such gaps are covered by bundles of scintillating fibers.

Each detector subsystem contributes one or more trigger primitive signals to the LAT trigger system. The TKR trigger is a coincidence of 3 adjacent paired layers within a single tower (a total of 6 consecutive SSD detector planes). The CAL provides two inputs to the global LAT trigger: in the standard configuration, discriminator thresholds are set at 100 MeV and 1 GeV energy deposition for each log, to form two separate trigger request signals. The ACD provides information used in the hardware trigger: a fast signal, to be used *e.g.* as charged-particle veto, and two separate, slower signal chains to measure the signal amplitude, *e.g.* to determine the pulse height from $\sim 0.1\,\mathrm{MIP}$ to hundreds of MIPs.

The LAT trigger collects information from the LAT subsystems and, when appropriate, initiates event readout. Because each readout cycle produces a minimum of $26.5\,\mu\mathrm{s}$ of dead time, the trigger was designed to be efficient for γ rays while keeping the total trigger rate, which is dominated by the much greater flux of charged particles, low enough to limit the dead-time fraction to less than about 10%. The triggering criteria allow additional, prescaled event streams for continuous instrument monitoring and calibration

during normal operation. In addition the LAT trigger periodically initiates a readout at a frequency of 2 Hz (*periodic trigger*).

To limit the data volume to the available telemetry bandwidth, collected data are passed to the on-board filter (OBF). Provided that the on-board filter processes at least the average incoming data rate no additional dead time will be accrued; in practice, the amount of dead time introduced by the on-board filter is negligible. The on-board filter allows the coexistence of different filtering algorithms and, in fact, in the nominal science data taking configuration all the events are presented to several different filters. One feature of the γ filter of particular importance is the so called *high-pass* feature, which allows all events with an energy deposition in the CAL above a programmable threshold (currently set to 20 GeV): the low particle flux at high energy causes no significant increase in the overall data volume.

3˙3. *The LAT operation.* – *Fermi* was launched into a 565 km altitude orbit with an inclination of 25.6° with a period of 96 minutes, while the orbital pole precesses about the celestial pole with a period of ~ 53.4 days. At this inclination *Fermi* spends about 13% of the time inside the South Atlantic Anomaly (SAA): science data taking is suspended while the observatory is within the SAA because of the high flux of trapped particles. When *Fermi* is in standard sky-survey mode the center of the LAT field of view is rocked north and south of the zenith direction on alternate orbits by a characteristic rocking angle. In 2009 September this rocking angle was increased from 35° to 50° in order to lower the temperature of the spacecraft batteries and thus extend their lifetime. As a result of this change, the amount of the γ-ray bright Earth limb that is subtended by the field of view of the LAT during survey-mode observations increased substantially.

Triggered events passing the on-board filter are downlinked and undergo event reconstruction, where electronic information is translated into physically meaningful quantities under the assumption of a γ ray impinging on the LAT from the front. Track candidates are generated from the TKR data, and associated in vertexes; several potential determination of the direction of the primary γ ray are evaluated with different algorithms. The energy deposited in the TKR is also evaluated. In the CAL the energy deposition cluster is determined and several estimates of the event energy are derived, taking into account the energy loss due to the gaps in the modular design of the LAT and the energy escaping from back and sides. TKR tracks are propagated to the ACD and relevant quantities, such as the track distance from any ACD tile with energy deposition, are evaluated.

After reconstruction, event analysis takes place. From the complex information describing the reconstructed event a simple photon event structure is assembled by selecting the best energy and direction estimates, based on the event topology, and the quantities to be written in the familiar FITS photon tables are computed. Background rejection is a key process during event analysis. Due to the overwhelming particle background in the LAT orbit, a background reduction of a factor $\sim 10^6$ is necessary; the LAT event analysis achieves this while preserving $\sim 75\%$ of γ rays. Event selection can be adjusted to reduce the background contamination and improve the LAT energy and angular resolution at the expense of reducing the γ-ray efficiency. In this way *event classes* can be defined to suit different scientific requirements, *e.g.* higher-background, high-efficiency datasets for the study of brief transients, high-purity datasets for the precise study of brighter sources, etc.

3˙4. *The LAT performance.* – The LAT collaboration provides a set number of predefined event classes to suit most analyses, with the necessary software tools for their

use. The *instrument response* is the key for translating the observed event counts into source properties. The instrument response is customarily factored into three terms, each dependent on the energy and incidence angle of the incoming γ ray.

- The *effective area* depends on the geometrical cross section of the LAT as well as the efficiency for converting and identifying incident γ rays; loosely speaking it is the LAT efficiency expressed in units of area: it translates an observed count rate into a source flux.

- The *point-spread function* (PSF) describes the LAT angular resolution as the probability distribution of the distance between true and reconstructed directions. It also describes the measured angular distribution of photons coming from a point source, hence the name.

- The *energy dispersion* describes the LAT energy resolution as the probability distribution of the difference between true and reconstructed energy; loosely speaking it describes the measured energy distribution for a monochromatic energy line.

The instrument response elements are evaluated from a dedicated Monte Carlo simulation of the LAT; *front* and *back* sections of the LAT have significantly different response, so each is addressed separately. Several event classes are publicly distributed with the *ScienceTools* science analysis package, and data can be selected accordingly in the online server or locally with the software tools. Available event classes should cover the needs of most users: "TRANSIENT" event classes provide large efficiency allowing a significant background rate, "SOURCE" classes are tailored to provide a good balance for the study *e.g.* of point sources, "CLEAN" classes provide low background contamination at the expense of effective area, especially at low energies, etc.

A detailed description of the current reconstruction and event analysis (labeled *Pass 7*), together with assessment of the associated systematics are given in [29]. Currently, a major revision of event reconstruction and analysis is underway: designated *Pass 8*, this new analysis aims for improved performance in all aspects. One of the main goals of this revision is to recover the efficiency lost to instrumental pile up effects, given that the current analysis process conservatively discards γ events with spurious signals in the LAT subsystems due to particles crossing within the electronic integration and readout times. While only a few percent of the events are affected, this leads to an overall reduction of efficiency than can now be restored (see fig. 2). The details of the new scheme and the current estimate of the impact on performance can be found in [34].

IRFs can change in time for two reasons.

- If data reconstruction and/or event analysis change, raw data must be reprocessed, the Monte Carlo simulation must incorporate the changes, and as a consequence the LAT response must be evaluated anew. An example of this is the change from "Pass 6" to "Pass 7" event analysis. In 2013 LAT data were reprocessed to profit from new calibration constants; the new dataset is labeled "Pass 7 REP".

- Occasionally, details of the representation of the IRFs are improved, such as *e.g.* the functional form describing energy dispersion and PSF; this obviously does not imply a change in the data but only in the IRFs: an increasing version number is used to indicate this, *e.g.* "V6".

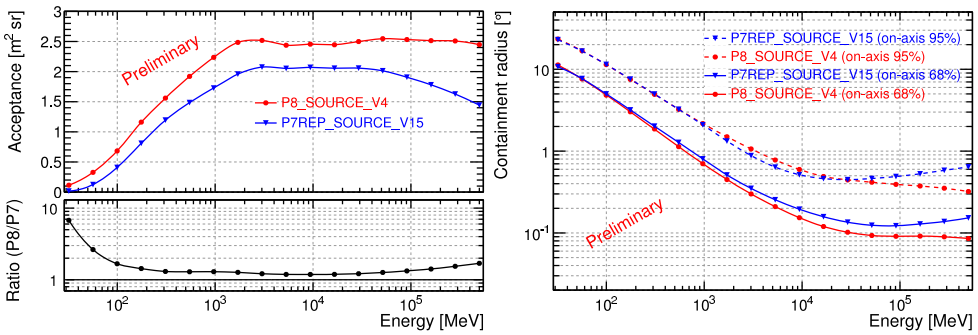

Fig. 2. – Left: LAT acceptance as a function of energy, for Pass 7 REP SOURCE class, compared to the current Pass 8 prototype. Right: PSF for normal incidence photons. From [33].

The residual charged-particle background flux, which is different for the different event classes, is conventionally included as part of the model for isotropic diffuse γ-ray emission (see sect. **3**˙5).

3˙5. *The LAT data and data products*. – LAT γ-ray data are publicly available; analysis software and high-level data products are also distributed [35]. The *ScienceTools* science analysis package includes tools to select event classes and regions of interest (ROI), apply additional quality cuts (*e.g.* on the measured zenith angle to reduce contamination from the bright Earth limb), and fit a model of the emission in the ROI to the observed counts. *Fermi*-LAT data products include a catalog of detected sources, a model of the Galactic diffuse emission and of the isotropic emission (see below), all of which are necessary ingredients for the standard science analysis procedure. The derivation of these models is of course deeply entangled, given the strong interdependence.

Standard LAT analysis based on a model fitting technique requires an accurate spatial and spectral model for the Galactic diffuse emission. The Galactic model is a spatial and spectral template; for the derivation see sect. **5**˙1.

In the case of the isotropic component, a spectral template describes the spectral form derived from a fit to the all-sky emission that is not represented in the Galactic diffuse model, including both extragalactic diffuse γ rays and remaining residual (misclassified) charged particles incident on the LAT. The isotropic model is determined under the assumption of a specified Galactic diffuse model and in particular depends strongly on the selection of an event class, since the background rates are extremely class-dependent.

The *Fermi*-LAT catalog, currently at the third iteration (3FGL, see fig. 3), accounts for 3033 sources and includes source locations and spectral descriptions [37]. Of these, 78 are flagged as potentially being due to imperfections in the model for Galactic diffuse emission. Table I summarizes all the detected classes of sources in 3FGL.

4. – The Solar System

Compared to extreme, remote sources, nearby sources can be detected even if the intrinsic luminosity is rather small thanks to their proximity. The Earth itself is in fact the brightest γ-ray source in the LAT sample. Earth, and the Earth atmosphere in particular, provide an ideal environment to indirectly determine the local flux of cosmic protons. Not only are the outer limits of the atmosphere (viewed along lines of sight

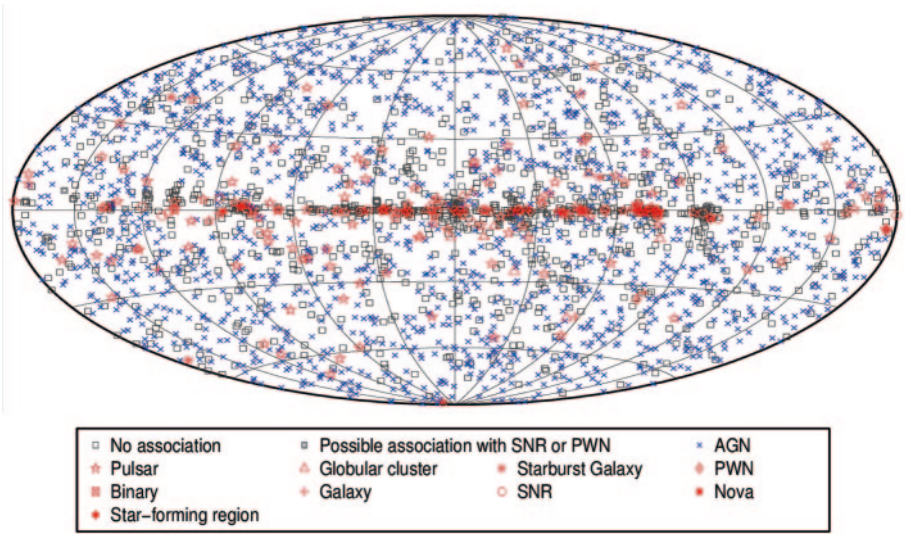

Fig. 3. – Sky map showing sources in 3FGL (see also table I), flagged by source class. Colors highlight the AGNs, non-AGNs and unassociated sources; from [37].

close to the horizon) a thin target, allowing a straightforward derivation of the primary CR spectrum, but in addition the Earth provides the magnetic field the LAT lacks to discriminate particles by charge. On the other hand, while the LAT is designed to reject charged CRs, nonetheless large amounts of CR events leak into the triggered and filtered sample and are collected: a direct measurement of the local particle flux is therefore possible.

TABLE I. – *Sources detected in the 3FGL divided by classes. "Other AGNs" includes: non-blazars, radio galaxies, Seyfert galaxies, Narrow line Seyfert 1 galaxies, AGNs of uncertain type. "Other" includes: high-mass binaries, binaries, novae, globular clusters, star-forming regions.*

Source class	Identified	Associated
Pulsar	143	24
Pulsar Wind Nebula	9	2
Supernova Remnants	12	11
Supernova remnant/Pulsar wind nebula	–	49
Quasars (steep and soft spectrum)	0	4
BL Lac blazars	18	642
FSRQ blazars	38	446
Other AGNs	10	588
Normal & Starburst galaxies	2	5
Other	6	15
Total	238	1786
Unassociated	–	1009

Solar and geomagnetic modulations of the CR spectrum complicate the situation below $\sim 10\,\mathrm{GeV}$. The former is given by the interaction of CR with the solar magnetic (SMF) field inside the heliosphere: charged particles drift in large-scale gradients of the SMF depending on their charge and on the SMF polarity, which changes periodically on time scales of ~ 11 years. The latter is caused by particles with low rigidity being prevented from reaching a particular location along the spacecraft orbit; in addition, identical particles with opposite charges gyrate in opposite directions before reaching the spacecraft, causing a characteristics east-west asymmetry due to the increased absorption of particles arriving along trajectories where the atmosphere is denser.

4˙1. *Earth in gamma rays and cosmic protons*. – While electron bremsstrahlung dominates below 50 MeV, at higher energy primarily contributors to the atmospheric γ-ray luminosity are hadronic cascades, by means of neutral pion and kaon production and decay. CR protons are the main responsible, with a small contribution from He nuclei. As a consequence analysis of the Earth γ-ray flux is particularly suited to determine the proton flux above $\sim 100\,\mathrm{GeV}$ [38, 39].

γ-ray emission can be described as a function of the angle from the local nadir, Θ_N. At the LAT altitude the Earth limb is located at $\Theta_N \sim 66.7^\circ$. At smaller angles, corresponding to secondary γ-ray emission from below the horizon, the LAT can collect γ rays from events back-scattering at a large angle; therefore the spectrum is soft. At the limb, γ rays are produced in the forward direction by primary protons impinging on the atmosphere along the line of sight, in this regime the γ-ray flux is determined by the primary proton flux. At large angles, the decrease in target thickness causes a drop of luminosity and emission from other celestial sources becomes relevant.

Let us focus on the thin target regime, above 15 GeV and up to 1 TeV, the upper limit of the energy range over which the LAT response is adequately validated. Background can be estimated by a ring surrounding the Earth, far enough that the PSF causes no contamination from the signal region. PSF spillover causes contamination from the bright thick-target region, and smearing of events from the signal region: the combined correction amounts to a decrease in the measured luminosity of $\sim 35\%$.

A model must be used to infer the proton spectrum from the γ-ray data, in [39] two models are used, with negligible difference to the results. A correction must be applied to remove the contribution from alpha particles (6–10% by primary number, 10–20% in γ-ray flux, depending on energy) with a minimal impact on the derived proton spectrum. The proton-to-gamma energy conversion factor is ~ 0.17; therefore our selection of photon energy translates into a proton energy range of 90 GeV–6 TeV. The resulting proton spectrum is well described by a power-law distribution with index 2.68 ± 0.04; there is no significant indication of a break in the proton spectrum. In fig. 4 the inferred CR proton spectrum is shown and fitted with two alternative models: power law and broken power law; the significance of the spectral break is only $\sim 1\sigma$. The spectral shape is in good agreement with results from PAMELA, ATIC-2 and CREAM, confirming a flattening of the proton spectrum at high energies. It is remarkable how this indirect measurement, based on rather limited statistics, still manages a high accuracy, *e.g.* within an order of magnitude from the precision of the PAMELA measurement.

4˙2. *Terrestrial gamma-ray flashes*. – Terrestrial Gamma-ray Flashes (TGF) were reported in 1994 by the BATSE burst monitor on CGRO [40]: they last typically 0.1–1 μs and reach energies up to $\sim 20\,\mathrm{MeV}$. From the very beginning the correlation with thunderstorms has been clear, thanks to the spatial and temporal coincidence between

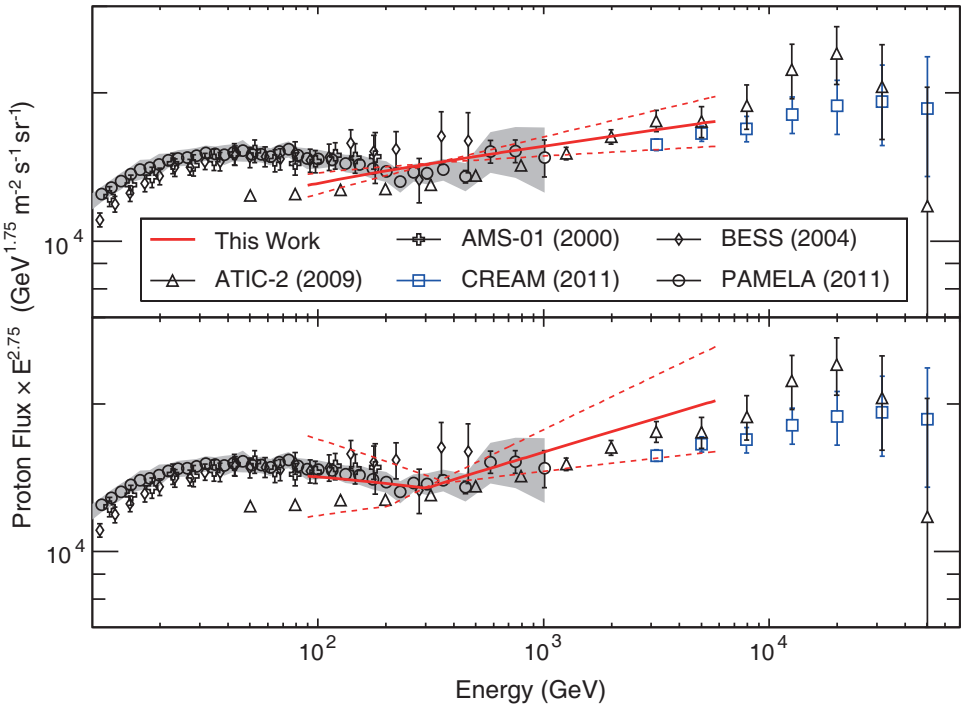

Fig. 4. – CR proton spectrum as derived from Earth γ-ray emission, from [39]. Top: fit with a power-law model; bottom: broken power-law model.

BATSE events and very low frequency radio signals from lightning, even if the precise sequence of events was not clear. RHESSI [41], AGILE-MCAL [42] and the *Fermi*-GBM [43] have observed the same phenomenon. In particular the latter observed TGF with a rate of one every ~ 3.7 days. Precise timing and localization demonstrated the contemporaneity of lightning and γ-ray bursts [44], and the observed hard spectrum was found to be consistent with bremsstrahlung emission by electrons accelerated in some electrical discharge process. In addition to the aforementioned LAT pointing strategy which usually avoids the Earth, observation is complicated by the event characteristics: typically several photons in the lowest energy range of the LAT sensitivity reach the instrument in a short time window comparable to the few μs shaping time of the readout electronics, so conventional event analysis is not particularly efficient. To date no events above ~ 50 MeV were reported [45], and a dedicated analysis effort to try recovering these challenging multiple γ-ray events is in progress.

4˙3. *Cosmic ray electrons*. – Once electrons (e^- and e^+) cross the ACD without being tagged, the event development is hardly distinguishable from photon-generated showers: in a sense the LAT is an electron detector with the addition of converter foils and an ACD. On the positive side this means that a precise direct measurement of the local cosmic electron spectrum is within the LAT capabilities. The trigger and filters are extremely flexible, and the only practical limitation is given by the increased deadtime and bandwidth consumption that would arise from allowing in a significant fraction of electrons. Even without tuning the trigger, the on-board filter (OBF) is set to pass all

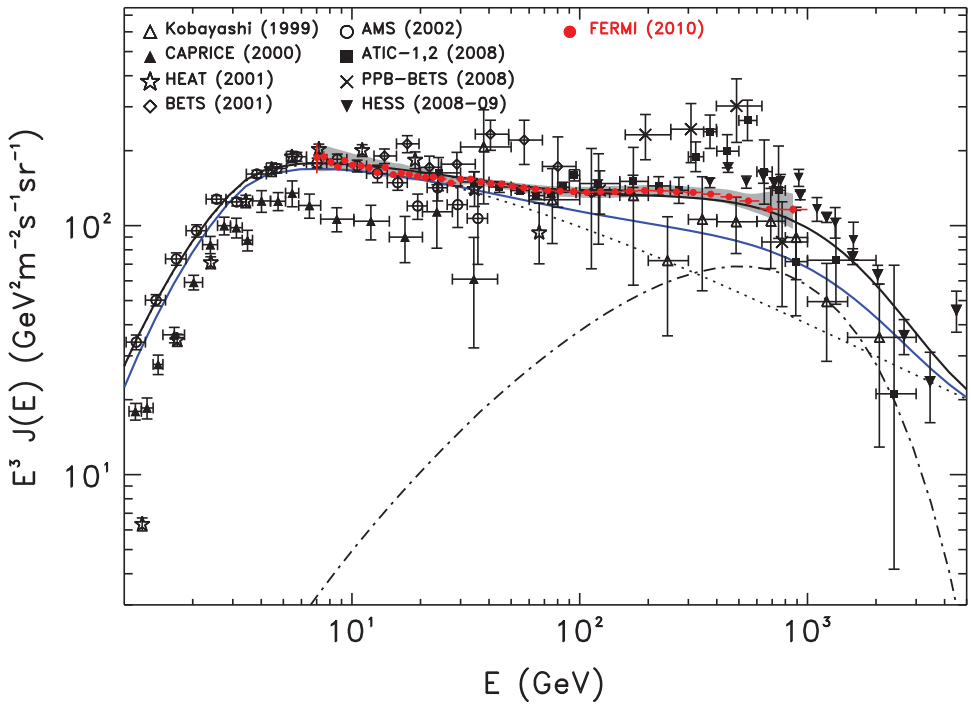

Fig. 5. – Electron spectrum, from [49]. Dotted line: conventional model; dashed line: additional component with hard injection spectrum and exponential cutoff. Solid blue line: e^- spectrum only; solid black line: total electron spectrum.

events with a calorimeter energy deposition greater that 20 GeV: given the rapidly falling spectra of all species this happens at the expense of a minimal increase in bandwidth consumption. Taking advantage of this, a first measurement of the electron flux was performed early in 2009 [46].

To lower the energy range the LAT Collaboration made use of a "diagnostic" trigger engine, selecting for downlink an unbiased fraction (1/250-th) of all triggering events. This led to a second analysis making use of two complementary datasets: *LE*, between 0.1 and 100 GeV, and *HE*, between 20 and 1000 GeV, with different systematics and a substantial overlap range to cross-check the analysis.

The event analysis and background rejection was carefully tuned to reject the large hadron background while keeping good electron efficiency end energy resolution.

The resulting electron spectrum is shown in fig. 5: below 50 GeV the spectrum is consistent with previous experiments, keeping in mind that measurements at low energies are affected by local magnetic modulations. At higher energies a deviation from a power-law spectrum is evident; this can be explained either by adjusting the injection spectra, or adding a source of electrons with a hard spectrum. In particular, if the high-energy particles come from a single source this must be located nearby: electrons lose energy rapidly due to synchrotron radiation and IC collisions, so 100 GeV electrons must originate within 1.6 kpc. Various scenarios have been discussed [47, 48] in an effort to explain this excess either by assuming a conventional astrophysical origin, such as a nearby pulsar, or exotic phenomena, such as dark matter annihilation.

As we mentioned previously, the Earth's magnetic field can be used to discriminate the sign of charged particles [50]. If one looks at the direction of the incoming e^-, the Earth would appear as a dark disk. Surrounding it the forward scattered interactions of energetic e^- in the atmosphere cause a bright ring, much like what happens for γ rays, and going outwards one finally observes the primary electrons. The secondary-electron ring is slightly deflected westwards as a function of the particle rigidity due to the geomagnetic field. If we now consider e^+, the curvature is reversed and the Earth appears slightly eastwards. At a given energy there are therefore 4 regions in the sky: one where primary electrons cannot reach the LAT because they are blocked by the Earth and its atmosphere, one crescent-like region where e^- are forbidden but e^+ are allowed, one where e^+ are forbidden but e^- are allowed, and the majority of the sky, where both charges are allowed. This allows us to measure separately the e^+ and e^- fluxes below 200 GeV, where the exclusive regions are large enough to provide good statistics; as a lower energy limit we take 20 GeV, corresponding to the threshold of the high-pass feature in the OBF.

While the e^- spectrum is consistent with what we discussed previously, the e^+ flux is well described by a power law with index 3.20 ± 0.06 where we indicate the total (statistical + systematic) uncertainty. This is consistent with the PAMELA measurement. Recently AMS-02 reported on the e^+ fraction, confirming the results from the previous observations of *Fermi*-LAT and PAMELA up to 350 GeV [51].

To differentiate between conventional propagation scenarios against a local source of electrons, one would naively look at the particle apparent origin in the sky; unfortunately the Galactic and local magnetic fields act to deviate the charged particles. Nonetheless, depending on the details of the source and on the propagation in the Galactic medium, an anisotropy in the directions of incoming electrons could be observed. A search for this based on 1 year of data did not allow identifying such a signature, providing upper limits on the dipole anisotropy ranging from $\delta \sim 10^{-2}$ above 100 GeV to $\sim 10^{-1}$ above 500 GeV at 90% C.L.; the limits for multipole anisotropy are of course less stringent [52].

4˙4. *Sun*. – Prior to the launch of *Fermi*, only 9 solar flares had been detected above 25 MeV, five by GRS/SMM in 1980s and four by EGRET in the 1990s; all of these were classified as X class flares, *i.e.* with peak fluxes (in the X-ray) in the range 10^{-4}–10^{-3} W/m^2. The picture changed dramatically in the *Fermi* era; the LAT has detected more than 40 solar flares in the first 6 years, more of half of these being M class events, with peak fluxes (in the X-ray) one order of magnitude lower.

To detect solar flares with the LAT, timing is a major issue: in addition to the typical short duration of flares, while *Fermi* operates in survey mode the Sun enters the LAT FOV for only 35 minutes every 3 hours, so direct imaging of a flare is a fortuitous occurrence. In addition, things are further complicated by the intense keV X-ray emission of flares: if enough of these photons pass the micrometeor shield and thermal blanket around the LAT and reach the ACD, the energy pile-up can cause a significant ACD signal and therefore the loss of events during the background rejection stage. (In principle an intense flare could deposit enough energy in the ACD tiles to veto a γ-ray event, but this has not occurred yet). In addition to the standard science analysis, the *Fermi*-LAT collaboration has developed a dedicated analysis for short transients (*LAT Low Energy, LLE*) where event classification cuts are significantly relaxed, providing great γ-ray efficiency at the expense of a high background; this new approach is also immune to the ACD pile-up effect.

SOL2010-06-12T00:57 is an example of an impulsive flare [53]. The GBM detected narrow and broad nuclear lines, indicating that protons and ions were accelerated above

$\sim 30\,\mathrm{MeV}$, while the LAT detected emission up to $\sim 400\,\mathrm{MeV}$; both pion decay and bremsstrahlung models are good fits to the observed spectrum in the LAT energy range, the latter being compatible with a simple power-law primary spectrum. An interesting feature is the apparent delay ($6 \pm 3\,\mathrm{s}$) observed between the GBM time profile (100–500 keV) and the LAT one ($> 30\,\mathrm{MeV}$): this would indicate that the primary particles responsible of the γ-ray emission, either protons or electrons according to the competing models, accelerate to $E > 100\,\mathrm{MeV}$ on time scales similar to electrons reaching hundreds of keV, with a time delay of a few seconds.

SOL2012-03-07 is an example of a flare showing sustained emission after the impulsive phase, being detected at LAT energies for more than 20 hours [54]. This flare also produced the most energetic photon ever detected in such episodes (4.5 GeV). The high-energy γ-ray spectrum is significantly curved: while it is easy to accommodate this within a hadronic scenario, bremsstrahlung models require a cutoff in the primary electron spectrum. Continuous acceleration of protons at the flare reconnection region can explain the long duration of the γ-ray production: particles are accelerated at the reconnection region, the proton spectrum softens in time as the turbulence weakens, and the γ-ray spectrum softens accordingly, as observed. An alternative possibility is to associate the flare with a Coronal Mass Ejection (CME). During these powerful eruptions, huge disturbances in the coronal magnetic fields release vast quantities of plasma into space; the shock in a CME is known to accelerate particles, at times above the 300 MeV required for pion production. In this scenario the predicted γ-ray flux would be too low, due mainly to the low density at the CME site: energetic particles must be transported to high-density regions below the corona by a field line connecting the two regions; the time scale sets the distance to ~ 0.4 A.U.

On 2013 August 11, $> 100\,\mathrm{MeV}$ emission from a solar flare was observed for $\sim 30'$, and the direction of the incoming γ rays matched the flaring region location. Surprisingly, the active region of the Sun's surface responsible for the flare was located behind the solar limb. In order to explain the LAT observation, localization of the site of γ-ray production (either in the corona or in the photosphere) will put stringent constraints on the flaring process (paper in preparation).

Flaring episodes aside, the quiescent Sun is a steady γ-ray emitter due to the interactions of hadronic CRs in its upper strata; in addition, IC scattering of the solar photon flux is observable given the LAT sensitivity [55]. The flux from the solar disk depends on the ambient CR proton spectrum in the immediate proximity of the solar atmosphere, in contrast to the solar IC emission, which is produced by electrons in a considerable part of the heliosphere and integrated along the line of sight. The LAT predecessor EGRET detected unresolved emission from the Sun, and a reanalysis of the original dataset in 2008 [56] separated the two emission components.

Given the LAT sensitivity and angular resolution, the Sun is a moderately bright, extended source moving across the sky at approximately 1°/day. As it is the case for the other Solar System objects, this large proper motion requires the use of special tools to work in a frame centered on the Sun. The approach to the background estimate is also unique: in the "fake-Sun" approach, a background model is derived by rebinning the LAT data around a fictitious source following the Sun along the ecliptic but offset by a large angle. Since emission is expected to be observable above backgrounds within $\sim 20^\circ$, in [55] several fake Suns were placed spaced by 40° along the ecliptic. All background estimates are essentially featureless, and they agree within a fraction of a percent, and are consistent with backgrounds as derived by an all-sky simulation of all LAT sources, including Galactic and isotropic diffuse components.

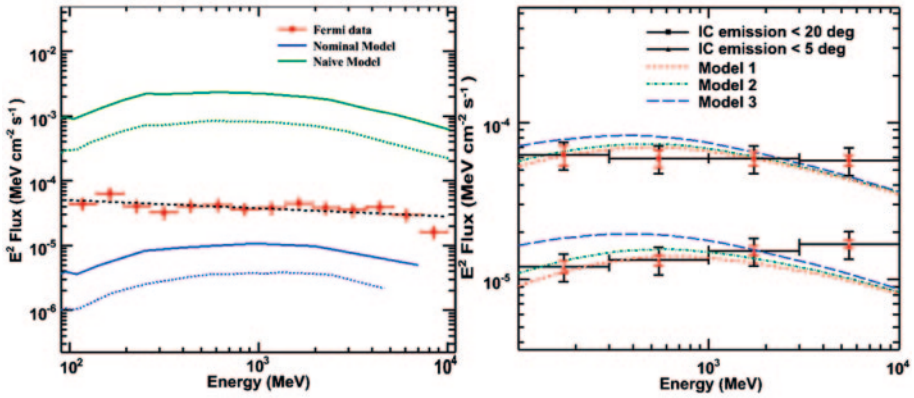

Fig. 6. – Energy spectra for the solar emission, from [55]. Left: spectrum of the disk emission, compared with model predictions; solid and dotted lines are calculated under different assumptions about CR cascade development in the solar atmosphere. Right: IC emission for elongation radii $< 5^\circ$ and $< 20^\circ$, compared with model predictions.

The solar γ-ray emission can be divided in a model-independent way in two components: a point-like one (the $\sim 0.^\circ 5$ disk is not resolvable) and an extended halo. The energy spectrum of the point-source component is shown in fig. 6, left: it is compatible with a simple power-law spectrum with index 2.11 ± 0.73 and intermediate between the two models described in [57]. It must be remarked that calculation of the disk emission relies on assumptions about CR transport in the inner heliosphere and in the immediate vicinity of the Sun, thus allowing for a broad range of models. The accurate measurements of the disk spectrum by the *Fermi*-LAT thus provides precious insights on the CR cascade development in the solar atmosphere. The spectrum of the extended component is shown in fig. 6, right, integrated within two elongation radii, $< 5^\circ$ and $< 20^\circ$. Here uncertainties are large, and none of the models in [57] is favored. Again, a single power law with index ~ 2 fits well.

Interestingly, the intensity of the IC component is found to be comparable to the intensity of the isotropic γ-ray background for relatively large elongation angles. Integrated for subtended angles $< 5^\circ$ above 100 MeV the former compares to about half of the flux of the isotropic template, while for subtended angles $< 20^\circ$ the flux of the IC component is still approximately one sixth of the isotropic emission. Therefore, it is important to take into account the broad non-uniform IC component of the solar emission when analyzing weak sources near the ecliptic. In addition, the relative importance of the IC component is bound to increase with time as more sources are discovered and removed from the isotropic template.

4·5. *Moon.* – The Moon emits γ rays due to the interaction of CRs on the lunar surface. The Moon enjoys a rare distinction, being one of the few extraterrestrial bodies of which we have surface samples: the composition of the regolite is well studied, and since the local CR spectrum is also well measured, observation of the lunar emission provides a good test of our model calculations. The spectrum is predicted to be steep, with a cutoff around 3–4 GeV, and, excitingly, a narrow pion decay line is expected at 67.5 MeV [58].

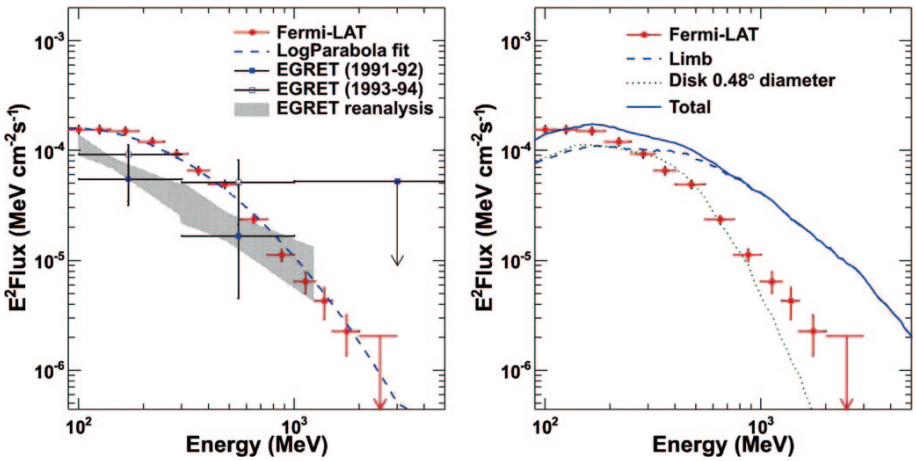

Fig. 7. – Left: γ-ray spectra for the Moon as observed by the *Fermi*-LAT, compared with EGRET measurements, in particular with the 2008 reanalysis in [56]. Right: comparison of the *Fermi*-LAT observed spectrum with the models in [58]. From [59].

EGRET detected the lunar emission in the years 1991-1994, in correspondence of a period of relatively high solar activity: later reanalysis of the EGRET data yielded a flux of $(5.55 \pm 0.65) \times 10^{-7}\,\mathrm{cm}^{-2}\,\mathrm{s}^{-1}$ above 100 MeV [56]. As in the case of the Sun, the observation of the Moon is complicated by its large proper motion ($\sim 13^\circ$ per day) and by the parallax due to the *Fermi*-LAT orbit ($\sim 0.6^\circ$ per orbit); the tools and analysis techniques described for the solar analysis are necessary. *Fermi*-LAT reported the measurement of the lunar emission after 2 years of data taking, hence covering the interval from 2008 August to 2010 August, corresponding to a deep solar minimum. Since the amount of Galactic CRs in the heliosphere is anti-correlated to the intensity of the solar wind, an enhanced lunar γ-ray emission was expected. Indeed *Fermi*-LAT reported a flux of $(1.04 \pm 0.10) \times 10^{-6}\,\mathrm{cm}^{-2}\,\mathrm{s}^{-1}$ [59], where we quote the systematic error, the statistical uncertainty being an order of magnitude smaller.

The observed spectrum is shown in fig. 7, left: a simple log-parabola curve is a good fit; EGRET measurements are superimposed even if, as discussed, they are not directly comparable due to the different primary CR spectrum. In fig. 7, right, the LAT measurement is compared with the calculation of the lunar γ-ray emission in [58]. It is remarkable that the limb emission, expected to be much brighter than the softer disk component (as happens for the Earth emission) appears instead to be negligible. In [59] this discrepancy is attributed to the roughness of the Moon surface, neglected in the simulations. Tantalizingly, the *Fermi*-LAT spectrum is derived above 100 MeV, due to the relatively large systematic uncertainties below such energy in the "Pass 7" dataset. A future paper, making use of the improved "Pass 8" event analysis, will have to address the existence of the pion decay line at 67.5 MeV.

4˙6. *Other Solar System bodies*. – Other Solar System bodies (planets, asteroids) emit γ rays via the same process as Earth and Moon, but no detection by *Fermi*-LAT was reported. Simply scaling the solar emission to the distance and size of Jupiter indicates that such emission is probably below the LAT sensitivity.

5. – The Milky Way

5˙1. *Diffuse emission from the interstellar medium.* – At *Fermi*-LAT energies, diffuse γ-ray emission from the Milky Way dominates the sky: above 50 MeV its intensity averaged over the sky is 5 times greater than the intensity produced by resolved sources. This abundant high-energy interstellar emission is produced by the interaction of energetic CRs with interstellar nucleons and photons: decay of secondary particles produced in hadron collisions, IC scattering of the interstellar radiation field and bremsstrahlung emission in the interstellar medium are the main contributors. Clearly the Galactic diffuse emission is a bright and structured foreground for detecting and characterizing point sources. On the other hand, observation of the γ-ray diffuse emission allows investigating both the population of energetic CRs and the density of interstellar matter and radiation across the Galaxy; the former in particular can otherwise be inferred only for leptons, through radio and synchrotron emission.

The amount of Galactic gas along a given line of sight can be derived by tracing emission of the various components at other wavelengths. Atomic hydrogen (H I) is mapped by the 21 cm hyperfine line: it extends out to 30 kpc from the Galactic center, with a maximum surface density of about $4M_\odot\,\mathrm{pc}^{-2}$ at $R = 7$–12 kpc and a characteristic thickness of 1–1.5 kpc from the Galactic plane. Molecular hydrogen (H_2) totals up to roughly the same amount as H I ($\sim 10^9 M_\odot$) but it is concentrated in dense clouds (density $\sim 10^3$–10^4 atoms/cm^3 and mass 10^4–$10^6 M_\odot$) within 10 kpc from the Galactic Center with a peak around 5 kpc. While H_2 cannot be traced directly at interstellar conditions, the dense clouds contain other suitable molecules, such as CO, traced at 2.6 mm (even though the derivation of H_2 density from CO emission is not exactly straightforward). Ionized hydrogen gas (H II) can be traced in many ways, *e.g.* thanks to the H_α line at 656 nm, and is abundant around massive O and B stellar complexes where the powerful stellar ultraviolet fields can ionize the surrounding gas. Notably, most tracers provide both density and velocity information. Making use of a rotation curve of the Galaxy the velocity estimate can be converted into a distance measurement. There will be simpler and more complex regions, *e.g.* looking along lines of sight in the Galactic plane within 90° of the Galactic Center a rotational speed could correspond to different distance estimates, but the distance from the Galactic Center is uniquely determined by the line-of-sight velocity (measured from the Doppler shifts of the 21 cm and 2.6 mm lines).

CO and H I have been known to not completely trace the neutral interstellar medium. An excess γ-ray brightness, relative to what is expected from the gas traced by CO and H I has been correlated with excess reddening, *i.e.*, regions for which the $E(B-V)$ reddening is not completely linearly correlated with CO and H I. Many LAT measurements confirm this and indicate this emission has the same spectrum as the H I component, pointing to a similar origin, namely CR interacting with gas. The unaccounted target mass can total up as much as to 50% of the molecular mass traced through CO. There are several possible explanations for this amount of gas not accounted for by conventional tracers: *e.g.* in the presence of high radiation fields CO dissociates more easily than H_2. The column density of dust is usually estimated by the reddening of starlight: the infrared and microwave emission of stars in a region are compared with unabsorbed counterparts of the same spectral band. The value is then scaled to equivalent reddening in the B and V bands (4300 and 5500 Å respectively), where the selective extinction $E(B-V)$) is taken to be proportional to the dust column density [60]; likewise E(B-V)) provides no distance information.

The interstellar radiation field comprises starlight, emission from dust particles and CMB; precise measurements of the radiation spectrum from IRAS, COBE and Planck are available. In contrast to the emission components associated with gas density there is no simple map or template approach to the IC emission: the emission skymap must be calculated with numerical codes. Several models for the CR diffusion in the Galaxy exist, and recently codes solving the propagation equation numerically have appeared, *e.g.* GALPROP [61]. Nonetheless, a wide range of parameters, such as local particle fluxes, must be adjusted to try and obtain the observed emission, species' abundances, etc. Several models are discussed in [60].

An all-sky maximum-likelihood fit is used to determine the intensities of the various components, including gas mass and IC templates, fluxes and spectra of the point sources from the *Fermi*-LAT catalog, and the intensity and spectrum of an isotropic background (including residual CRs that were misclassified as γ rays, see sect. **3**˙5). Excesses or deficits are found when comparing the model to *Fermi*-LAT observations. These depend on the assumptions made, namely that the CR flux is uniform within bins of galactocentric radius, the distribution of CR sources used to derive the IC intensity is axisymmetric, the uniform spin temperature for optical depth corrections for H I column densities, not accounting for H I self absorption, the linear relation between $W(\mathrm{CO})$ and $N(\mathrm{H_2})$, and the validity of the interstellar radiation field model. A large excess of γ rays associated with the Loop I giant radio continuum loop and two hard-spectrum lobe-shaped excesses extending North and South from the direction of the Galactic center (*Fermi* Bubbles, see sect. **5**˙4) were for example observed in the residuals after subtracting the model. There is no accurate *a priori* template for the γ-ray emission of those large structures; so they are usually modeled with the radio continuum emission and with *ad hoc* patches of spatially uniform intensity, to derive the gas emissivities and IC renormalization. In addition, a map of the residual intensity of the Earth limb γ-ray flux that is not removed from the data by a zenith angle cut is important below 200 MeV.

Remarkably, a diffuse excess at GeV energies is observed in the direction of the Galactic Center, a discussion and a review of some possible origins are presented in sect. **7**˙1.2.

5˙2. *Probing the CR content in the Galaxy.* – Given the information on the local CR species made available by the current experiments, and given the wealth of data provided by *Fermi*-LAT, which can be used to infer CR densities all around the Galaxy, a new era of precise measurements of CR and Galactic gas properties has begun.

The typical LAT analysis of a portion of the Galaxy proceeds as follows: H density maps are obtained by separately binning the H I, $\mathrm{H_2}$, H II maps as a function of the galactocentric radius, and deriving the dark gas components by correlating $E(B-V)$) with $N(\mathrm{H\,I})$ and $W(\mathrm{CO})$. Point sources and an isotropic term are added to the model and everything is fitted to the observed γ-ray emission in a given narrow energy band with the *Fermi* Science Tools. We note that this procedure relies on the different components of the interstellar emission model having different distributions on the sky, and therefore as we move toward the low end of the LAT energy range the decreasing angular resolution makes the fit more difficult. Once local γ-ray emissivity per Hydrogen atom are estimated, to translate these into a CR density measurement nuclear production models are required; on the other hand, the emissivity per H atom can be compared in a model-independent way: in fig. 8 a comparison of *Fermi*-LAT observations is shown. γ-ray emissivity is derived at intermediate latitude, so as to depend mainly on the local (closer than $\sim 2\,\mathrm{kpc}$) abundance of CRs, for regions covering the entire sky: the agreement is remarkable, indicating a similar CR spectrum in all directions around the Earth.

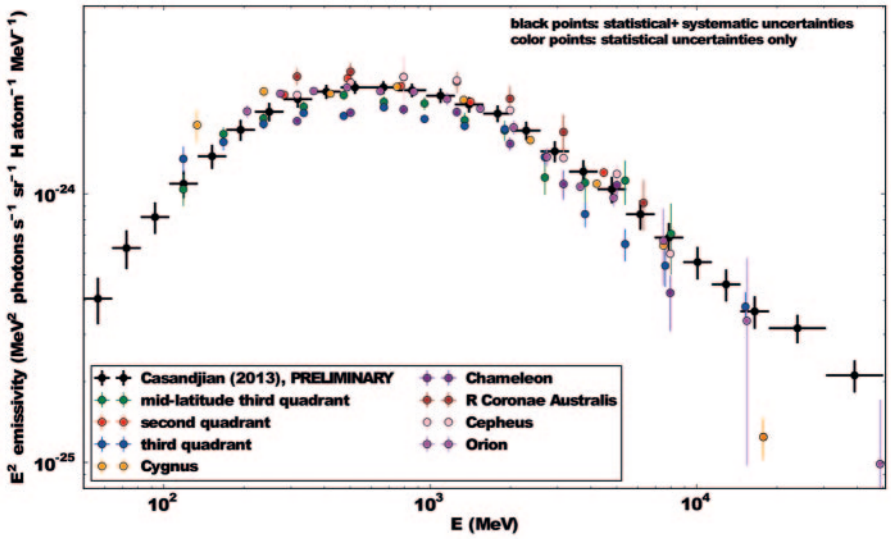

Fig. 8. – *Fermi*-LAT γ-ray emissivity per H atom in the local interstellar space, as measured for the whole sky at intermediate Galactic latitudes; from [62].

To quote one outstanding issue, let us discuss the so-called *gradient problem*. One input of any CR diffusion model is the distribution across the Galaxy of CR sources. All estimates of CR source densities agree on a decrease beyond the solar circle; in spite of this, the γ-ray emissivity is observed to be approximately constant beyond a galactocentric radius of $\sim 10\,\mathrm{kpc}$. One way to reconcile the model predictions with this is to increase the thickness of the Galactic halo in which CRs propagate (see fig. 9, left). On the other hand, the locally measured isotopic abundances limit the halo thickness to a maximum $z \sim 10\,\mathrm{kpc}$. Assuming the commonly assumed pre-*Fermi* value of $z = 4\,\mathrm{kpc}$, one would need a flat CR source density beyond the solar circle (fig. 9, right). Currently no tentative explanation for this inconsistency appears to agree with all observations.

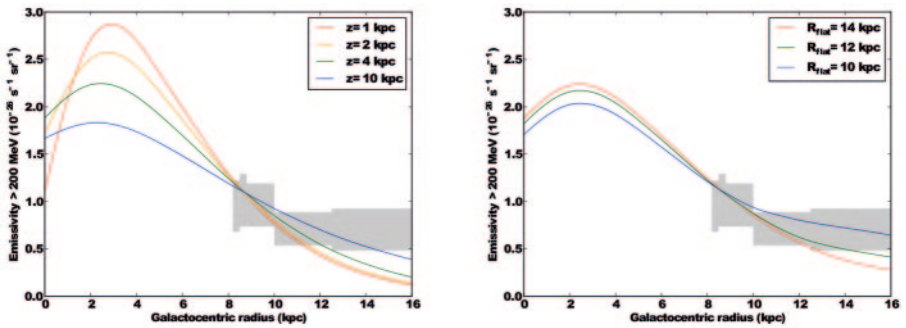

Fig. 9. – *Fermi*-LAT γ-ray emissivities ($> 200\,\mathrm{MeV}$) as a function of galactocentric radius, compared with model predictions as a function of the height of the CR propagation halo (left) and of a radius beyond which CR source density is assumed constant (right). From [62].

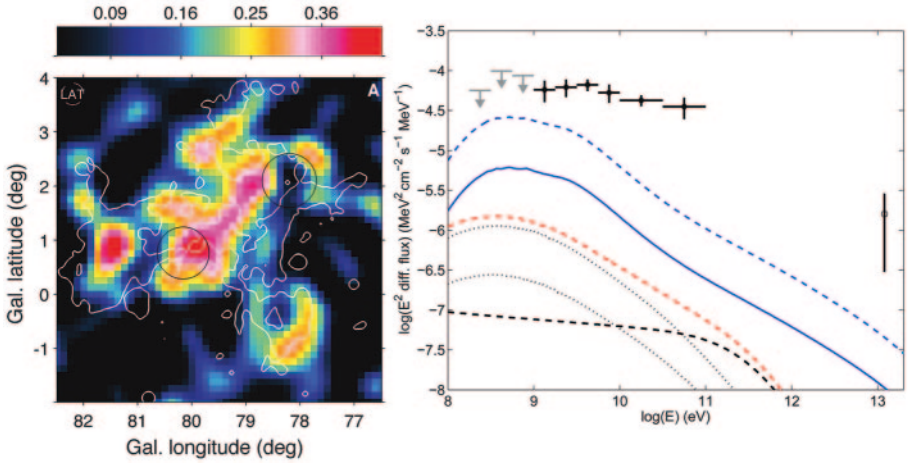

Fig. 10. – Left: γ-ray photon count map from in the Cygnus region, once all known astrophysical sources and the isotropic background are removed; overlaid 8 μm intensity contours. Right: spectrum of the emission from the Cocoon, including to the far right the estimate derived from Milagro observations, compared to emission models assuming local CR spectrum. The blue curves show the expectations from the Local CR spectrum pervading the ionized gas for different electron densities: $10\,\mathrm{cm}^{-3}$ (solid) and $2\,\mathrm{cm}^{-3}$ (dashed). The black curves give the expectations from the Local CR electron spectrum up-scattering the stellar light from Cyg OB2 (upper dotted curve) and NGC 6910 (lower dotted curve), and the interstellar radiation present in the cavity and photon-dominated regions (dashed curve). The red curve sums all IC emissions. From [63].

5˙3. *Star-forming regions*. – From isotopic abundances, roughly 80% of Galactic CRs have the same composition as Solar System material, with the remaining 20% being synthetized by Wolf-Rayet (WR) stars [6]. CRs then require a turbulent medium in which they are confined and re-accelerated in shock waves. WR stars are the evolutionary product of OB stars, which exist in OB associations that are forming superbubbles. These star-forming regions are a natural place to look for young CRs being accelerated before they are released into the Galactic medium.

Cygnus X is located at $\sim 1.5\,\mathrm{kpc}$ from the Solar System distance. It is associated with one of the largest known molecular clouds and it contains several massive-star associations. Inside it, the powerful stellar winds have rearranged the surrounding material creating low-density cavities; the compressed edges of these bubbles can be observed in infrared. *Fermi*-LAT observations reveal a complex region, including the presence of pulsars and SNRs (including γ-Cygni) [63]. Diffuse γ-ray emission in the 0.1–100 GeV range indicates that within 20% the average local CR flux and spectrum is consistent with the one in the Solar neighborood. Once the backgrounds are subtracted, a residual emission remains, clearly observed above 1 GeV up to 100 GeV (see fig. 10, left). The estimated local CR intensity and the target gas mass, derived by measuring the bremsstrahlung emission of the ionized gas, are inconsistent with the hardness of the observed γ-ray spectrum: an additional hard CR component is necessary, pointing to freshly accelerated particles filling the cloud cavities. As seen in fig. 10, right, the observed γ-ray spectrum cannot be reconciled with the local CR spectrum, even freely varying the target mass density. The nature of the accelerating source remains uncertain: both the Cyg OB2 star complex and the γ-Cygni SNR are plausible candidates.

5˙4. *The Fermi bubbles*. – The center of a galaxy is often home to energetic activity, and our Galaxy is no exception. In particular, a residual microwave signature was observed by WMAP when synchrotron, bremsstrahlung, thermal and spinning dust and CMB components were subtracted from the observed emission [64]. This extended component, with no significant associated X-ray emission and no structure in Hα maps, is consistent with a weak synchrotron radiation from a hard-spectrum CR electron population, as well as DM annihilation scenarios. The search for counterparts in other wavelengths led to the discovery of a large-scale high-energy feature in the *Fermi*-LAT skymap [65-67]. Labeled "*Fermi* bubbles", these structures extend 55° above and below the Galactic Center. While this can be a chance alignment, the nice symmetry of the emission lobes counterindicates alternative associations with nearby regions in the foreground of the Galactic core. If indeed centered on the Galactic core, the vertical size can be inferred to be about 10 kpc. Differently from a central haze, the bubbles have a sharp edge and relatively large luminosity at high latitudes. What is perhaps the most striking feature of this new source of γ rays is the clear signature that appears in the *Fermi* skymap: the lobes can be clearly seen directly in high-energy LAT count maps.

A dedicated study of the morphology and of the spectral properties of the bubbles can be found in [68]. The spectrum of the γ-ray emission is approximately E^{-2}, with a clear cutoff above ~ 100 GeV, and no variation of the spectral shape can be observed across the bubbles' surface. As is often the case, both IC and hadronic models (including secondary IC emission) fit the γ-ray counts well. The leptonic model has the advantage that target photons at high latitude are abundant, but to transport energetic leptons across such distances before cooling implies supersonic speed and hence would imply formation of shocks, which are not observed neither as synchrotron emission nor as ionization emission lines. The hadronic model has the advantage in terms of both cooling requirements and lack of secondary emission, but the density of target gas at high latitude is small, and one has to assume some means of effective CR entrapment to produce such a bright emission. In the hadronic model the bubbles are formed by SN explosions in the Galactic plane, and structures in the Galactic magnetic field can account for the sharp edges. In the leptonic model the bubbles can be powered from several kinds of outflows from the Galactic Center: a jet-like phenomenon, strong stellar wind from star formation in the bulge, outflow from the black hole, etc. Observation of a jet structure would be a way to settle the issue, but such claims currently cannot be confirmed.

5˙5. *Pulsars*. – CGRO detected 7 pulsars in γ rays (1 MSP), folding the signals into the pulsar rotational phase using radio ephemerides and observing emission peaks at given phase angles (an additional 3 marginal detections were reported). Besides this radio-informed search, an alternative is to search for pulsation in the γ-ray signal itself ("blind search"): this requires high computational resources to scan the vast allowed parameter space (2 orders of magnitude in period, 6 in period derivative for normal pulsars); MSPs, which are commonly in binary systems, have additional complications due to the orbital parameters (orbital period, projected eccentricity and position uncertainty). *Fermi*-LAT employed both approaches: known radio and X-ray pulsars were searched for pulsed signal at γ-ray energies, and a blind search campaign was launched to look for radio-quiet pulsars. To limit the sample of blind search candidates, "pulsar-like" objects were selected, characterized by low flux variability and curved spectra. All pulsars are actually characterized by hard spectra ($1 < \gamma < 2$) with an exponential cutoff in the few GeV range. The *Fermi*-LAT localization capabilities are more than adequate: $10'$ localization

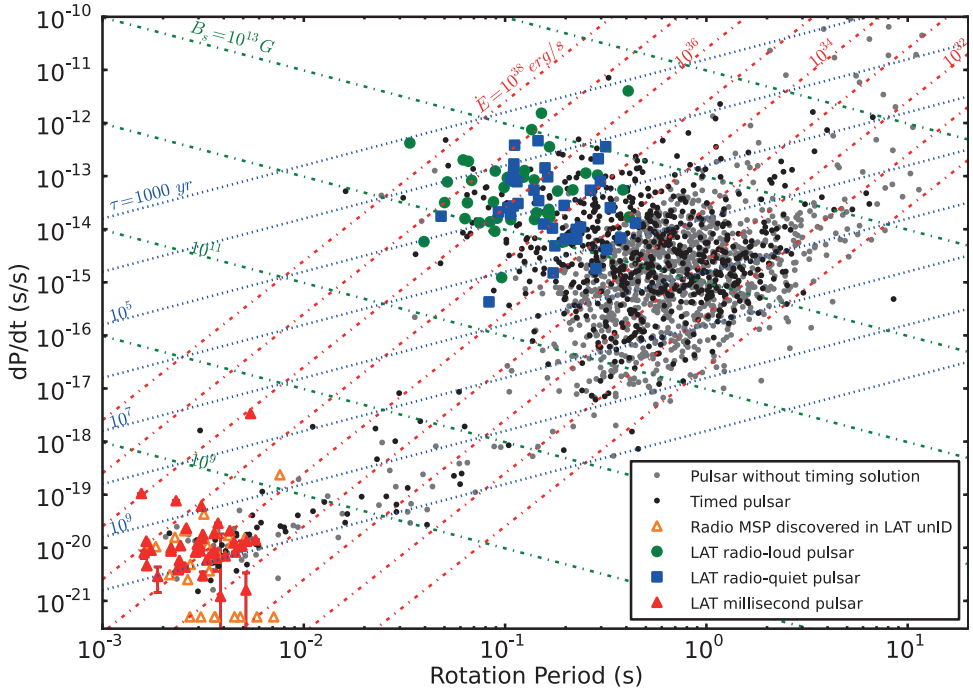

Fig. 11. – Pulsar spindown rate *vs.* period for sources in the second LAT pulsar catalog, from [69]. The picture includes radio MSPs discovered at the positions of previously unassociated LAT sources for which we have not (yet) seen γ-ray pulsations (open triangles); for a few $\mathrm{d}P/\mathrm{d}t$ is unavailable.

is comparable to radio telescope beams. Moreover, suitable unidentified sources were the targets of dedicated radio programs, yielding an unexpected trove of MSPs, many of which were later detected as γ-ray pulsars.

As of 2014 August, 45 radio- and X-ray "normal" pulsars are seen pulsing at γ-ray energies, and 40 additional sources were detected by the γ-ray pulsation alone. Sixty-one radio-selected MSPs and one γ-ray-selected MSP complete the picture [69]. The latter features the shortest known binary orbital period of all pulsars: 93 min; a follow-up radio observation detected the pulsation [70], thus reversing the conventional order of detection. The blind search for MSPs in the Galactic disk was a great success [71]: more than 1/4 of currently known MSPs in the Galactic disk were identified by the LAT.

In fig. 11 spindown rate *vs.* rotational period is shown for the 117 pulsars in [69]. The normal (top right) and MSP (bottom left) populations can be easily separated. The energy loss isocurves emphasize how this is a sensitivity-limited sample, where detected pulsars lie in the part of the plane corresponding to high energy loss. Among the 514 LAT sources detected above 10 GeV in 3 years, 27 are associated with pulsars; of these 20(12) have significant pulsation above 10(25) GeV [72]. This finding (preceded by Čerenkov detections of pulsations in the Crab at very high energies) indicates that the spectrum cannot actually be exponentially cut off.

With ~ 100 young and middle-aged pulsars having been detected, often with enough statistics to build detailed spectra and light curves, it is now possible to discriminate

between the emission geometry models based on a significant sample of the source population. Many works address the issue by correlating the observations with simulations of the emission geometry with full-scale radiation models. *E.g.* in [73] the *Fermi*-LAT light curves for the sources in [69] are analyzed, including information from the radio emission profiles when available. In general, none of the assumed emission geometries can explain the variety of the LAT sample. The outer magnetosphere models, slot gap, outer gap and one pole caustic (see sect. **2**˙2) seem to best describe the observed LAT pulsar light curves. First of all polar models describe a larger gap region, with broad emission peaks in the folded lightcurve, which are not observed. This geometrical trend concurs with the absence in most (but not all) of the LAT pulsars of a super-exponential cut-off in their spectra, as expected for a polar cap origin of the high-energy beam near the neutron star surface due to γ-B absorption. On the other hand, the fact that none of the assumed emission geometries is able to explain all the observed light curves suggests that the γ-ray emission may be a combination of slot- and outer gap models, and that the observed features are dependent on viewing angle. It is reassuring that while the individual pulsar estimates can change according to the fitting strategy used, the collective properties of the LAT pulsar population are robust.

A similar abundance of MSP pulsars (~ 40) is providing input to population studies. *E.g.* in [74] a greater variety of light curve morphology than the young γ-ray pulsars is derived for MSP. While most MSP light curves are similar to those of young pulsars, showing the correlation of increasing radio lag with decreasing γ-ray peak separation, a much larger number show phase alignment of radio and γ-ray peaks and a new phenomenon, γ-ray peaks leading the radio peaks, not observed in the young pulsar population. MSP light curves resembling those of young γ-ray pulsars are indeed well fit by the narrow gap models that best describe young pulsars. MSP light curves in which the γ-ray peaks lead the radio peak(s) are better fitted with polar cap models where γ-ray emission occurs over the whole open-field volume and the observed early phase is due to relativistic aberration.

Glitches are historically observed in radio pulsars: in such occurrences there is a sudden increase in the spin rate, typically accompanied by a sudden increase in the spin-down rate; the glitch is followed by a transient phase of exponential recovery (on time scales varying from minutes to weeks). Glitches are very likely to occur in the young population of LAT pulsars, and several were indeed observed. Early γ-ray observations suggested glitch-associated pulse and flux changes in the Crab and Vela pulsars, but remained unconfirmed by additional observations, until *Fermi*-LAT reported a variation in the γ-ray flux in radio-quiet J2021+4026 [75]. AGILE had reported variability in 1AGL J2022+4032, positionally coincident with J2021+4026 between 2007 and 2009, concluding that it was more likely due to another source along the line of sight [76]. In 2011 October the *Fermi*-LAT flux above 100 MeV suddenly varied over a time scale shorter than a week, decreasing by $\sim 20\%$ with high significance; simultaneously, the frequency spin-down rate increased by $\sim 4\%$ (at 3σ). Significant changes in the pulse profile and marginal changes in the emission spectrum occurred at the same time. There is also evidence for a small, steady flux increase over the preceding 3 years. In [75] the jump of J2021+4026 is tentatively attributed to a shift in the magnetic field structure; if the slow variation in the pulsar flux before the jump is substantiated by additional study, this might plausibly be associated with a more gradual change in geometry preceding the glitch.

An analysis of *Fermi*-LAT data from 13 globular clusters has revealed 8 significant, point-like and steady γ-ray sources that are spatially consistent with the locations of

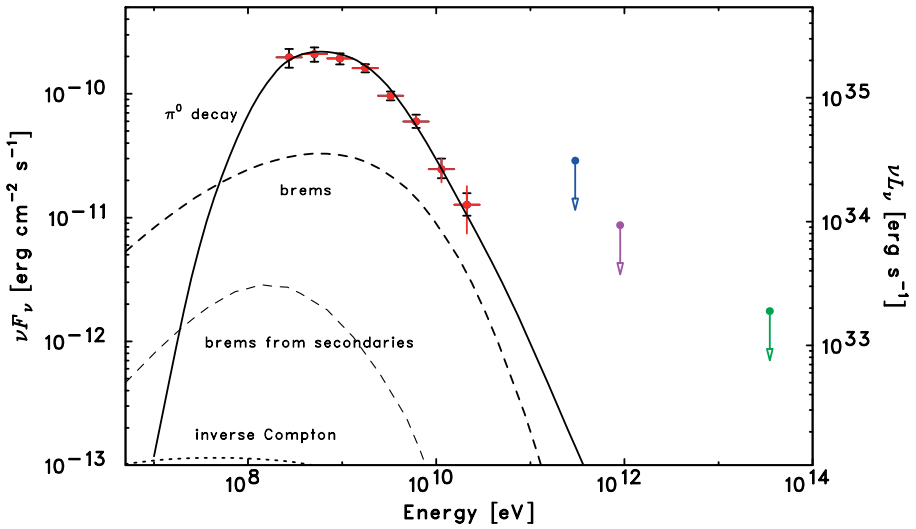

Fig. 12. – W44 spectrum, from [78]. Crosses: *Fermi*-LAT measurement, upper limits from left to right: Whipple, HEGRA, Milagro.

the clusters. Five of them (47 Tuc, Omega Cen, NGC 6388, Terzan 5, and M 28) show hard spectral power-law indexes ($0.7 < \gamma < 1.4$) and clear evidence for an exponential cut-off in the range 1.0–2.6 GeV, which is the characteristic signature of magnetospheric emission from MSPs [77]. Three of them (M 62, NGC 6440 and NGC 6652) also show hard spectral indexes, however the presence of an exponential cutoff cannot unambiguously be established. From the observed γ-ray luminosities the total MSP populations amount to tens to few hundreds in these clusters, in agreement with theoretical predictions.

5˙6. *Supernova remnants*. – *Fermi*-LAT has detected several SNRs, and has provided evidence of both leptonic and hadronic acceleration.

The characteristics of γ-ray emission from SNRs interacting with molecular clouds, such as W44 (see fig. 12) [78] and IC 443 [79], clearly favor hadronic models. In such bright SNRs the sharp decrease in flux with decreasing energy around 100 MeV indicates pion origin, caused by accelerated protons colliding with the dense ($\sim 100\,\mathrm{cm}^{-3}$) medium of the molecular cloud.

In particular, W44 is an interesting example of the amount of information that can be inferred about CR interaction with molecular clouds. Significant emission is detected by the *Fermi*-LAT above the local Galactic and isotropic backgrounds. If the source morphology is assumed to be consistent with the radio synchrotron map of W44, the SNR emission can be included in the background model and subtracted. After this step two regions of excess γ-ray emission become evident, just outside the radio map contours [80]; the residual peak count rate is about 1/10 of the removed SNR contribution. These two hot spots are coincident with the molecular cloud complex surrounding W44, as observed in CO maps (see sect. **5**˙1). Explaining such enhanced emission in terms of an imperfect molecular column density estimate from CO maps would imply a factor > 5 underestimate of the interstellar gas mass, or the presence of untraced gas of at least $\sim 10^6 M_\odot$. A local excess of CR is a more viable solution; this would imply CRs are escaping the W44 SNR and interact with the nearby molecular clouds: the energetics

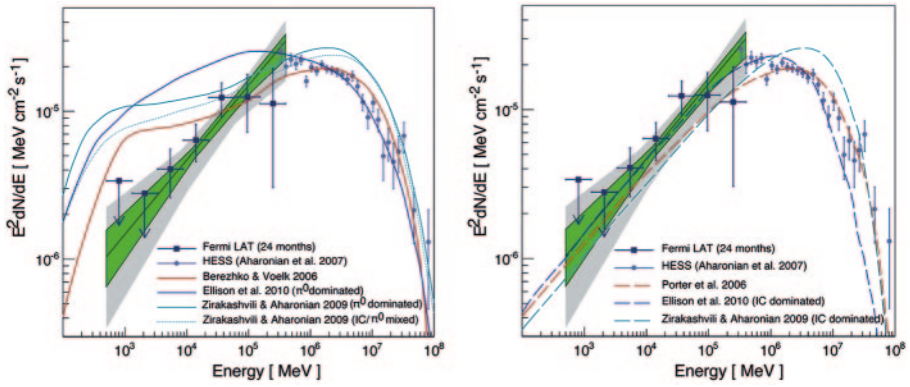

Fig. 13. – RX J1713.7−3946 spectrum, from [81]. Left: comparison with hadronic model, right: leptonic model.

of this process provide an estimate of the total amount of energy converted into CRs of the order of $(0.3\text{–}3) \times 10^{50}$ erg, in good agreement with the value of $\sim 0.4 \times 10^{50}$ erg corresponding to the total kinetic energy of protons in the SNR.

Cas A [82] is a much younger and fainter SNR, with no interaction with a molecular cloud. The spectral signature still indicates hadronic acceleration; the target proton density being much lower than in the previous cases the γ-ray flux is correspondingly 10 times lower.

The spectrum of RX J1713.7−3946 [81] is clearly different, and compatible with purely leptonic emission due to inverse Compton scattering (see fig. 13). For this second young and faint SNR, though, the dominant leptonic emission does not imply scarcity of accelerated protons. Indeed, since there is no interaction with a nearby molecular cloud, the target density is necessarily small: to explain the observed thermal X-ray component in terms of a hadronic model the derived target gas density would be only $\leq 0.2\,\mathrm{cm}^{-3}$, several hundred times less than what is usually assumed for W44. In [81] the upper limit on the accelerated proton population is derived and found to be consistent with the estimates for W44.

As the discriminating factor between leptonic and hadronic models is given by the observed flux in the lowest part of the LAT energy range, expectations are for significant advances with the *Pass 8* upgrade: a factor 2 in the sensitivity around and below 100 MeV would imply a significant advance in the discriminating capabilities of the LAT observations.

The Crab SNR historically has been used as a standard candle for high-energy γ-ray instruments, *e.g.* Čerenkov telescope sensitivities are usually quoted in terms of fractions of the Crab flux per observation time. In 2010 September AGILE reported a flare, and a previous episode in 2007 October, before *Fermi*-LAT observations, was also announced [83]. *Fermi*-LAT reported two flaring events, 2009 February and the 2010 September one [84]. The flux above 100 MHz varied by a factor 4 and 6 respectively, in a time scale of 16 and 4 days respectively, see fig. 14; the pulsar γ-ray emission in the same time intervals show no variation. Spectral analysis shows a variation in the synchrotron component of the plerion emission, remarkably with no significant correlated variation at IR and X-ray energies. The brevity of the γ-ray flares is in clear agreement with this: if the flare were instead produced by IC radiation or Bremsstrahlung, the cooling time of

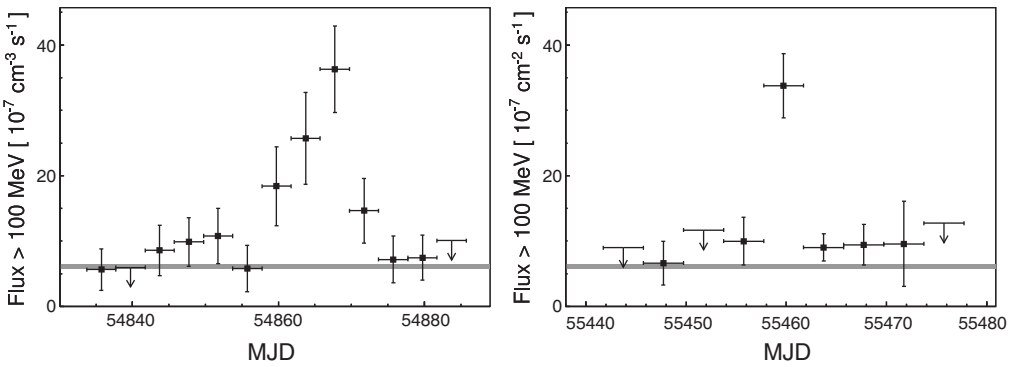

Fig. 14. – γ-ray flux above 100 MeV for the synchrotron component of the Crab nebula, in 4-day time bins for 2009 February and September 2010; from [84]. The gray band indicates the average flux measured over the entire period.

the emitting electrons given the particle densities in the SNR would greatly exceed the flare duration ($> 10^6$ y), while synchrotron cooling time based on the estimated magnetic field in the nebula is in good agreement (less than ~ 15 days). Incidentally, the detection of synchrotron photons at energies > 1 GeV implies that electrons are accelerated to energies ≥ 1 PeV in the nebula; this poses serious challenges to particle acceleration theories, especially since synchrotron losses are very efficient.

5·7. *High-Mass Binaries.* – X-ray binaries (XRBs) are interacting binaries where matter from a donor star accretes onto the compact partner, either a black hole or a neutron star. Conversion of gravitational energy into radiation by accretion on a compact object is an extremely efficient process: efficiencies in the conversion into X-rays are estimated to be $\sim 10\%$ or more. Microquasars are a subclass, characterized by strong, variable radio emission, often resolved into a pair of relativistic jets. Incidentally, precise determination of the compact object mass in XRBs provides the strongest evidence of the existence of black holes (or at least of stellar objects with mass above any reasonable limit in the neutron star equation of state).

XRBs are usually classified as a function of the donor mass. In low-mass binaries the only way for the donor star to transfer mass to the compact object is by overflow of the Roche limit. Such systems are extremely bright in X-rays, and emission at longer wavelengths is mostly due to reprocessing of the X-ray flux within the accretion flow. In high-mass binaries (HMB), the donor can transfer mass even without overflowing, by means of powerful stellar winds. Such systems are dominated by the optical luminosity of the massive companion ($> 10 M_\odot$). HMBs are short-lived, due to the short lifetime of the massive companion star, and are generally found along the Galactic plane; the short time scales imply that there is no significant evolution of the compact object's magnetic fields, and many HMBs feature an accretion-powered pulsar. For a more detailed review see *e.g.* [85].

γ-ray emission from XRBs is expected in both the case of microquasars and systems containing energetic pulsars. γ-ray emitting binaries can show secular modulation of the flux, due to different conditions at different orbital phases, *e.g.* a smaller or larger separation of the pair. *Fermi*-LAT has observed four XRB systems. Differences in the orbital semi-axes, periastron and apastron distances and orbital plane inclination ensure

that the observed morphology of these systems can vary significantly between each other, so similarities and differences between sources are expected.

Cygnus-X3 is a bright high-mass microquasar known since the 1960s, when the 4.8-hour orbital period was first measured. It is composed of a Wolf-Rayet star and a black hole candidate. The LAT easily detected emission in about one year of data [86], phase-masking the nearby pulsar (J2032+4127) located very close to the system ($\sim 30'$). Orbital modulation is not apparent in the entire dataset, but can be enhanced by restricting the time range to two active periods ($\sim$ 2 months each). The emission region must be away from the accretion disk, to prevent excessive absorption, but within the system, since the orbital modulation is observed; this favors a scenario in which energetic electrons of unknown origin upscatter the abundant UV photons provided by the high-mass companion, and the γ-ray maximum corresponds to a superior conjunction, *i.e.* the compact object is behind the Wolf-Rayet star and electrons hit UV photons head-on towards the observer.

LSI I 61°303 and LS 5039 are high-mass XRB systems, and the former in particular is one of the brightest X-ray sources in the sky. In both cases EGRET detected a positionally coincident source with high significance in the γ-ray band, but the uncertainty radius was too large to claim a firm identification and no variability or periodicity could be established. AGILE confirmed the association of LSI I 61°303, observing it at EGRET flux levels [87], and even the MAGIC, VERITAS and H.E.S.S. Čerenkov observatories reported TeV emission from the two sources. The LAT analysis revealed both sources at high significance [88, 89], with spectra with a marked cutoff at GeV energies (~ 6 GeV and ~ 2.1 GeV for LSI I 61°303 and LS 5039, respectively). Timing analysis confirmed modulation of the flux in correspondence to the orbital period: again the maximum occurs close to superior conjunction, favoring a leptonic interpretation of the emission with upscattering of photons from the companion's solar wind. On the other hand, differences are evident. The binary period of LSI I 61°303 is ~ 26.6 days; flux determination in each of the individual nine orbits covered by LAT data at the time of the analysis revealed a modulation of a factor 3, indicating variation on a scale significantly shorter than the known radio super-orbital period of ~ 4.5 y; no significant variation of the spectral shape from orbit to orbit was observed. Phase-dependent spectroscopy of LS 5039 showed instead anticorrelated intensity and spectral hardness: maximum flux with soft spectrum at superior conjunction, minimum flux with hard spectrum at inferior conjunction; see fig. 15.

Similarly to the pulsar search campaign, the *Fermi*-LAT Collaboration has performed a blind search for orbital modulation in a set of XRB candidates. A strong signature of periodic emission was detected for source 1FGL J1018.6−5856, corresponding to a period $T \sim 16.6$ days [90]. The spectral analysis reveals an exponential cutoff at $E \sim 2.5$ GeV, consistent with values quoted above. A follow-up observation at keV energies with *Swift*-XRT found only one source in the LAT error circle, and confirmed variability at the orbital modulation period. Optical observations permitted identification of an O-type star, very similar to the main sequence member of LS 5039. Remarkably, phase-dependent spectroscopy showed instead an opposite behavior than for LS 5039: for this new candidate XRB the spectrum is harder at maximum.

PSR B1259−63/LS 2883 is a rather peculiar system, composed of a pulsar and a blue Be star on a very eccentric orbit (~ 0.87); radio observations indicate that the pulsar is eclipsed for about 40 days out of 1237 when it goes behind the massive-star companion [91]. An equatorial disk surrounds the star, and the pulsar is believed to cross the disk plane twice each orbit, immediately before and after periastron. The source is

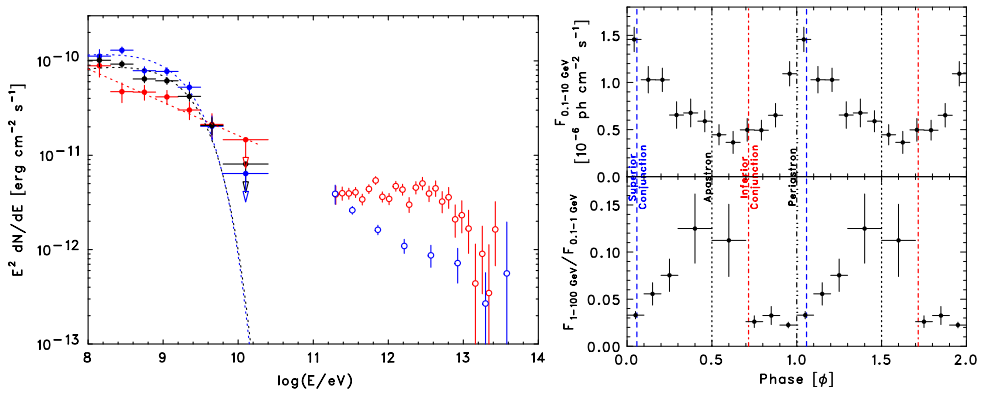

Fig. 15. – Left: LAT data points and fitted spectrum of LS 5039, phase averaged (black), at superior conjunction (blue) and at inferior conjunction; (non-contemporaneous) corresponding H.E.S.S. observations are shown (empty dots). Right: integrated flux (top) and spectral hardness (bottom) *versus* orbital phase. From [89].

thoroughly monitored: *e.g.* H.E.S.S. reported detection at TeV energies at the periastra in 2004, 2007 and 2010–2001, without observing any significant variability [92]. The LAT detected no γ-ray emission before the 2010 periastron; approaching the periastron the source became visible at LAT energies [93]. Unexpectedly, 30 days after periastron γ-ray flux increased over a period of a few days to values 30 times that seen during the pre-periastron period, but with a softer spectrum. For the following month, it was seen to be variable on daily time scales before starting to fade. The total γ-ray luminosity observed during this period is comparable to the spin-down power of the pulsar. Simultaneous radio and X-ray observations of the source showed no corresponding changes in radio and X-ray flux between the pre-periastron and post-periastron flares. While the modulated emission from the system is well known, being attributed to the interaction of the pulsar wind with the stellar wind of the companion star, the flare episode suggested several possible explanations, involving a sudden change in the of the physical conditions of the system, an anisotropy of the γ-ray emission, or the appearance of a new emission component. With no clear indication of a favored scenario, only additional observations can shed some additional light on the process at work in this puzzling source.

5˙8. *Novae*. – In 2010 the LAT observed a γ-ray transient temporally and spatially coincident with a nova, Nova V407 Cyg [94]. Novae take place in binary systems, when mass from a larger star overflows the Roche limit and falls on the companion white dwarf: the hydrogen accretes on the surface of the white dwarf until fusion ignites and blows the material away. This is a relatively minor occurrence: both stars remain intact after the episode. Nova V407 Cyg is a rare recurrent symbiotic nova, in which the companion star is a red giant blowing out a strong stellar wind. A possible explanation of the γ-ray emission is the collision of the fast-moving nova ejecta with the dense stellar wind.

After years of quiet, suggesting the peculiarity and perhaps uniqueness of Nova V407 Cyg, in 2012 June two separate novae were observed by the LAT. Nova V1354 Sco and Nova V959 Mon both emitted a detectable flux at a time corresponding to their optical peaks [95]; indeed Nova V959 Mon was detected in the γ-ray band before its optical counterpart was discovered. Surprisingly, both novae are classical novae, *i.e.* the white

dwarf star companion is a main sequence star. This implies that there is no dense stellar wind like in the case of Nova V407 Cyg. *S*wift X-ray observations showed no corresponding source near Nova V1354 Sco, but did find one in Nova V959 Mon. Both objects were observed at radio frequencies: Nova V959 Mon shows a bipolar structure with optically thick bremsstrahlung emission by energetic electrons [96, 97]; instead only a faint detection of Nova V1354 Sco, which appears to be a fairly standard classical nova, was reported [98].

In 2013 the LAT has detected other classical novae, Nova V339 Del [99], and Nova V1369 Cen [100].

Remarkably all classical Novae are very similar when observed at LAT energies: they show soft spectra that take 3–5 days to rise to the peak, lasting 2–3 days, and then fade over a time scale of 2–3 weeks. Both hadronic and leptonic models can explain the observed emission spectra within statistical uncertainties [101].

6. – Local group and beyond

6˙1. *Star-forming galaxies*. – Star-forming galaxies host kpc-scale regions of intense star-forming activity; their non-thermal emission is interpreted as prevalently diffuse in origin and not tightly linked to the activity of a central engine. In such galaxies, young, massive stars emit most of their energy in the UV band: since UV radiation is efficiently absorbed by interstellar dust and subsequently re-emitted in the IR band, the IR luminosity (in the 8–1000 μm range) is a reliable tracer of star-forming systems [104].

Massive stars rapidly conclude their lives with gravitational collapse, terminating in supernova explosions. The ejected material drives shock waves, which propagate in the interstellar medium creating supernova remnants (see sect. **5**˙6). In addition to enormous IR luminosities, a strong radio continuum emission is usually associated with starbursts: radio synchrotron emission is induced by CR interaction with the interstellar magnetic fields. γ rays are produced by the same CRs via inverse Compton scattering of the interstellar radiation fields, via bremsstrahlung, or via inelastic collisions with ambient gas (through π^0 and $\pi^{\pm}$ decay).

During the EGRET era, the Large Magellanic Cloud was the only external galaxy detected in γ rays, although γ-ray emission was generally predicted for starbursts and suspected to be detectable with EGRET. Nowadays, galaxies whose γ-ray emission is powered by CR interactions are an emerging source class in the *Fermi*-LAT sky survey.

The recent detection of starburst galaxies M82 and NGC 253 at high and very high energies naturally encouraged the study of the other star-forming systems, starting from the most promising γ-ray candidates, namely galaxies with high IR emission and abundant molecular gas. A sample of 69 dwarf, spiral, and luminous and ultraluminous IR galaxies was selected for closer scrutiny [103]: only a few of those have been significantly detected individually, while for the remaining objects flux upper limits have been derived. The analysis revealed that γ-ray luminosity significantly correlates with both the radio continuum luminosity and the total IR luminosity (see fig. 16), confirming that galaxies with significant star-forming activity are more luminous at γ-ray energies than their quiescent relatives. Furthermore, the established relationship between IR luminosity and γ-ray luminosity offers a valuable method to quantify the contribution of such objects to the isotropic diffuse γ-ray background (see sect. **6**˙4).

6˙2. *Active galactic nuclei*. – The extragalactic γ-ray sky is completely dominated by active galaxies, where *active* indicates that a significant fraction of the emitted energy

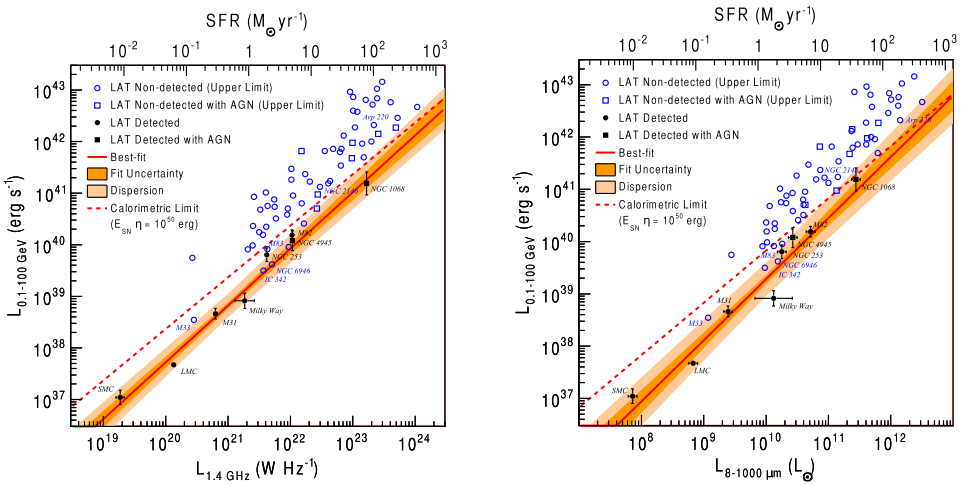

Fig. 16. – Left: γ-ray luminosity (0.1–100 GeV) *versus* radio continuum luminosity at 1.4 GHz. Galaxies significantly detected by the LAT are indicated with filled symbols whereas galaxies with γ-ray flux upper limits (95% confidence level) are marked with open symbols. Galaxies hosting Swift-BAT AGN are shown with square markers. The upper abscissa indicates star-formation rates estimated from the radio continuum luminosity according to [102]; Right: same symbols but with γ-ray luminosity (0.1–100 GeV) plotted *versus* IR luminosity (in the 8–1000 μm band); from [103].

is not linked to the standard components of a galaxy (*i.e.* stars, stellar remnants and the interstellar medium). Every detected active galaxy appears to be powered by a compact region at the core, motivating the common denomination of Active Galactic Nuclei (AGN). The central engine of an AGN is commonly believed to be powered by the infall of matter onto a collapsed object, such as a massive black hole [105].

Among AGNs, blazars constitute a distinct subclass, showing a relativistic jet of plasma oriented at a small angle from the line of sight. Emission from these objects is dominated by the non-thermal radiation in the jet, and it is characterized by clear relativistic beaming effects which dramatically boost the observed photon energies and luminosity.

The typical spectral energy distribution (SED) of blazars shows two broad peaks. The low-frequency emission, from radio to optical or X-rays, is interpreted as synchrotron radiation produced by the high-energy electrons inside the jet. The high-energy emission, peaking in γ rays, can be interpreted as the result of inverse Compton scattering of low-energy photons by the same energetic electrons responsible for the aforementioned synchrotron emission. The seed photons come from the synchrotron emission itself ("synchrotron self-Compton") or are external photons that originate in regions outside the jet ("external Compton").

Observations by EGRET identified blazars as a major class of γ-ray emitters. *Fermi*-LAT enabled the first population studies of AGNs in the γ-ray band, doubling the EGRET sample of 66 objects [13] in the first few months of observations. In fact, the first 3 months of sky survey allowed the identification of 132 bright sources at high galactic latitude $|b| > 10°$ with significance greater than 10σ [12]. The third LAT AGN catalog (3LAC) [14], based on 4 years of data, counts 1591 sources located at high $b > 10°$.

1563 of these are associated with radio-loud (*i.e.* jet-dominated) AGNs: this represents a substantial fraction of the total 3FGL sample (72% of the 2192 $|b| > 10^\circ$ 3FGL sources).

The large majority of these AGNs are blazars, which are historically subdivided into "Flat Spectrum Radio Quasars" (FSRQs) or "BL Lacertae" (BL Lac) objects, depending on the presence or absence, respectively, of emission lines in the optical spectrum. A further classification is based on the position of the synchrotron peak frequency ($\nu^S_{\rm peak}$) in the source rest frame: we distinguish low-energy-peaked BL Lac objects (LSPs) when $\nu^S_{\rm peak}$ is lower than 10^{14} Hz, intermediate-synchrotron-peaked sources (ISPs) when $< \nu_{\rm peak}$ is within 10^{14}–10^{15} Hz, and high-synchrotron-peaked (HSP) whenever $\nu^S_{\rm peak} > 10^{15}$ Hz [106]. 3LAC describes 467 FSRQs, 632 BL Lacs, 460 blazar candidates and 32 non-blazar AGNs (probably misaligned radio-loud AGNs).

6˙2.1. Blazars. The population of blazars detected so far by the *Fermi*-LAT extends to redshift $z = 3.1$. While BL Lacs are preferentially found at relatively low redshift, the distribution having a maximum at $z = 0.3$ and an extended tail at higher redshifts, the number density of FSRQs grows dramatically up to $z \simeq 0.5$–2.0, to decline thereafter [14].

The evolution (*luminosity function*) of the different blazar classes has been the focus of several investigations. Evolution of the source abundance is defined as *positive* when numerical abundance decreases with time (correspondingly, increases with redshift); observations indicate that FSRQs undergo positive evolution, while BL Lacs do not show any clear pattern. In the *Fermi*-LAT sample, FSRQs show a positive evolution [108], up to a redshift cutoff that depends on luminosity. The deficit of FSRQs at lower redshift may be explained by an increasing accretion efficiency in the central engine at later cosmic times, possibly driven by galaxy merging events becoming more common, and by richer environments.

On the other hand, the evolution of BL Lac objects, and their relation to FSRQs, remains matter of debate, with claims of no evolution [109, 110], positive [111] or even negative evolution [112]. Detailed studies of both GeV-detected populations and samples complete up to greater redshifts [107] seem to favor scenarios in which BL Lacs are an accretion-starved end-state of an earlier, merger-driven and gas-rich phase [113, 114]. The increase in the volumetric density of BL Lacs (driven in particular by the high-synchrotron-peaked ones) at the same epoch as the turn off of FSRQs reinforces the idea of a transition from FSRQ to BL Lac, the latter representing the final stage of an FSRQ-like class. The evolution of different luminosity classes, sketched in fig. 17, appears to support this interpretation. This remains an attractive speculation, though, as it relies on several assumptions on critical blazar parameters such as black hole mass, beaming factor and host galaxy environment, and a so more accurate knowledge of these fundamental physical quantities is required.

Even after selection effects are taken into account, observations suggest that BL Lac spectra become softer with increasing luminosity. This effect is not as striking as claimed in some previous works [115], but might still be interpreted in terms of a different accretion regime and disk efficiency([4]), as expected if particles cool faster in luminous objects [116].

([4]) Material falling in nearly circular orbits onto a black hole loses gravitational energy corresponding to a fraction of its rest mass energy during the infall. The lost energy is emitted as an outflow of radiation and particles (and potentially Poynting flux). The efficiency η depends on the fraction of mass inflow $\dot{M}$ converted to radiation $L_{\rm bol}$, $\eta = L_{\rm bol}/\dot{M}c^2$.

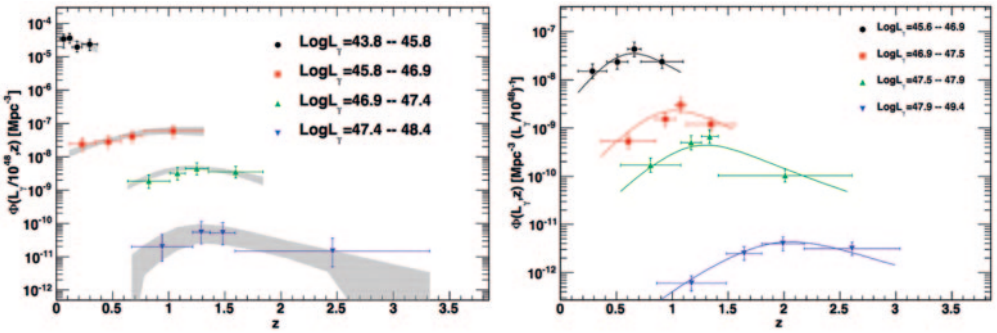

Fig. 17. – Growth and evolution of blazars, separated by luminosity class. Left: BL Lacs exhibit quasar-like evolution, which slows down at low γ-ray luminosity: for $L_\gamma < 10^{46}\,\mathrm{erg\,s^{-1}}$ the evolution becomes negative: *e.g.* the density of BL Lacs increases for decreasing redshift. Right: the bulk of the population of FSRQs (low-luminosity objects) lies at smaller redshifts, while the most luminous FSRQs are found earlier in the history of the Universe. From [107] and [108].

6˙2.2. Location of the γ-ray emission site in blazars. Variability studies provide precious evidence to pinpoint the emission region in blazars: elementary kinematics correlates the time scale of flux variations t_{var} to the emission region size R, so that $R \leq c\delta t_{\mathrm{var}}/(1+z)$, where δ is the relativistic Doppler factor([5]). Blazars exhibit flux variability on different time scales, from minutes up to several years. The shortest variability time scales indicate that at least in some instance γ rays are produced close to the black hole, probably within the broad line region (BLR) as found, *e.g.*, for FSRQ 4C+21.35 [117]. The detection of VHE emission from the latter, however, appears as a new challenge to our current understanding of blazars, since the observed VHE flux, if produced close to the central region, would be highly attenuated by e^+e^- pair production with BLR photons [118].

Investigation of the *spectral break in blazar spectra* similarly allows probing the mechanisms and energetics of the central engine. It is well known that some blazars exhibit a noticeable curvature in their γ-ray spectra. For the brightest of these objects, 3C 454.3, the spectrum is found to be better described by a power law with exponential cutoff [119]. With the statistics accumulated in more than six years of *Fermi*-LAT operation, other bright FSRQs show spectra with a similar feature, and the energy at which the cutoff occurs seems to be remarkably constant as a function of flux. Several hypotheses have been proposed to explain this curvature, such as an intrinsic break in the energy distribution of the radiating particles [119], Klein-Nishina effects when jet electrons scatter the BLR radiation in a near-equipartition regime [120], hybrid scattering [121] and γ-ray absorption due to e^+e^- pair production against the photon field of the BLR [122]. So far no clear evidence favoring one process over the others has been found; the confirmation of one scenario would offer unique information on the blazar mechanics; in particular, the pair-production hypothesis would unequivocally locate the γ-ray emission within the BLR. The interpretation is further complicated because in some cases the spectral break disappears during flares [123].

([5]) $\delta = [\Gamma(1-\beta\cos\theta)]^{-1}$, where β is the emitting region velocity, θ the angle of its motion with respect to our line of sight and Γ the bulk Lorentz factor.

Historically the correlation between the amount of radiation emitted in different energy bands has been thoroughly investigated and is now extensively used to disentangle possible coexistent production sites in blazars [124]. For example, the remarkable detection of high-energy flaring episodes in coincidence with radio and optical flares and with changes in the polarization angle in FSRQ 3C 279 suggests that γ rays can be produced in the pc-scale region where radio emission originates [125]. The general picture that emerges tells us that there is no unique prescription suitable for all blazar flares, as different observations lead to different conclusions (*e.g.* [126]), revealing a complex range of behaviors even for a single source at different epochs [127].

6˙2.3. Gravitationally Lensed Blazars. The detection of gravitationally lensed systems at γ-ray energies was foreseen by the *Fermi*-LAT team before launch [128]. So far, two known lensed blazars have been observed with the *Fermi*-LAT, and detailed studies triggered by LAT observations indicate that a third object (GB 1310+487 [129]) might be subject to gravitational lensing effects.

Though the sample is limited, an interesting variety of properties, as well as controversial results, have been pointed out. The best candidates for studying this phenomenon at γ-ray energies are the two FSRQs PKS 1830−211 and B0218+357. The former, which is also among the brightest *Fermi*-LAT AGNs, does not display convincing evidence for lensing signatures in the γ-ray band (see the different conclusions in [130] and [131]), despite the detection of lensing at other wavelengths [132]. Since gravitational lensing is an achromatic process, γ-ray observations suggest different structures and emission mechanisms in this class of sources as a function of energy. On the other hand, B0218+357 allowed the first estimate of gravitational lensing parameters in γ rays, yielding a competitive measurement of the time delay [133]. In addition, the firm detection of lensing signatures correlated to flaring events in B0218+357, and the consequent measurement of the lensing time delay, led to the first measurements of Hubble's constant using γ-ray observations. The resulting value ($h = 0.64 \pm 004$) is interestingly close to recent results (*e.g.* the one of the Planck collaboration [134]) but it has to be noted that it may be affected by systematic errors in the lens modeling and to uncertainties in the line-of-sight geometry. In this regard, the measurement of the time lag in a different system by the LAT would provide an independent γ-ray based constraint on Hubble's constant. Notably, the example of B0218+357 has demonstrated that such measurements are possible, in turn paving the way for a new research area, looking for similar lensing signatures in other blazars.

6˙2.4. Misaligned AGNs. AGNs not belonging to the blazar subclass represent only 2% of the 3LAC sample and include a large variety of objects, in particular misaligned AGNs (MAGNs, *i.e.* AGNs with jet not aligned along the line-of-sight) such as radio galaxies, compact steep-spectrum sources, steep-spectrum radio quasars and Seyfert galaxies. The radio morphology determines the division of MAGNs into two subclasses, Fanaroff-Riley I (FRI) or Fanaroff-Riley II (FRII): double jet structures appear in FRI radio galaxies, while edge-brightened radio lobes characterize FRII radio galaxies [135].

Under the current AGN unified model [136], an increase in the angle of the jet from the line of sight implies a de-amplification of the jet emission that can be quite severe, even at relatively small angles. As a matter of fact, objects with jets oriented at large angles from the line of sight should not be detectable in γ rays if a pure one-zone, homogeneous, synchrotron self-Compton model is adopted. This simple conjecture was soon questioned by the first EGRET γ-ray detections of radio galaxies (*i.e.* Cen A [137], NGC 6251 [138]),

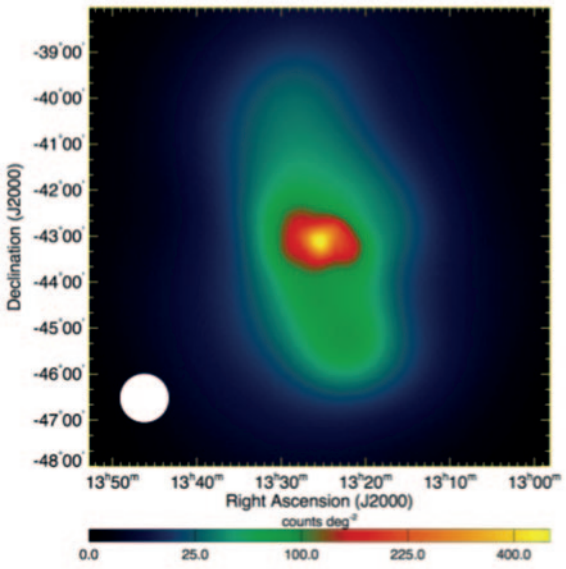

Fig. 18. – The *Fermi*-LAT γ-ray ($> 200\,\mathrm{MeV}$) counts map resulting from ~ 10 months of all-sky survey data clearly shows a prominent γ-ray emission consistent with the Cen A core and extended emission from the southern giant lobe. Because the northern lobe is characterized by lower surface brightness emission (in radio), it is not immediately apparent from a by-eye inspection of the γ-ray counts map. The white circle with a diameter of 1° is approximately the width of the LAT PSF. From [142].

and later further disfavored by TeV observations (*e.g.* of M87 [139]). This suggests a more complex jet structure, and notably offers the opportunity for systematic studies of relativistic jets under different geometries.

The *Fermi*-LAT MAGN sample (describing objects reported in the 3FGL catalog [37]) includes twelve FRI (low-power) radio galaxies, and nine FRII (high-power) radio sources. Cen A, M87 and NGC 1275 are among the detected sources, and remarkably are also observed at VHE. Exactly where γ rays originate in MAGN remains an open question. Several results seem to indicate that the GeV emission is most likely dominated by the beamed radiation of the relativistic jets, observed at intermediate viewing angles, contextually identifying small regions (10^{16}–$10^{18}\,\mathrm{cm}$) near the radio core (as in the case of NGC 1275 [140] and M87 [141]). Nevertheless, γ-ray emission also has been associated with large extended regions, as seen in Cen A, where the > 100's kpc-scale structures have been observed in γ rays [142] (see fig. 18). The *Fermi*-LAT result implies the presence of 0.1–1 TeV electrons in the Cen A lobes to upscatter low-energy photons to γ-ray energies. Given that their radiative lifetimes (< 1–$10\,\mathrm{Myr}$) approach plausible electron transport time scales across the lobes, these particles have either been accelerated *in situ* or efficiently transported from regions close to the core. It is presently unclear how common this scenario is in the other radio galaxies.

6˙3. *Galaxy clusters*. – Galaxy clusters are unique environments to study CR acceleration given their capability to confine CRs up to energies of at least 1 PeV for a time longer than the Hubble time. With respect to Galactic acceleration sites, such as

supernova remnants, they differ by the presence of large-scale structure formation and associated shocks, gigantic radio structures and high-temperature weakly magnetized plasma. Observations have already established the presence of leptonic CRs in their Mpc-scale diffuse radio halos and relics. Besides these, theories predict the presence of relativistic hadronic particles, whose interactions give rise to π^0 decay signatures [143]. So far, acquiring evidence of hadronic CRs by detection of diffuse γ-ray emission has proven elusive, even after deep searches with Čerenkov telescopes and more than six years of *Fermi*-LAT survey.

The γ-ray non-detection cases are puzzling, when considering that the CR electrons responsible for the radio continuum emission must be constantly replenished, and that CR nuclei, accelerated in large-scale shocks and accumulated in the intra-cluster medium over Gyr time scales, must produce some level of high-energy emission. Within the hadronic scenario, inelastic collisions of CR ions with the thermal protons of the intra-cluster medium produce pions that, in turn, decay into γ rays and e^+e^-. The secondary leptons can in turn produce γ rays via inverse-Compton scattering against the background radiation fields, but this emission is always subdominant compared to the neutral pion decay. Therefore, high-energy upper limits from individual radio halo clusters imply lower limits on the strength of intra-cluster magnetic fields.

The most stringent GeV constraints for CR protons in galaxy clusters to date are based on 4 years of *Fermi*-LAT all-sky data. In a search for high-energy emission originating from 50 X-ray luminous galaxy clusters, only the three clusters Abell 1367, Abell 3112 and Abell 400 show significant individual excesses [144]; their emission is unlikely to be associated with the intracluster medium due to several problematic issues: spatial offset, hard spectra, inferred normalization larger than other clusters and, above all, presence of plausible radio counterparts. While the hunt for the first detection of high-energy γ rays from galaxy clusters is still ongoing, the γ-ray non-detection provides the most direct limits on the abundance of CR protons, showing that the volume-averaged CR energy density is $< 1\%$ of the thermal intra-cluster medium, and confining the hadronic injection efficiency by intermediate shocks associated with large-scale structure formation to be less than 25% (in the Mach number range $\sim$ 3–4). On a side note, a better understanding of the γ-ray contribution from galaxy clusters will naturally translate into constraints on more exotic scenarios such as annihilation or decay of dark matter particles.

6˙4. *Diffuse extragalactic background radiation.* – The electromagnetic radiation that permeates the Universe across the whole electromagnetic spectrum is usually referred to as *diffuse extragalactic background radiation* (DEBRA). It can be interpreted as the integrated light of all photon sources along the line of sight; it is therefore composed of the contribution of individual sources (stars, galaxies, AGNs, etc.) and of truly diffuse emission, such as the CMB.

When looking at the Universe in γ rays we examine the DEBRA with complementary approaches. On one hand, we study the extragalactic γ-ray background (EGB), the sum of an isotropic diffuse γ ray background (IGRB)([6]), which is statistically uniform on large angular scales, and of resolved γ-ray sources. We must note therefore that the intensity attributed to the IGRB is instrument-dependent, since more sensitive telescopes

([6]) The IGRB comprises extragalactic emissions too faint or too diffuse to be resolved in a given survey, as well as any residual Galactic foregrounds that are approximately isotropic and the residual instrument background of misclassified charged particles in the LAT data.

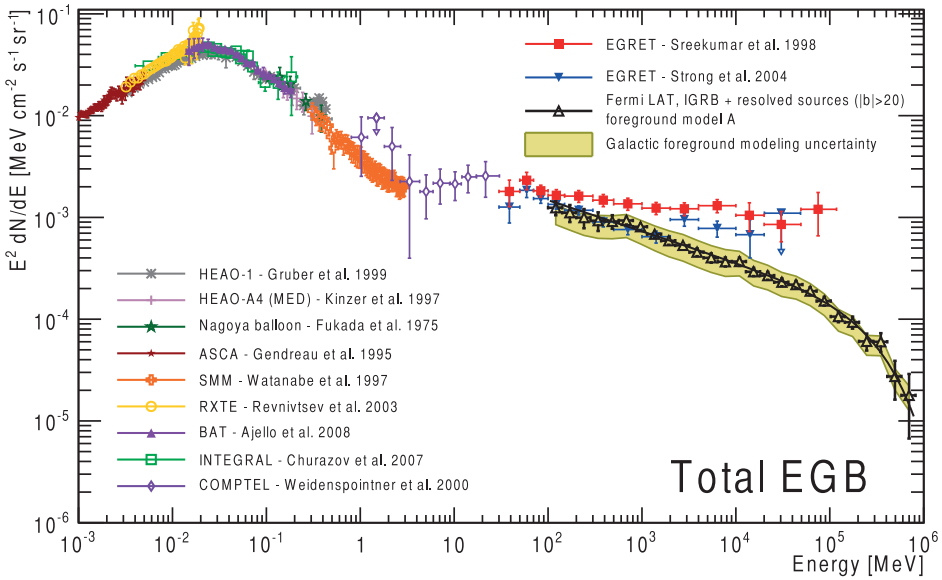

Fig. 19. – The total EGB intensity measured by the *Fermi*-LAT is plotted together with other measurements of the X-ray and γ-ray background; from [146].

are capable of resolving and extracting fainter sources. On the other hand, we use an indirect approach and investigate the imprint that extragalactic background light (EBL) leaves on the spectra of sources at cosmological distances. The EBL refers to the fraction of DEBRA lying in the UV-to-far-IR bands and accounts for radiation emitted by star-formation processes (starlight and star light absorbed/re-emitted by dust) plus a small contribution from AGNs integrated over all redshifts.

Although the origin of the IGRB is suspected to be mainly extragalactic, many various astrophysical γ-ray source classes are expected to contribute, *e.g.* AGNs, star-forming galaxies, galactic MSPs, as well as hypothetical, more exotic contributors. Consequently, elusive, diverse origin of the IGRB also motivates speculations about yet undiscovered contributors, or new physical γ-ray emission processes, such as *e.g.* annihilation and/or decay of dark matter particles (see sect. **7**˙1.1). Several efforts have been directed to comparing of the theoretical expectations for the amount of EBL in the γ-ray band, *i.e.* the EGB, with observations, *i.e.* IGRB and single-population contributions. The first estimate of the EGB spectrum reported by the *Fermi*-LAT Collaboration was based on 10 months of data and showed that the diffuse γ-ray spectrum was consistent with a single power law in the energy range 0.2–100 GeV [145]. Recent updates make use of 50 months of observations [146] and show an overall agreement with the aforementioned estimate between 100 MeV and 100 GeV, but with strong evidence of a high-energy cutoff (see fig. 19). The spectrum is well described by a power law with exponential cutoff from 100 MeV up to 820 GeV, with the cutoff energy $\sim$ 250 GeV. Its intensity and spectral shape in this range well reproduce the spectral properties of blazars, star-forming galaxies and radio galaxies, while the observed high-energy cutoff can naturally be explained as attenuation of the blazar high-energy emission by EBL UV–IR photons. Thanks to the unprecedented statistics collected by the *Fermi*-LAT, most of the EGB can now be

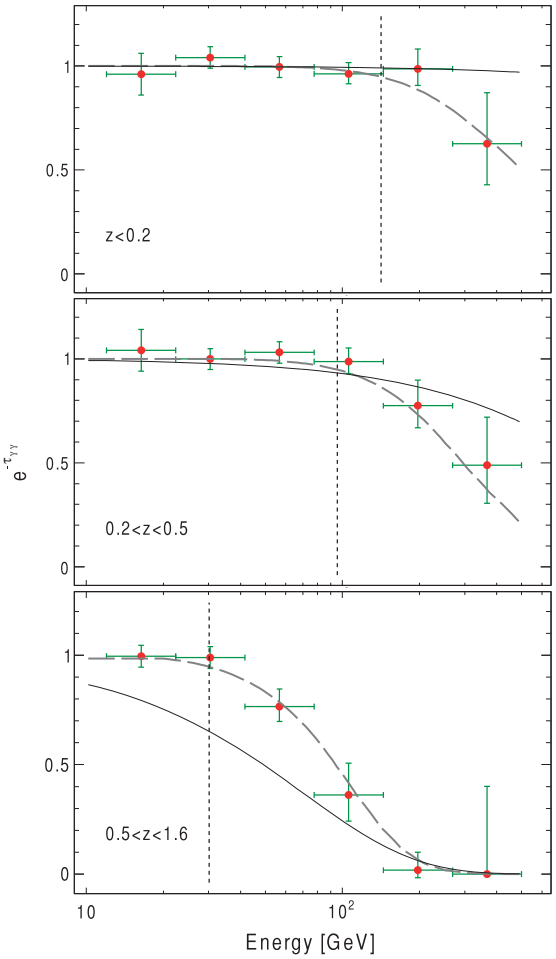

Fig. 20. – Absorption feature present in the spectra of BL Lac objects as a function of increasing redshift (data points, from top to bottom). The dashed curves show the attenuation expected for the sample of sources. The vertical line shows the critical energy below which less than 5% of the source photons are absorbed by the EBL. The thin solid curve represents the best-fit model assuming that all the sources have an intrinsic exponential cutoff and that blazars follow the blazar sequence model of [154]. The EBL model of [23] was used; from [152].

explained by known γ-ray sources, identifying blazars, and low-luminosity hard-spectrum nearby sources like BL Lacs in particular, as the dominant contributors. Blazar emission can account for $51^{+10}_{-15}\%$ of the EGB photons ($> 0.1\,\mathrm{GeV}$) [147]. This partition leaves only modest room for other contributions: in particular, limits on dark matter components are getting tighter with time, though more detailed studies are needed to derive more robust conclusions (see [148] and sect.**7**˙1.1). A complementary, powerful approach for probing the diffuse radiation fields in the UV-to-far-IR bands is through γ-γ absorption of high-energy photons [149-151]. Pair production (e^+e^-) against EBL photons with wavelengths from UV to IR is effective at attenuating γ rays with energy above $\sim 10\,\mathrm{GeV}$.

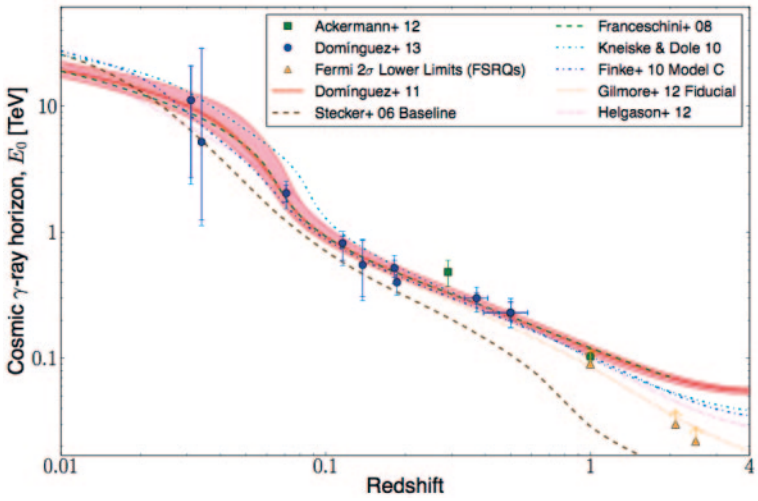

Fig. 21. – Estimation of the CGRH obtained from blazars in the sample of [156] (blue circles); from [156].

This process occurs for head-on collisions when (*e.g.*) $E_\gamma \times E_{\rm EBL} \geq 2(m_e c^2)^2$, where $m_e c^2$ is the rest mass energy of the electron, and introduces an attenuation in the spectra of γ-ray sources above a critical energy of $\sim 170(1+z)^{-2.38}$ GeV. The major effect is a redshift- and energy-dependent attenuation of the γ-ray flux of extragalactic sources such as blazars and GRBs. Striking evidence of this was provided using stacked samples of blazars (see fig. 20). This distinct EBL imprint on the γ-ray spectra of distant sources can be used to constrain the EBL intensity [152, 153]: all recent measurements favor models with a minimal level of EBL, consistent with the estimated contribution from resolved galaxies.

6˙5. *The high-energy horizon.* – As noted in the previous section, γ rays originating from distant sources may be absorbed by EBL photons during their travel across cosmological distances. The cosmic γ-ray horizon (CGRH) is defined, as a function of redshift, as the energy at which the optical depth due to photon-photon pair production becomes unity. Correspondingly, the CGRH can be thought as the distance that HE-VHE photons can travel through the Universe. Given the exponential behavior of the flux attenuation, the optical depth is the energy at which the intrinsic spectrum is attenuated by the EBL by a factor of $1/e$. Precise detection of the point at which the γ-ray flux becomes strongly attenuated was one of the primary scientific drivers of *Fermi* [155]. The direct determination of the CGRH from the spectra of blazars has proven challenging, mainly due to observational difficulties: first of all due to the lack of knowledge of the intrinsic, unattenuated spectra at HE/VHE, followed by the previous lack of a considerable sample of blazars in the GeV band. Several predictions were derived from EBL models in the past, and different methodologies used γ-ray observations of remote blazars and GRBs to derive lower limits [153], but most of the CGRH estimates before *Fermi* were strongly dependent on the assumed EBL model. *Fermi*-LAT data allowed the detection of a large number of blazars in the GeV energy range, making statistical analysis possible. Contextually, recent literature claims the first measurement of the CGRH using

multiwavelength observations of blazars [156]. Starting from a few physically motivated assumptions on the blazar inner engine, the authors model the intrinsic γ-ray fluxes and compare theoretical expectations with detections by *Fermi*-LAT and by Čerenkov observatories. The ratios between the predicted and detected fluxes are interpreted as an estimate of the EBL optical depth. By means of a maximum likelihood approach, independent of any EBL model, they derive the CGRH for each blazar and estimate the trend as a function of redshift as shown in fig. 21 [157]. As the γ-ray data set collected by *Fermi*-LAT increases in time, and more blazars and GRBs are detected at affected energies, the opacity of the universe to γ rays could be estimated over a wider energy and redshift range. This will not only provide further understanding how the EBL intensity evolves over cosmic time, but could also allow us to estimate the cosmological parameters with a novel and independent methodology, as proposed by several authors [158].

6˙6. *Gamma-ray bursts*. – Gamma-ray bursts (GRBs) are cosmological explosions thought to originate from the collapse of massive stars or from the merging of compact objects (such as neutron stars or black holes). In these objects a prompt emission lasting for 0.01–100 s is usually observed in the γ-ray band, and can be accompanied by later emission observable at lower frequencies, *e.g.* in the optical and radio bands, that can last for thousands of seconds. Typically one or two GRBs occur per day, but their origin and the particle acceleration mechanisms involved remain uncertain.

Before the launch of *Fermi*, GRBs were mainly studied in the energy band from a few keV to a few MeV, and the largest available sample was provided by the catalog of the Burst And Transient Source Experiment (BATSE) onboard CGRO [159]. Emission in the γ-ray band was demonstrated by the detection a few GRBs by EGRET above 100 MeV, the observations suggesting complex temporal and spectral behaviour at high energies. Particular concern arose after GRB 940217 was observed [19], since it displayed high-energy emission up to $\sim$ 90 minutes after the low-energy trigger provided by BATSE. With the purpose of investigating similar events, and to extend the study of GRB afterglow emission to high energies, *Fermi* was built with the capability to repoint in the direction of a bright GRB and keep it near the center of the LAT field-of-view (where efficiency is maximum) for several hours (5 hr initially, 2.5 hr since 2010 November), subject to constraints due to occultation by the Earth. This repointing occurs autonomously, following requests from either the GBM or the LAT (Autonomous Repoint Request), with adjustable brightness thresholds and led to more than 80 extended GRB observations so far.

Prior to *Fermi*, GRB spectral properties were known up to $\sim$MeV energies and the spectra were typically described in terms of the phenomenological Band function (consisting of two power laws smoothly joint together at the peak [21]), or a power law with an exponential cutoff (also called Comptonized model), or a smoothly broken power law [160]. More recently, a logarithmic parabola [161] was also introduced, and shown to provide a good representation. A first major result by *Fermi* was to break this paradigm of a single component being able to describe the whole GRB spectrum. The greatly broadened energy coverage provided by *Fermi* required the introduction of multi-component spectral models, at least for some GRBs. In fact, the brightest LAT bursts are usually characterized by a power-law spectral component that dominates at LAT energies, but there is no single recipe to fit all *Fermi* GRBs.

Several theories have tried to explain this high-energy excess over the main low-energy component. In early afterglow models this component could arise early in the prompt phase, when the fireball is still coasting, due to the forward shock propagating into the

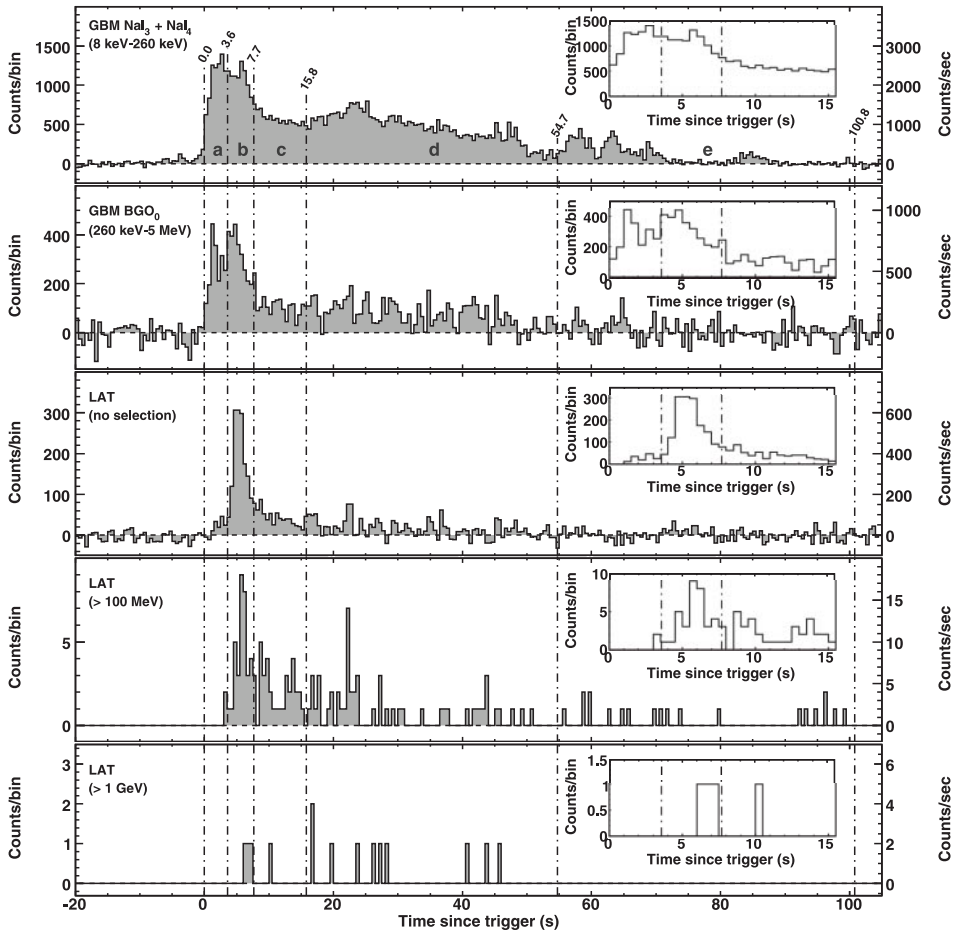

Fig. 22. – Light counts for GRB 090816C as observed with the GBM (background subtracted, top 2 panels) and the LAT (after onboard filter, bottom 3 panels) with different energy selections. Insets: counts *versus* time after trigger; a delay in the high-energy component is evident; from [164].

external medium surrounding the GRB. Other hypotheses involve inverse Compton scattering by relativistic electrons of soft target photons, either photospheric or produced by synchrotron radiation, or hadronic emission, either proton/ion synchrotron radiation or photopion-induced cascade radiation. In addition, *Fermi*-LAT observed for the first time a high-energy cutoff which required the addition of an exponential cutoff to the power-law spectral component [162,163], for a total of three components (Band, power law and exponential cutoff). These significant cutoffs in the additional power-law component suggest the presence of e^+e^- pair production by high-energy photons against keV–MeV photons.

Another remarkable breakthrough achieved by study of *Fermi*-LAT data is the observation of a delay between the LAT-detected emission and the GBM signal. The typical delay is of a few seconds [164] (see fig. 22), although delays of up to 40 s have been detected in long bursts. The cause of the delayed onset of the high-energy LAT emission

is poorly understood but the effect offers an important clue to the nature of GRBs.

The early afterglow model for temporally-extended LAT-detected emission can explain both the delayed onset and the additional component [165-168]. On the other hand it cannot account for the sharp spikes seen in coincidence with the prompt soft γ-ray emission, and competing models involving internal shocks cannot be ruled out. Future detections of additional bright bursts will help in characterizing and explaining spectral cutoffs, determining the bulk Lorentz factors and constraining GRB energetics.

Remarkably, LAT GRB observations allow investigating other related fields, such as measuring the opacity of the Universe and searching for Lorentz invariance violations. The former relies on the interaction of high-energy γ rays ($\sim 10\,\mathrm{GeV}$) from high-redshift GRBs with the optical/UV photons of the Extragalactic Background Light, allowing a more precise determination of the radiation content of the Universe (see sect. **6**˙4); for the latter see sect. **7**˙3.

Interestingly, new challenges arose from the observation of the exceptionally bright GRB 130427A [169]. This burst displayed the largest fluence, most energetic photon (95 GeV, corresponding to 128 GeV in the rest frame given the redshift $z = 0.34$), longest duration of γ-ray emission (20 hours), and one of the largest isotropic energy releases ever observed from a GRB. Analysis of this GRB challenges the widely accepted model that the non-thermal, high-energy emission of GRB afterglows is generated by synchrotron emission radiated by electrons accelerated by an external shock [169, 170].

7. – Fundamental physics

7˙1. *Dark matter*. – We have already mentioned in sect. **4**˙3 how the observation of an overabundant positron fraction can be explained in terms of a DM component. If DM annihilates directly into e^+-e^- one would expect a quasi-monochromatic peak; continuum e^+ spectra derive from either hadronic (from π^+) or leptonic (μ^+ and τ^+) final states. In the latter case, even accounting for energy loss from propagation, a typical cutoff appears at half the DM particle mass. Recent interpretation, taking into consideration the results from *Fermi*-LAT, Pamela and especially AMS-02, places stringent limits on DM with mass below $\sim 300\,\mathrm{MeV}$; see *e.g.* [171] where strong limits are derived, firmly excluding thermal cross section values for a neutalino mass $m_\chi \leq 80\,\mathrm{GeV}$.

Moving to γ-ray observations, the *Fermi*-LAT pursued a rich program including both diffuse (*e.g.* the Galactic center) and point sources (*e.g.* dwarf satellites and galaxy clusters). No evidence of a DM signal was observed, and corresponding upper limits have been derived. In this section we summarize the most interesting results.

7˙1.1. Isotropic signal. The isotropic γ-ray sigmal was discussed in sect. **6**˙4; here we focus on the DM implications of the *Fermi*-LAT observations.

Models of the expected isotropic DM signal, integrating contributions from clumps of DM at all scales and at all redshifts, are particularly affected by the uncertainties on the "astrophysics" term, see sect. **2**˙4. In particular, numerical simulations do not resolve structures below $\sim 10^5 M_\odot$: this implies that going down to the lower limit of the structure spectrum, as many as 10 orders of magnitude are described by extrapolating what is found at the highest mass concentrations. In [172] the uncertainty is addressed by considering three extreme scenarios: a first in which only structures resolved in numerical calculation are considered ("conservative" case), a second in which substructures down to $10^{-6} M_\odot$ are included in a way to maximize the corresponding contribution to the γ-ray signal ("optimistic" case), and a third, intermediate scenario with a semi-analytical

derivation of the structure spectrum. Different final state channels are considered: into quarks ($b\bar{b}$), producing γ rays via hadronization and π^0 production, into leptons ($\mu^+\mu^-$) and into γ-γ pairs.

The procedure can be summarized easily. In a simple approach, cross section upper limits are obtained requesting that the DM flux does not surpass the observed isotropic diffuse emission in any energy range. In a more realistic approach, the estimated contribution to the isotropic diffuse emission due to unresolved starburst galaxies (sect. **6**˙1) and blazars (sect. **6**˙2) are taken into account: two power-law contributions, with power-law indexes 2.7 and 2.4 respectively, are included in the emission model and the normalizations are allowed to vary freely. Upper limits are evaluated in this case by estimating how much DM signal is allowed before a chi-square analysis reveals the additional component on top of the two power-law spectra. We note than in principle this procedure assumes there is no Galactic DM component. Indeed, in addition to the conventional, main Galactocentric component, annihilation in the halo in which the Galaxy is embedded could potentially give an additional isotropic term of Galactic origin (whether the latter can be present with no indication of the former remains an open point). In principle this would imply an entirely different analysis, with DM templates to be included in the derivation of the Galactic diffuse model, and a consequent determination of a (different) isotropic diffuse emission. The additional complication associated with this analysis, the uncertainties in the modeling of the Galactic diffuse emission, and the overlap between the Galactic and extragalactic signals in this scenario suggest a different approach with an independent limit on the isotropic, extragalactic γ-ray emission based on the current measurements.

Given the severe uncertainties, the most conservative and most optimistic limits on cross sections span three orders of magnitude: while the most conservative constraints barely reach exclusion of theoretically motivated DM cross sections, more optimistic descriptions of the DM halos and sub-halos would allow excluding most such models. Better knowledge of the conventional extragalactic astrophysical contributions and of the Galactic γ-ray foreground model would also further improve the understanding and interpretation of the IGRB. A new paper using 5 year statistics is in preparation, with a new modeling procedure and robust determination of the amount of unresolved starburst and active galaxies [173]. In parallel, the range of uncertainty in the DM model predictions is expected to decrease from 3 to ~ 1 orders of magnitude thanks to a new numerical determination of the spatial power spectrum for low-mass sub-halos. The preliminary constraints on DM cross sections are expected to become as stringent as the ones derived for dwarf spheroidals (see sect. **7**˙1.3) [174].

7˙1.2. Galactic center. The GC is a crowded region where many astrophysical processes produce a bright γ-ray background, making it difficult to disentangle a DM signature. Nonetheless, many models predict the GC to be the brightest γ-ray source powered by DM annihilation; in particular a helping hand is given by the baryon abundance itself, since the cooling of gas in the centers of DM halos is expected to lead to a more concentrated DM distribution [175].

In 2011 an excess between 300 MeV and 10 GeV was reported [176,177]. Both a point-like source and an extended excess at the GC location were detected after removing point sources in the second *Fermi*-LAT source catalog (2FGL) [36] and having parametrized the Galactic diffuse component with an analytical distribution. Many subsequent works reported similar results; for an example of an analysis using the diffuse emission templates distributed by the *Fermi*-LAT Collaboration, see *e.g.* [178]. We must remark that the

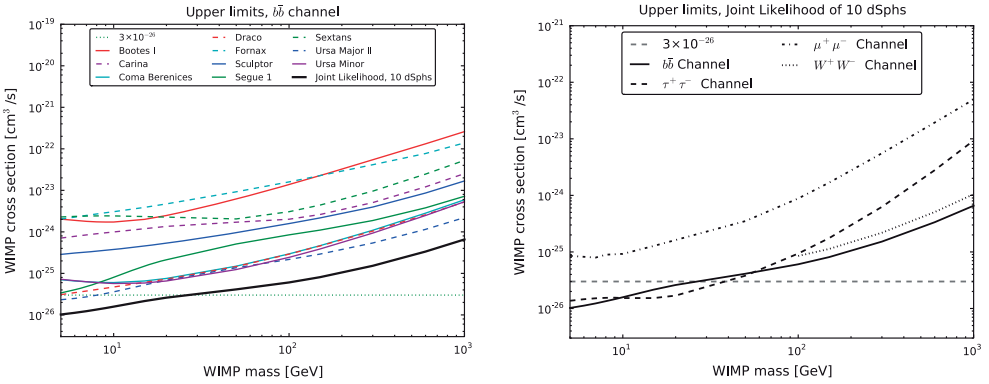

Fig. 23. – 95% upper limits for WIMP annihilation, from observation of 10 dwarf spheroidals [184]. Left: cross section limits for the individual spheroidals and for the stacked sample, for $b\bar{b}$ channel; right: comparison of combined upper limits for $b\bar{b}$, $\tau^+\tau^-$, $\mu^+\mu^-$, W^+W^- channels.

amount of excess is strongly dependent to the details of the Galactic emission model, see [60] and sect. **5**˙1.

Several astrophysical scenarios can produce a similar spatial/spectral distribution of γ-ray emission without resorting to exotic phenomena. The spectrum of the excess is consistent with what is observed in globular clusters [179, 180] (see sect. **5**˙5) and indeed the central stellar cluster is expected to feature an abundant millisecond pulsar population as in globular clusters for the same reason, namely the enhanced probability of formation of binary systems. Radio observations show the synchrotron signature from a population of energetic electrons; emission at GeV energies due to non-thermal bremsstrahlung is consistent with the LAT excess [181]. If the excess is ascribed to DM annihilation, cross sections can be derived and compared with existing upper limits from other analyses, notably the stringent ones in sect. **7**˙1.3. In [178] annihilation into the leptonic channel appears to be in tension with current limits, but some space remains for hadronic channels. Notably, limits on the DM parameters are strongly model dependent. In [182] a very conservative approach requires only the DM signal to be less than the entire observed γ-ray emission, assuming some well motivated spatial distributions. Still, models accounting for DM profile contraction due to baryonic collapse on the GC impose stringent limits excluding the thermal cross section for masses below $\sim 500\,\mathrm{GeV}$, depending on the annihilation channel.

7˙1.3. Dwarf spheroidals. Dwarf spheroidals are satellite galaxies of the Milky Way and are the largest Galactic DM substructures predicted by DM scenarios. With light-to-mass ratios as large as 100–1000, these structures have negligible γ-ray emission from conventional astrophysical processes, having no detectable interstellar gas and little or no star formation. In [183] 14 dwarf spheroidals were analyzed using the first year of LAT data, and no significant γ-ray emission was observed. To derive cross section upper limits for DM annihilation, the amount of mass in the spheroidals was evaluated from the observed line-of-sight-stellar motion. The cross section limit was subsequently improved by the combined analysis of 10 spheroidals using 2-year statistics [184]. One significant uncertainty is given by the "astrophysics" term defined in sect. **2**˙4 ("J factors" in [184]): line-of-sight mass integrals are derived from stellar velocity dispersion data

under some assumptions (*e.g.* of Gaussian distribution, of subdominant measurement errors, etc.) which can cause a bias of $\sim 50\%$. To address this, J factors are left free to adjust in the likelihood analysis; the measurement uncertainties are accounted for in the evaluation of the likelihood. Other free parameters are the normalization of the Galactic and isotropic diffuse components, and the brightness of nearby point sources and of course the velocity-averaged annihilation cross section $\langle \sigma v \rangle$. For the first time the annihilation cross section limits have been pushed below the canonical thermal relic cross section of $3 \times 10^{-26}\,\mathrm{cm}^3\,\mathrm{s}^{-1}$ for DM masses below $\sim 20\,\mathrm{GeV}$; see fig. 23. It is reassuring that repeating the analysis with models present in the literature for shallower DM cusps leads to upper limits in agreement within 10% of the aforementioned results, proving that the procedure is almost insensitive to the assumed DM profile. A recently updated analysis, using 4 years of *Fermi*-LAT data for 25 dwarf spheroidals, and determining the amount of DM in 18 of these from stellar kinematics, sets the tightest constraints to date in the range between 2 GeV and 10 TeV [185].

Recently DM searches with *Fermi*-LAT have also been extended to high velocity clouds in the halo of the Milky Way [186,187], leading to remarkably strong limits to the WIMP cross sections under the assumption of a relevant DM content in these peculiar H I substructures.

7˙1.4. Line signal. Observation of a spectral γ-ray peak compatible with a monochromatic signal would certainly be a formidable evidence for DM annihilation, as no other astrophysical phenomenon is known that can produce such a feature. *Fermi*-LAT first results on a search for a line signal from direct annihilation to γ rays were based on 1 year of observation in the range $20 < E < 300\,\mathrm{GeV}$, using data processed with the older "Pass 6" event analysis framework [188] (see sect. **3˙**4). This forced the use of a few additional quality cuts, to further reduce background contamination, and to allow only one of the possible energy determination algorithms (see sect. **3˙**3), to reduce the presence of spectral artifacts. The dataset used excluded most of the Galactic plane, where the γ-ray background due to the diffuse emission is large, but included the Galactic Center, where an enhanced DM signal is expected. The line search procedure searched *Fermi*-LAT event counts for the presence of an excess on top of the overall background spectrum; the signal template at a given energy was calculated as the local acceptance-averaged response of the LAT to a monochromatic line. The resulting upper limits on $\langle \sigma v \rangle$ were determined to be 1 order of magnitude weaker than cross section values expected for a typical thermal WIMP.

A subsequent analysis, making use of twice the statistics (2 years) and an improved event class with reduced background and a similarly selected sky region [189] was performed in the range $7 < E < 300\,\mathrm{GeV}$. The appearance of spectral features at 7 and 10 GeV led to the identification of one cut in the event analysis as source of spectral artifacts ("PSF cut"): the systematic nature of this feature was confirmed by the appearance of the same lines in the Earth limb dataset, which provides a smooth reference spectrum. The fit was repeated at these two energies with a modified dataset where the troublesome cut was disabled in the event analysis. In fig. 24 an example of the analysis procedure is shown (at $E = 7\,\mathrm{GeV}$, no "PSF cut"). Background (modeled as a power law) and signal (parametrized LAT energy resolution as derived from from Monte Carlo simulations) are fitted to the photon spectrum inside the sliding window. In the maximum likelihood approach the background index and the line signal fraction are free parameters. On the right of fig. 24 the likelihood contour corresponding to a 1σ error is shown, and the likelihood profile as a function on the signal fraction only are shown

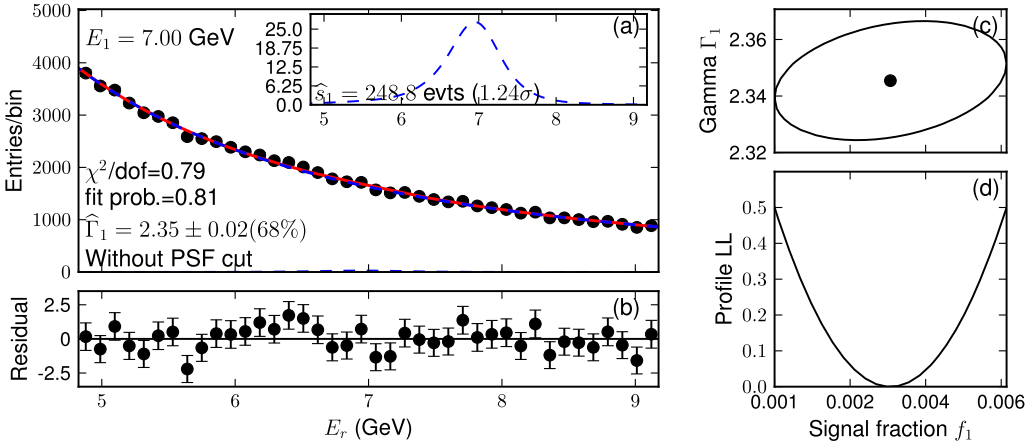

Fig. 24. – Line fitting example, from [189]. (a) Fitted background and signal components (blue dashed), combined fitted spectrum (solid red, almost coincident with the background curve); signal is shown also in the inset. (b) Normalized residuals for the composite fit. (c) Standard error (1σ) CL error ellipse. (d) Profile of the log-likelihood for the signal fraction.

for completeness. The largest signal was observed close to 7 GeV; after refinement of the search window range this led to a best energy of 6.5 GeV, corresponding to a 2.6σ significance (*pre-trials*); correcting for the number of trials factors caused the decrease of this value to 1.2σ. Since no signal was observed, 95% upper limits were calculated and the implications for a DM annihilation/decay scenario were discussed. In particular, cross section upper limits represented an improvement over the previous estimate in [188] of roughly a factor 2 for $\gamma\gamma$ final state.

Widespread excitement resulted in 2012, with reports of a line feature in the LAT photon spectrum at ~ 130 GeV in the Galactic halo with post-trials significance just above 3σ [190, 191]. Once more, appearance of an analogous feature in the Earth limb dataset seemed to indicate a systematical artifact [192]. A new detailed analysis, using 3.7 years of data reprocessed with an improved event analysis (see sect. **3**˙4), indicate a local significance of 3.3σ, amounting to 1.5σ post-trial. In addition to the appearance of the line feature in the Earth limb dataset, the line width is found to be too narrow with respect to the expected LAT resolution at a level of 2–3σ, further disfavoring the DM signal interpretation [193]. Together with the reprocessed dataset and the new, improved event analysis, a new modeling of the response to a monochromatic signal was introduced. As we mentioned in sect. **3**˙3 one can fine-tune the event analysis to improve the energy resolution at the expense of event statistics. In [193] the line profile is parametrized not only as a function of observed energy, but also as a function of a parameter P_E giving an event-by-event estimate of the quality of the energy reconstruction; see fig. 25, left. This "2D" likelihood fit gives a lower significance than the previous "1D" fit, indicating that the line feature narrows, as a function of harsher quality cuts, in a way that is not compatible with a monochromatic γ-ray signal; see fig. 25, right. A possible interpretation as statistical fluke is gaining favor since the line significance was reported to be decreasing in time [194]. To conclude, similar searches below 10 GeV down to 100 MeV failed to show any signal [195].

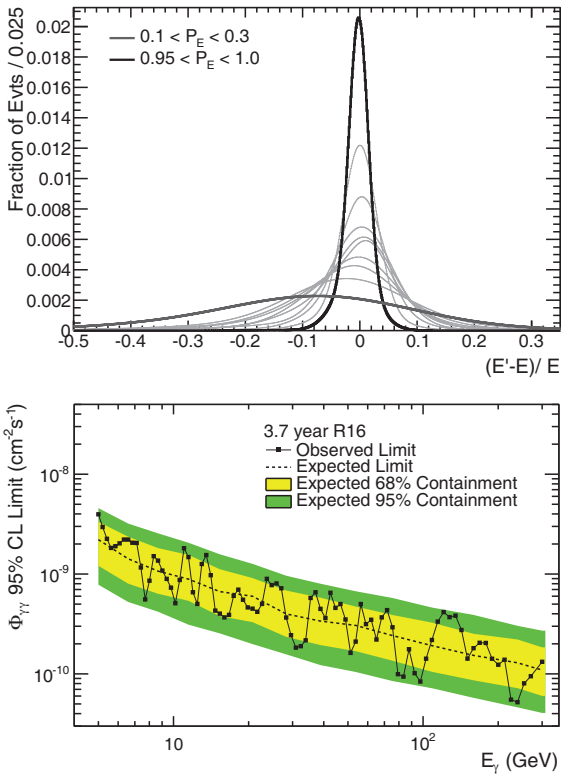

Fig. 25. – Upper panel: LAT response to a 100 GeV monochromatic signal, as a function of the event parameter P_E, estimating the quality of the energy reconstruction. Lower panel: 95% C.L. for the γ-ray flux from a monochromatic signal at the Galactic center; yellow (green) bands show the 68% (95%) expected containment from no-signal Monte Carlo simulations; from [193].

7˙2. *Intergalactic magnetic field*. – The intergalactic magnetic field (IGMF) is expected to be the seed for the (significantly stronger) magnetic fields observed in galaxies and even galaxy clusters. While mechanisms are proposed by which small fields can be amplified to the observed values in a galactic environment, the situation for galaxy clusters is more uncertain, and the origin of this seed field in the early universe is unknown [15].

The presence of weak magnetic fields on cosmological scales has an interesting consequence for high-energy AGN observations. TeV photons from these point-like sources interact with the EBL (sect. **6˙4**) producing electron pairs which can then upscatter photons to GeV energies; depending on the IGMF intensity and correlation length, pairs can be deflected enough to produce an observable GeV halo around active galaxies at cosmological distances.

To date several searches for the effects of the IGMF have reported evidence for its detection using *Fermi*-LAT data but such investigations are particularly complicated due to instrumental effects, in turn yielding controversial results to be taken with care. Early observations with *Fermi*-LAT were complicated by imperfect representation of the LAT angular resolution: it was announced early on that "Pass 6" angular response was broader than Monte Carlo estimates, to the effect that measurement of AGN halos was

entangled with experimental determination of the LAT PSF using flight data. Contrary to instrumental effects, the broadening due to IGMF would be correlated to the source distance, suggesting that a promising approach to discriminating the effects would be to split the AGN sample into redshift classes. Despite early claims of a redshift-dependent halo [196], subsequent analysis did not confirm this [197, 198]. The angular resolution derived in [197] was then adopted as the experimentally determined PSF, replacing the Monte Carlo version; since the "Pass 7" response was evaluated no experimental corrections have been needed of the PSF. At TeV energies MAGIC searched for spatially extended emission around the bright blazars Mrk 421 and Mrk 501, excluding IGMF strengths in the range 4–10 fG [199]. The general consensus seems to be converging on ruling out both very large and very small values of the IGMF strength [200] with different limits provided by several authors (*e.g.* a lower bound $\geq 3 \times 10^{-16}$G on the strength of intergalactic magnetic fields [201] but see also [202, 203]).

7˙3. *Lorentz invariance violation.* – Lorentz invariance, the postulate at the base of Einstein's theory of special relativity, assumes that all observers measure exactly the same speed of light in vacuum. In particular this implies that c is independent of the photon energy, *i.e.* there is no chromatic aberration. Relativity is a classical theory, though, and the quantum nature of spacetime on a very small scale is expected to alter the picture. In particular, one possibility is that the speed of light may show dependence on the photon wavelength at high energies. A powerful test for such deviations can be made based on the short time delays observed in *Fermi*-LAT GRBs between low- and high-energy events, taking advantage of the enormous distances over which photons propagate before reaching us. Assuming that the observed delay between high- and low energy γ rays is to be attributed to such deviations from special relativity, *Fermi* measurements disfavor quantum gravity theories where the dependence of the speed of light from energy is linear [204, 205], while little can be said about non-linear models.

8. – Conclusion

After more than half of the expected mission duration, the *Fermi* Gamma-ray Space Telescope has radically changed our picture of the high-energy Universe. Some fields have been revolutionized, *e.g.* the study of Galactic sources, and several surprising phenomena were observed, *i.e.* emission from classical novas. In summary, the scientific payback has exceeded the expectations, high as they were before launch.

One major ingredient of this success can be found in the technological improvements incorporated in the LAT, with respect to the previous generation instruments. Of particular note is the stability of the detectors' performance, thanks to the lack of consumables and conservative design. Indeed, to achieve a comparable jump in observational capabilities in the next generation of observatories, new technologies will be necessary and some are currently being evaluated for space operation.

The second major ingredient is the intensive cooperation with other instruments operating at different wavelengths, from radio to very-high-energy γ rays, and observing energetic leptons and hadrons. In view of the expected deployment of new observatories, such as the ASTRO-H X-ray observatory in space and the Čerenkov Telescope Array (CTA) on ground to mention only two, an exciting new season is approaching. Therefore it is not surprising that the ground-based γ-ray community is strongly in favor of continuing operation of the *Fermi*-LAT mission for longer than the nominal mission duration.

With potentially several years of operations remaining, increasing exposure and improvements in the analysis of LAT data allow us to foresee more exciting discoveries.

* * *

The authors thank all colleagues in the *Fermi*-LAT Collaboration for the pleasant and fruitful environment. In particular we thank the colleagues who read the manuscript and provided very helpful comments: D. J. Thompson, C. C. Cheung, J. Finke, A. Domínguez, J. Cohen-Tanugi, J. Granot, P. Caraveo, F. Longo, G. Busetto. We sincerely thank the anonymous referee for the thorough review and for providing many useful suggestions, which significantly improved the quality of the manuscript.

REFERENCES

[1] Hillas A. M., "Cosmic Rays: Recent Progress and some Current Questions", arXiv:astro-ph/0607109.
[2] Wiedenbeck M. E. *et al.*, "An Overview of the Origin of Galactic Cosmic Rays as Inferred from Observations of Heavy Ion Composition and Spectra", *Space Sci. Rev.*, **130** (2007) 415.
[3] Chang J. *et al.*, "An excess of cosmic ray electrons at energies of 300–800 GeV", *Nature*, **456** (2008) 362.
[4] Aharonian F. *et al.*, "Probing the ATIC peak in the cosmic-ray electron spectrum with H.E.S.S.", *Astron. Astrophys.*, **508** (2009) 561.
[5] Adriani O. *et al.*, "An anomalous positron abundance in cosmic rays with energies 1.5–100 GeV", *Nature*, **458** (2009) 607.
[6] Binns W. R. *et al.*, "Cosmic-Ray Neon, Wolf-Rayet Stars, and the Superbubble Origin of Galactic Cosmic Rays", *Astrophys. J.*, **634** (2005) 351.
[7] Sturrock P. A., "A Model of Pulsars", *Astrophys. J.*, **164** (1971) 529.
[8] Arons J., "Pair creation above pulsar polar caps-Geometrical structure and energetics of slot gaps", *Astrophys. J.*, **266** (1983) 215.
[9] Cheng K. S. *et al.*, "Energetic radiation from rapidly spinning pulsars. I-Outer magnetosphere gaps. II-VELA and Crab", *Astrophys. J.*, **300** (1986) 500.
[10] Romani R. W. and Watters K. P., "Constraining Pulsar Magnetosphere Geometry with Gamma-ray Light Curves", *Astrophys. J.*, **714** (2010) 810.
[11] Ransom S. M., "Twenty Years of Searching for (and Finding) Globular Cluster Pulsars", *AIP Conf. Proc.*, **983** (2008) 415.
[12] Abdo A. A. *et al.*, "Fermi Large Area Telescope Bright Gamma-ray Source List", *Astrophys. J. Suppl.*, **183** (2009) 46.
[13] Hartman R. C. *et al.*, "The Third EGRET Catalog of High-Energy Gamma-Ray Sources", *Astrophys. J. Suppl.*, **123** (1999) 79.
[14] Ackermann M. *et al.*, "The Third Catalog of Active Galactic Nuclei Detected by the Fermi Large Area Telescope", in preparation.
[15] Elyiv A. *et al.*, "Gamma-ray induced cascades and magnetic fields in the intergalactic medium", *Phys. Rev. D*, **80** (2009) 3010.
[16] Kouveliotou C. *et al.*, "Identification of two classes of gamma-ray bursts", *Astrophys. J.*, **413** (1993) 101.
[17] Woosley S. E., "Gamma-Ray Bursts from Stellar Collapse to a Black Hole?", *Astron. Astrophys.*, **182** (1993) 5505.
[18] Paczynski P., "Gamma-ray bursters at cosmological distances", *Astrophys. J.*, **308** (1986) 43.
[19] Hurley H. *et al.*, "Detection of a gamma-ray burst of very long duration and very high energy", *Nature*, **372** (1994) 652.
[20] Gonzalez M. M. *et al.*, "A γ-ray burst with a high-energy spectral component inconsistent with the synchrotron shock model", *Nature*, **424** (2003) 749.

[21] Band D. *et al.*, "BATSE observations of gamma-ray burst spectra. I-Spectral diversity", *Astrophys. J.*, **413** (1993) 281.
[22] Fazio G. G. and Stecker F. W., "Predicted High Energy Break in the Isotropic Gamma Ray Spectrum: a Test of Cosmological Origin", *Nature*, **226** (1970) 135.
[23] Franceschini A. *et al.*, "Extragalactic optical-infrared background radiation, its time evolution and the cosmic photon-photon opacity", *Astron. Astrophys.*, **26** (2008) 837.
[24] Natarajan A. and Yoshida N., "The Dark Ages of the Universe and Hydrogen Reionization", arXiv:1404.7146.
[25] Roos M., "Dark Matter: The evidence from astronomy, astrophysics and cosmology", arXiv:1001.0316.
[26] Ade P. A. R. *et al.*, "Planck 2013 results. XV. CMB power spectra and likelihood", arXiv:1303.5075.
[27] Gamma Ray Astronomy Program Working Group, *Recommended Priorities for NASA'S Gamma Ray Astronomy Program–1996-2010*, http://heasarc.gsfc.nasa.gov/docs/cgro/epo/brochures/grapwg, 1997.
[28] Atwood W. B. *et al.*, "The Large Area Telescope on the Fermi Gamma-Ray Space Telescope Mission", *Astrophys. J.*, **697** (2009) 1071.
[29] Ackermann M. *et al.*, "The Fermi Large Area Telescope on Orbit: Event Classification, Instrument Response Functions, and Calibration", *Astrophys. J. Suppl.*, **203** (2012) 4.
[30] Atwood W. B. *et al.*, "Design and initial tests of the Tracker-converter of the Gamma-ray Large Area Space Telescope", *Astropost. Phys.*, **28** (2007) 422.
[31] Grove J. E. and Johnson W. N., "The calorimeter of the Fermi Large Area Telescope", Proc. SPIE, **7732** (2010) 773205.
[32] Moiseev A. A. *et al.*, "The anti-coincidence detector for the GLAST large area telescope", *Astropost. Phys.*, **27** (2007) 339.
[33] Bruel P. *et al.*, "Performance of Pass 8 Event Analysis of the Fermi Large Area Telescope", Fermi Symp. Proc., 2014, http://fermi.gsfc.nasa.gov/science/mtgs/symposia/2014/program.
[34] Atwood W. B. *et al.*, "Pass 8: Toward the Full Realization of the Fermi-LAT Scientific Potential", Fermi Symp. Proc., 2012, arXiv:1303.3514.
[35] "Fermi-LAT Data Products", http://fermi.gsfc.nasa.gov/ssc/data/access.
[36] Nolan P. L. *et al.*, "Fermi Large Area Telescope Second Source Catalog", *Astrophys. J. Suppl.*, **199** (2012) 31.
[37] The Fermi-LAT collaboration, "Fermi Large Area Telescope Third Source Catalog", submitted to *Astrophys. J. Suppl. Ser.*, arXiv:1501.02003.
[38] Abdo A. A. *et al.*, "Fermi large area telescope observations of the cosmic-ray induced gamma-ray emission of the Earth's atmosphere", *Phys. Rev. D*, **80** (2009) 122004.
[39] Ackermann M. *et al.*, "Inferred Cosmic-Ray Spectrum from Fermi Large Area Telescope Gamma-Ray Observations of Earth's Limb", *Phys. Rev. Lett.*, **112** (2014) 151103.
[40] Fishman G. J. *et al.*, "Discovery of Intense Gamma-Ray Flashes of Atmospheric Origin", *Science*, **264** (1994) 1313.
[41] Smith D. M. *et al.*, "Terrestrial Gamma-Ray Flashes Observed up to 20 MeV", *Science*, **307** (2005) 1085.
[42] Fuschino F. *et al.*, "AGILE View of TGFs", *AIP Conf. Proc.*, **1118** (2009) 46.
[43] Briggs M. S. *et al.*, "First results on terrestrial gamma ray flashes from the Fermi Gamma-ray Burst Monitor", *J. Geophys. Res.*, **115** (2010) A07323.
[44] Connaughton V. *et al.*, "Associations between Fermi Gamma-ray Burst Monitor terrestrial gamma ray flashes and sferics from the World Wide Lightning Location Network", *J. Geophys. Res.*, **115** (2010) A012307.
[45] Grove J. E. and Chekhtman A., "A Four-Year Fermi Large Area Telescope Survey of Terrestrial Gamma-ray Flashes", HEAD, **13** (2013) 127.27.
[46] Abdo A. A. *et al.*, "Measurement of the Cosmic Ray $e^+ + e^-$ Spectrum from 20 GeV to 1 TeV with the Fermi Large Area Telescope", *Phys. Rev. Lett.*, **102** (2009) 181101.

[47] Grasso D. *et al.*, "On possible interpretations of the high energy electron-positron spectrum measured by the Fermi Large Area Telescope", *Astropost. Phys.*, **32** (2009) 140.
[48] Bergström L. *et al.*, "Dark Matter Interpretation of Recent Electron and Positron Data", *Phys. Rev. Lett.*, **103** (2009) 1103.
[49] Ackermann M. *et al.*, "Fermi LAT observations of cosmic-ray electrons from 7 GeV to 1 TeV", *Phys. Rev. D*, **82** (2010) 092004.
[50] Ackermann M. *et al.*, "Measurement of Separate Cosmic-Ray Electron and Positron Spectra with the Fermi Large Area Telescope", *Phys. Rev. Lett.*, **108** (2012) 011103.
[51] Aguilar M. *et al.*, "First Result from the Alpha Magnetic Spectrometer on the International Space Station: Precision Measurement of the Positron Fraction in Primary Cosmic Rays of 0.5–350 GeV", *Phys. Rev. Lett.*, **110** (2013) 141102.
[52] Ackermann M. *et al.*, "Searches for cosmic-ray electron anisotropies with the Fermi Large Area Telescope", *Phys. Rev. D*, **82** (2010) 092003.
[53] Ackermann M. *et al.*, "Fermi Detection of Gamma-Ray Emission from the M2 Soft X-Ray Flare on 2010 June 12", *Astrophys. J.*, **745** (2012) 144.
[54] Ajello M. *et al.*, "Impulsive and Long Duration High-energy Gamma-Ray Emission from the Very Bright 2012 March 7 Solar Flares", *Astrophys. J.*, **789** (2014) 20.
[55] Abdo A. A. *et al.*, "Fermi Large Area Telescope Observations of Two Gamma-Ray Emission Components from the Quiescent Sun", *Astrophys. J.*, **734** (2011) 116.
[56] Orlando E. and Strong A. W., "Gamma-ray emission from the solar halo and disk: a study with EGRET data", *Astron. Astrophys.*, **480** (2008) 847.
[57] Seckel D. *et al.*, "Signatures of cosmic-ray interactions on the solar surface", *Astrophys. J.*, **382** (1991) 652.
[58] Moskalenko I. V. and Porter T. A., "The Gamma-Ray Albedo of the Moon", *Astrophys. J.*, **670** (2007) 1467.
[59] Abdo A. A. *et al.*, "Fermi Observations of Gamma-Ray Emission from the Moon", *Astrophys. J.*, **758** (2012) 140.
[60] Ackermann M., "Fermi-LAT Observations of the Diffuse Gamma-Ray Emission: Implications for Cosmic Rays and the Interstellar Medium", *Astrophys. J.*, **750** (2012) 3.
[61] Strong A. W. and Moskalenko I. V., "Propagation of cosmic-ray nucleons in the Galaxy", *Astrophys. J.*, **509** (1998) 212.
[62] Tibaldo L., "A Tale of Cosmic Rays Narrated in Gamma Rays by Fermi", ICRC Conf. Proc. 2013, `arXiv:1311.2896`.
[63] Ackermann M. *et al.*, "A Cocoon of Freshly Accelerated Cosmic Rays Detected by Fermi in the Cygnus Superbubble", *Science*, **334** (2011) 1103.
[64] Finkbeiner D. P., "Microwave Interstellar Medium Emission Observed by the Wilkinson Microwave Anisotropy Probe", *Astrophys. J.*, **614** (2004) 186.
[65] Dobler G., Finkbeiner D. P., Cholis I., Slatyer T. and Weiner N., "The Fermi Haze: A Gamma-ray Counterpart to the Microwave Haze", *Astrophys. J.*, **717** (2010) 825.
[66] Su M., Slatyer T. R. and Finkbeiner D. P., "Giant Gamma-ray Bubbles from Fermi-LAT: Active Galactic Nucleus Activity or Bipolar Galactic Wind?", *Astrophys. J.*, **724** (2010) 1044.
[67] Su M. and Finkbeiner D. P., "Evidence for Gamma-Ray Jets in the Milky Way", *Astrophys. J.*, **753** (2012) 61.
[68] Ackermann M. *et al.*, "The Spectrum and Morphology of the Fermi Bubbles", *Astrophys. J.*, **793** (2014) 64.
[69] Abdo A. A. *et al.*, "The Second Fermi Large Area Telescope Catalog of Gamma Ray Pulsars", *Astrophys. J. Suppl.*, **208** (2013) 17.
[70] Ray P. S. *et al.*, "Radio Detection of the Fermi-LAT Blind Search Millisecond Pulsar J1311-3430", *Astrophys. J. Lett.*, **763** (2013) L13.
[71] Caraveo P. A., "Gamma-Ray Pulsar Revolution", *Astron. Astrophys.*, **52** (2014) 211.
[72] Ackermann M. *et al.*, "The First Fermi-LAT Catalog of Sources above 10 GeV", *Astrophys. J. Suppl.*, **209** (2013) 34.

[73] Pierbattista M. *et al.*, "Light-curve modelling constraints on the obliquities and aspect angles of the young Fermi pulsars", submitted to *Astron. Astrophys.* (2014) arXiv:1403.3849.
[74] Johnson T. J. *et al.*, "Constraints on the Emission Geometries and Spin Evolution of Gamma-Ray Millisecond Pulsars", *Astrophys. J. Suppl.*, **213** (2014) 6.
[75] Allafort A. *et al.*, "PSR J2021+4026 in the Gamma Cygni Region: The First Variable Gamma-Ray Pulsar Seen by the Fermi LAT", *Astrophys. J. Lett.*, **777** (2103) 2.
[76] Chen A. W. *et al.*, "Study of the gamma-ray source 1AGL J2022+4032 in the Cygnus region", *Astron. Astrophys.*, **525** (2011) 33.
[77] Abdo A. A. *et al.*, "A population of gamma-ray emitting globular clusters seen with the Fermi Large Area Telescope", *Astron. Astrophys.*, **524** (2010) 75.
[78] Abdo A. A. *et al.*, "Gamma-Ray Emission from the Shell of Supernova Remnant W44 Revealed by the Fermi LAT", *Science*, **327** (2010) 1103.
[79] Abdo A. A. *et al.*, "Observation of Supernova Remnant IC 443 with the Fermi Large Area Telescope", *Astrophys. J.*, **721** (2010) 459.
[80] Uchiyama Y. *et al.*, "Fermi Large Area Telescope Discovery of GeV Gamma-Ray Emission from the Vicinity of SNR W44", *Astrophys. J. Lett.*, **749** (2012) 35.
[81] Abdo A. A. *et al.*, "Observations of the Young Supernova Remnant RX J1713.7-3946 with the Fermi Large Area Telescope", *Astrophys. J.*, **734** (2011) 28.
[82] Abdo A. A. *et al.*, "Fermi-Lat Discovery of GeV Gamma-Ray Emission from the Young Supernova Remnant Cassiopeia A", *Astrophys. J. Lett.*, **710** (2010) 92.
[83] Tavani M. *et al.*, "Discovery of Powerful Gamma-Ray Flares from the Crab Nebula", *Science*, **331** (2011) 736.
[84] Abdo A. A. *et al.*, "Gamma-Ray Flares from the Crab Nebula", *Science*, **331** (2011) 739.
[85] Psaltis D., " Accreting Neutron Stars and Black Holes: A Decade of Discoveries", arXiv:astro-ph/0410536.
[86] Abdo A. A. *et al.*, "Modulated High-Energy Gamma-Ray Emission from the Microquasar Cygnus X-3", *Science*, **326** (2009) 1512.
[87] Pittori C. *et al.*, "First AGILE catalog of high-confidence gamma-ray sources", *Astron. Astrophys.*, **506** (2009) 1563.
[88] Abdo A. A. *et al.*, "Fermi LAT Observations of LS I + 61°303: First Detection of an Orbital Modulation in GeV Gamma Rays", *Astrophys. J. Lett.*, **701** (2009) 123.
[89] Abdo A. A. *et al.*, "Fermi/LAT observations of LS 5039", *Astrophys. J. Lett.*, **706** (2009) 56.
[90] Ackermann M. *et al.*, "Periodic Emission from the Gamma-Ray Binary 1FGL J1018.6-5856", *Science*, **335** (2012) 189.
[91] Wang N. *et al.*, "13 years of timing of PSR B1259-63", *Mon. Not. R. Astron. Soc.*, **351** (2004) 599.
[92] Abramowski A. *et al.*, "H.E.S.S. observations of the binary system PSR B1259-63/LS 2883 around the 2010/2011 periastron passage", *Astron. Astrophys.*, **551** (2013) 94.
[93] Abdo A. A. *et al.*, "Discovery of High-energy Gamma-ray Emission from the Binary System PSR B1259-63/LS 2883 around Periastron with Fermi", *Astrophys. J. Lett.*, **736** (2011) 11.
[94] Abdo A. A. *et al.*, "Gamma-Ray Emission Concurrent with the Nova in the Symbiotic Binary V407 Cygni", *Science*, **329** (2010) 817.
[95] Cheung C. C. *et al.*, "Fermi Discovers a New Population of Gamma-ray Novae", Fermi Symp. Proc., 2012, arXiv:1304.3475.
[96] O'Brien T. J. *et al.*, "Nova Mon 2012 Resolved as a Double Radio Source", ATel #4408.
[97] Fuhrmann L. *et al.*, "Follow up radio observations of Nova Mon 2012 at 10–142 GHz", ATel #4376.
[98] Chomiuk L. *et al.*, "Radio Monitoring of Nova Sco 2012", ATel #4288.
[99] Hays E. *et al.*, "Detection of gamma rays from Nova Delphini 2013", ATel #5302.
[100] Cheung C. C., "Fermi-LAT Gamma-ray Observations of Nova Centauri 2013", ATel #5649.

[101] Ackermann M. *et al.*, "Fermi Establishes Classical Novae as a Distinct Class of Gamma-Ray Sources", *Science*, **345** (2014) 554.
[102] Yun M. S. *et al.*, "Radio Properties of Infrared-selected Galaxies in the IRAS 2 Jy Sample", *Astrophys. J.*, **554** (2001) 803.
[103] Ackermann M. *et al.*, "GeV Observations of Star-forming Galaxies with the Fermi LAT", *Astrophys. J.*, **755** (2012) 164.
[104] Sanders D. B. and Mirabel I. F., "Luminous Infrared Galaxies", *Annu. Rev. Astron. Astrophys.*, **34** (1996) 749.
[105] Blandford R. D. and Znajek R. L., "Electromagnetic extraction of energy from Kerr black holes", *Mon. Not. R. Astron. Soc.*, **179** (1977) 433.
[106] Abdo A. A. *et al.*, "The Spectral Energy Distribution of Fermi Bright Blazars", *Astrophys. J.*, **716** (2010) 30.
[107] Ajello M. *et al.*, "The Cosmic Evolution of Fermi BL Lacertae Objects", *Astrophys. J.*, **780** (2014) 73.
[108] Ajello M. *et al.*, "The Luminosity Function of Fermi-detected Flat-Spectrum Radio Quasars", *Astrophys. J.*, **751** (2011) 108.
[109] Caccianiga *et al.*, "On the Cosmological Evolution of BL Lacertae Objects", *Astrophys. J.*, **566** (2002) 181.
[110] Padovani P. *et al.*, "The Deep X-Ray Radio Blazar Survey. III. Radio Number Counts, Evolutionary Properties, and Luminosity Function of Blazars", *Astrophys. J.*, **662** (2007) 182.
[111] Marcha M. J. M. and Caccianiga A., "The CLASS BL Lac sample: The Radio Luminosity Function", *Mon. Not. R. Astron. Soc.*, **430** (2013) 2464.
[112] Rector T. A. *et al.*, "The Properties of the X-Ray-selected EMSS Sample of BL Lacertae Objects", *Astron. J.*, **120** (2000) 1626.
[113] Cavaliere A. and DElia V., *Astrophys. J.*, **571** (2002) 226.
[114] Bottcher M. and Dermer C. D., *Astrophys. J.*, **564** (2002) 86.
[115] Ghisellini G. *et al.*, "The Fermi blazars' divide", *Mon. Not. R. Astron. Soc.*, **396** (2009) 105.
[116] Ghisellini G. *et al.*, "A theoretical unifying scheme for gamma-ray bright blazars", *Mon. Not. R. Astron. Soc.*, **301** (1998) 451.
[117] Aleksić J. *et al.*, "MAGIC Discovery of Very High Energy Emission from the FSRQ PKS 1222+21", *Astrophys. J.*, **730** (2011) 6.
[118] Dermer C. D. *et al.*, "Variable Gamma-Ray Emission Induced by Ultra-high Energy Neutral Beams: Application to 4C +21.35", *Astrophys. J.*, **755** (2012) 147.
[119] Abdo A. A. *et al.*, "Early Fermi Gamma-ray Space Telescope Observations of The Quasar 3C 454.3", *Astrophys. J.*, **699** (2009) 817.
[120] Cerruti M. for the VERITAS Collaboration, "VERITAS results from a three-year observing campaign on the BL Lac object 1ES 0229+200", `arXiv:1303.3514`.
[121] Finke J. and Dermer C. D., "On the Break in the Fermi-Large Area Telescope Spectrum of 3C 454.3", *Astrophys. J.*, **714** (2010) 303.
[122] Poutanen Y. and Stern B., "GeV breaks in blazars as a result of gamma-ray absorption within the broad-line region", *Astrophys. J. Lett.*, **717** (2010) 118.
[123] Pacciani *et al.*, "Exploring the Blazar Zone in High-energy Flares of FSRQs", *Astrophys. J.*, **490** (2014) 95.
[124] Max-Moerbeck W. *et al.*, "OVRO 40 m Blazar Monitoring Program: Location of the gamma-ray emission region in blazars by the study of correlated variability at radio and gamma-rays", `arXiv:1303.2131`.
[125] Abdo A. A. *et al.*, "A change in the optical polarization associated with a γ-ray flare in the blazar 3C279", *Nature*, **463** (2010) 919.
[126] Marscher A. P. *et al.*, "The inner jet of an active galactic nucleus as revealed by a radio-to-gamma-ray outburst", *Nature*, **452** (2008) 966.
[127] Buson S. *et al.*, "Unusual flaring activity in the blazar PKS 1424-418 during 2008-2011", *Astron. Astrophys.*, **569** (2014) 40.

[128] Atwood W. B., "The Violent Universe", in the Les Houches Winter School, CEA-Saclay (2007).
[129] Sokolovsky K. *et al.*, "Two active states of the narrow-line gamma-ray-loud AGN GB1310+487", *Astron. Astrophys.*, **565** (2014) 26.
[130] Barnacka B. *et al.*, "First evidence for a gravitational lensing-induced echo in gamma rays with Fermi LAT", *Astron. Astrophys.*, **528** (2011) 3.
[131] Abdo A. A. *et al.*, "Gamma-ray flaring activity from the gravitationally lensed blazar PKS 1830-211 observed by Fermi LAT", *Astrophys. J.*, **799** (2014) 143.
[132] Lovell J. E. J. *et al.*, "The Time Delay in the Gravitational Lens PKS 1830−211", *Astrophys. J.*, **508** (1998) 51.
[133] Cheung C. C. *et al.*, "Fermi Large Area Telescope Detection of Gravitational Lens Delayed Gamma-ray Flares from Blazar B0218+357", *Astrophys. J. Lett.*, **782** (2014) 14.
[134] Planck Collaboration *et al.*, "Planck 2013 results. XVI. Cosmological parameters", *Astron. Astrophys.*, **571** (2014) 16.
[135] Fanaroff B. L. and Riley J. M., "The morphology of extragalactic radio sources of high and low luminosity", *Mon. Not. R. Astron. Soc.*, **167** (1974) 31.
[136] Urry C. M. and Padovani P., "Unified Schemes for Radio-Loud Active Galactic Nuclei", *Publ. Astron. Soc. Pacific*, **107** (1995) 803.
[137] Sreekumar *et al.*, "GeV emission from the nearby radio galaxy Centaurus A", *Astropost. Phys.*, **11** (1999) 211.
[138] Mukherjee M. *et al.*, "Is the EGRET Source 3EG J1621+8203 the Radio Galaxy NGC 6251?", *Astrophys. J.*, **574** (2002) 693.
[139] Aharonian F. *et al.*, "Is the giant radio galaxy M 87 a TeV gamma-ray emitter?", *Astron. Astrophys.*, **403** (2003) 1.
[140] Abdo A. A. *et al.*, "Fermi Discovery of Gamma-ray Emission from NGC 1275", *Astrophys. J.*, **699** (2009) 31.
[141] Abdo A. A. *et al.*, "Fermi Large Area Telescope Gamma-Ray Detection of the Radio Galaxy M87", *Astrophys. J.*, **707** (2009) 55.
[142] Abdo A. A., "Fermi Gamma-Ray Imaging of a Radio Galaxy", *Science*, **328** (2010) 725.
[143] Pinzke A. and Pfrommer C., "Simulating the γ-ray emission from galaxy clusters: a universal cosmic ray spectrum and spatial distribution", *Mon. Not. R. Astron. Soc.*, **409** (2010) 449.
[144] Ackermann M. *et al.*, "Search for cosmic-ray induced gamma-ray emission in Galaxy Clusters", *Astrophys. J.*, **787** (2014) 18.
[145] Ackermann M. *et al.*, "Fermi Large Area Telescope Study of Cosmic Rays and the Interstellar Medium in nearby Molecular Clouds", *Astrophys. J.*, **755** (2012) 22.
[146] Ackermann M. *et al.*, "The spectrum of isotropic diffuse gamma-ray emission between 100 MeV and 820 GeV", accepted by Astrophys. J., `arXiv:1410.3696`.
[147] Ajello M. *et al.*, "The Origin of the Extragalactic Gamma-Ray Background and implications for Dark-Matter Annihilation", `arXiv:1501.05301`, accepted for publication by Astrophys. J. Lett.
[148] The Fermi-LAT collaboration, "Limits on dark matter from 4 years measurement of the Isotropic Gamma-Ray Flux with the Fermi LAT", in preparation.
[149] Fazio G. G. *et al.*, "Predicted High Energy Break in the Isotropic Gamma Ray Spectrum: a Test of Cosmological Origin", *Nature*, **299** (1998) 433.
[150] Gould R. J. and Schreder G., "Opacity of the Universe to High-Energy Photons", *Phys. Rev. Lett.*, **16** (1966) 252.
[151] Stecker F. W. *et al.*, "TeV gamma rays from 3C 279—A possible probe of origin and intergalactic infrared radiation fields", *Astrophys. J.*, **390** (1992) 49.
[152] Ackermann M. *et al.*, "The Imprint of The Extragalactic Background Light in the Gamma-Ray Spectra of Blazars", *Science*, **338** (2012) 1190.
[153] Abdo A. A. *et al.*, "Fermi Large Area Telescope Constraints on the Gamma-ray Opacity of the Universe", *Astrophys. J.*, **723** (2010) 1082.
[154] Fossati G. *et al.*, "A unifying view of the spectral energy distributions of blazars", *Astrophys. J.*, **390** (1992) 49.

[155] Hartmann D. H., "Probing The Extragalactic Background With GLAST", *AIP Conf. Proc.*, **921** (2007) 24.
[156] Dominguez A. *et al.*, "Detection of the Cosmic Gamma-Ray Horizon from Multiwavelength Observations of Blazars", *Astrophys. J.*, **770** (2013) 77.
[157] Blanch O. and Martinez M., "Exploring the gamma-ray horizon with the next generation of gamma-ray telescopes. Part 1 Theoretical predictions", *Astropost. Phys.*, **23** (2005) 588.
[158] Dominguez A. and Prada F., "Measurement of the Expansion Rate of the Universe from Gamma-Ray Attenuation", *Astrophys. J.*, **771** (2013) 34.
[159] Kaneko Y. *et al.*, "The Complete Spectral Catalog of Bright BATSE Gamma-Ray Bursts", *Astrophys. J. Suppl.*, **166** (2006) 298.
[160] Ryde F., "Smoothly Broken Power Law Spectra of Gamma-Ray Bursts", *Astrophys. Lett.*, **39** (1999) 281.
[161] Massaro F. *et al.*, "Gamma-ray Bursts in the Fermi Era: The Spectral Energy Distribution of the Prompt Emission", *Astrophys. J.*, **714** (2010) 299.
[162] Ackermann M. *et al.*, "Detection of a Spectral Break in the Extra Hard Component of GRB 090926A", *Astrophys. J.*, **729** (2011) 114.
[163] Ackermann M. *et al.*, "Constraining the High-energy Emission from Gamma-Ray Bursts with Fermi", *Astrophys. J.*, **754** (2012) 121.
[164] Abdo A. A. *et al.*, "Fermi Observations of High-Energy Gamma-Ray Emission from GRB 080916C", *Science*, **323** (2009) 1688.
[165] Ghisellini G. *et al.*, "GeV emission from gamma-ray bursts: a radiative fireball?", *Mon. Not. R. Astron. Soc.*, **403** (2010) 926.
[166] Kumar P. and Barniol Duran, "On the generation of high-energy photons detected by the Fermi Satellite from gamma-ray bursts", *Mon. Not. R. Astron. Soc.*, **403** (2010) L75.
[167] Razzaque S., "A Leptonic-Hadronic Model for the Afterglow of Gamma-ray Burst 090510", *Astrophys. J.*, **724** (2010) L109.
[168] De Pasquale M. *et al.*, "Swift and Fermi Observations of the Early Afterglow of the Short Gamma-Ray Burst 090510", *Astrophys. J.*, **709** (2010) L146.
[169] Ackermann M. *et al.*, "Fermi-LAT Observations of the Gamma-Ray Burst GRB 130427A", *Science*, **343** (2014) 42.
[170] Kouveliotou C. *et al.*, "NuSTAR Observations of GRB 130427A Establish a Single Component Synchrotron Afterglow Origin for the Late Optical to Multi-GeV Emission", *Astrophys. J.*, **779** (2013) 1.
[171] Bergstrom L. *et al.*, "New Limits on Dark Matter Annihilation from Alpha Magnetic Spectrometer Cosmic Ray Positron Data", *Phys. Rev. Lett.*, **111** (2013) 1101.
[172] Abdo A. A. *et al.*, "Constraints on cosmological dark matter annihilation from the Fermi-LAT isotropic diffuse gamma-ray measurement", *J. Cosmol. Astrophys. Phys.*, **04** (2010) 14.
[173] Ajello M. *et al.*, "The resolved and unresolved components of the Isotropic Gamma-ray Background", AAS HEAD meeting, `#14, #400.06`, 2014.
[174] Zaharijas G. *et al.*, "Constraints on the Galactic Dark Matter signal from the Fermi-LAT measurement of the diffuse gamma-ray emission", Fermi Symp. Proc., 2012, `arXiv:1304.2547`.
[175] Gnedin O. Y. *et al.*, "Response of dark matter halos to condensation of baryons: cosmological simulations and improved adiabatic contraction model", *Astrophys. J.*, **616** (2004) 16.
[176] Hooper D. and Goodenugh L., "Dark Matter Annihilation in The Galactic Center As Seen by the Fermi Gamma Ray Space Telescope", *Phys. Lett. B*, **697** (2011) 412.
[177] Hooper D. and Linden T., "Origin of the gamma rays from the Galactic Center", *Phys. Rev. D*, **84** (2011) 123005.
[178] Abazajian K. N. and Kaplinghat M., "Detection of a gamma-ray source in the Galactic Center consistent with extended emission from dark matter annihilation and concentrated astrophysical emission", *Phys. Rev. D*, **86** (2012) 083511.

[179] Abazajian K. N., "The consistency of Fermi-LAT observations of the galactic center with a millisecond pulsar population in the central stellar cluster", *J. Cosmol. Astrophys. Phys.*, **03** (2011) 010.
[180] Mirabal N., "Dark matter *versus* pulsars: catching the impostor", *Mon. Not. R. Astron. Soc.*, **436** (2013) 2461.
[181] Yusef-Zadeh F. *et al.*, "ALMA Observations of the Galactic Center: SiO Outflows and High-mass Star Formation near Sgr A*", *Astrophys. J. Lett.*, **767** (2013) 32.
[182] Gómez-Vargas G. A. *et al.*, "Constraints on WIMP Annihilation for Contracted Dark Matter in the Inner Galaxy with the Fermi-LAT", *J. Cosmol. Astrophys. Phys.*, **10** (2013) 029.
[183] Abdo A. A. *et al.*, "Observations of Milky Way Dwarf Spheroidal Galaxies with the Fermi-Large Area Telescope Detector and Constraints on Dark Matter Models", *Astrophys. J.*, **712** (2010) 147.
[184] Ackermann M. *et al.*, "Constraining Dark Matter Models from a Combined Analysis of Milky Way Satellites with the Fermi Large Area Telescope", *Phys. Rev. Lett.*, **107** (2011) 1302.
[185] Ackermann M. *et al.*, "Dark matter constraints from observations of 25 Milky, Way satellite galaxies with the Fermi Large Area Telescope", *Phys. Rev. D*, **89** (2014) 042001.
[186] Drlica-Wagner A. *et al.*, "Searching for Dark Matter Annihilation in the Smith High-velocity Cloud", *Astrophys. J.*, **790** (2014) 24.
[187] Nichols M. *et al.*, "The Smith Cloud and its dark matter halo: survival of a Galactic disc passage", *Mon. Not. R. Astron. Soc.*, **442** (2014) 2883.
[188] Abdo A. A. *et al.*, "Fermi Large Area Telescope Search for Photon Lines from 30 to 200 GeV and Dark Matter Implications", *Phys. Rev. Lett.*, **104** (2010) 1302.
[189] Ackermann M. *et al.*, "Fermi LAT search for dark matter in gamma-ray lines and the inclusive photon spectrum", *Phys. Rev. D*, **86** (2012) 2002.
[190] Bringmann T. *et al.*, *J. Cosmol. Astrophys. Phys.*, **07** (2012) 054.
[191] Weniger C., "A tentative gamma-ray line from Dark Matter annihilation at the Fermi Large Area Telescope", *J. Cosmol. Astrophys. Phys.*, **08** (2012) 007.
[192] Finkbeiner D. P. *et al.*, "Is the 130 GeV line real? A search for systematics in the Fermi-LAT data", *J. Cosmol. Astrophys. Phys.*, **01** (2013) 029.
[193] Ackermann M. *et al.*, "Search for gamma-ray spectral lines with the Fermi Large Area Telescope and dark matter implications", *Phys. Rev. D*, **88** (2013) 2002.
[194] Zacharijaz G., "Recent results on dark matter search with the Fermi-LAT", Astroparticle Physics 2014 conference, `http://indico.cern.ch/event/278032/overview`.
[195] Albert A. *et al.*, "Search for 100 MeV to 10 GeV gamma-ray lines in the Fermi-LAT data and implications for gravitino dark matter in the $\mu\nu$SSM", `arXiv:1406.3430`.
[196] Ando S. and Kusenko A., "Evidence for Gamma-ray Halos Around Active Galactic Nuclei and the First Measurement of Intergalactic Magnetic Fields", *Astrophys. J. Lett.*, **722** (2010) 39.
[197] Ackermann M. *et al.*, "Determination of the Point-spread Function for the Fermi Large Area Telescope from On-orbit Data and Limits on Pair Halos of Active Galactic Nuclei", *Astrophys. J.*, **765** (2013) 54.
[198] Neronov A. *et al.*, "No evidence for gamma-ray halos around active galactic nuclei resulting from intergalactic magnetic fields", *Astron. Astrophys.*, **526** (2011) 90.
[199] Aleksić J. *et al.*, "Search for an extended VHE gamma-ray emission from Mrk 421 and Mrk 501 with the MAGIC Telescope", *Astron. Astrophys.*, **524** (2010) A77.
[200] Finke *et al.*, "Constraints on the Intergalactic Magnetic Field from Gamma-Ray Observations of Blazars", Fermi Symp. Proc., 2012, `arXiv:astro-ph/1303.5093`.
[201] Neronov A. *et al.*, "Evidence for strong extragalactic magnetic fields from Fermi observations of TeV blazars", *Science*, **328** (2010) 73.
[202] Tavecchio F. *et al.*, "The interalactic magnetic field constrained by Fermi/LAT observations of the TeV blazar 1ES 0229+200", *Mon. Not. R. Astron. Soc.*, **406** (2010) 70.

[203] Dolag K. *et al.*, "Lower limit on the strength and filling factor of extragalactic magnetic fields", *Astrophys. J.*, **727** (2011) L4.
[204] Abdo A. A. *et al.*, "A limit on the variation of the speed of light arising from quantum gravity effects", *Nature*, **462** (2009) 331.
[205] Vasileiou V. *et al.*, "Constraints on Lorentz invariance violation from Fermi-Large Area Telescope observations of gamma-ray bursts", *Phys. Rev. Lett.*, **87** (2013) 122001.